On the Origins of the Electrical Impedance Cardiogram

Alexander Emanuel Hoetink

VRIJE UNIVERSITEIT

On the origins of the Electrical Impedance Cardiogram

ACADEMISCH PROEFSCHRIFT

ter verkrijging van de graad van doctor aan
de Vrije Universiteit Amsterdam,
op gezag van de rector magnificus
prof.dr. T. Sminia,
in het openbaar te verdedigen
ten overstaan van de promotiecommissie
van de faculteit der Geneeskunde
op 18 maart 2005
in de aula van de universiteit,
De Boelelaan 1105

door

Alexander Emanuel Hoetink

geboren te Apeldoorn

promotor: prof.dr. R.M. Heethaar

copromotor: dr.ir. Th.J.C. Faes

Contents

Chapter 1 Introduction

Background

Electrical impedance cardiography, sometimes called bio-impedance cardiography or thoracic impedance cardiography, was introduced as a low-cost non-invasive method to monitor function parameters of heart and circulation. The method aims to calculate heart function related parameters from a change in the electrical impedance measured across the thorax. To do so, an electrical current is injected into the body by means of one set of electrodes and with a different set of electrodes voltage changes across the thorax are measured as a function of time. Figure 1 shows an example of a typical measurement setup. This arrangement was introduced by Woltjer, cf. Woltjer et al. (1996a), and will be referred to in this thesis as the Woltjer-arrangement. From the measured voltage and current the magnitude and phase angle of the thoracic impedance can be calculated. The magnitude of the thoracic impedance is generally revered to as the electrical impedance (EI) of the thorax (an example is shown in figure 2).

One of the heart function related parameters that might be determined from the thoracic EI signal is the amount of blood pumped by the heart into the aorta. This is called Stroke Volume (SV) if the amount of blood ejected with each beat is considered and Cardiac Output (CO) if the amount of blood ejected into the aorta per minute is of interest. The rational behind the method is that when blood is injected into the aorta, its cross-sectional surface area increases and consequently its EI decreases. Therefore, a heart contraction synchronous decrease of the measured thoracic EI is assumed to be related to SV and CO. Although this line of reasoning seams simple, the extensive literature on the subject shows that it contains several pitfalls.

Several reviews are available that give the history of the development of EI Stroke Volume estimators, e.g. Mohapatra (1981); Lamberts, Visser, & Zijlstra (1984) and Sherwood et al. (1990). In the 1950's the first attempts were made independently by Bonjer and Nyboer [Bonjer (1950) and Nyboer (1950)],

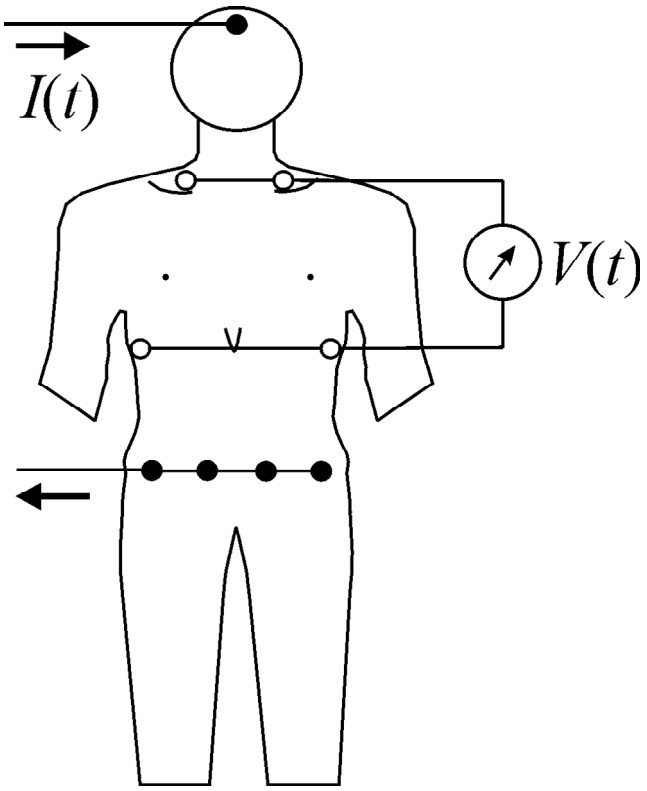

Figure 1. An example of a typical measurement setup, the so-called Woltjer-arrangement.

based on the assumption that the thorax can be represented electrically by a homogeneous cylinder enclosing another cylinder that represents the aorta (the so-called parallel cylinder model). They obtained a relationship between SV and the measured thoracic EI change that reads

$$V_S = \rho_{bl} \frac{L^2}{Z_0^2} \Delta Z \qquad (1.1)$$

Where V_S is the SV (ml), Z_0 (Ω) is the maximum of the thoracic EI signal, and ΔZ (Ω) is the (extrapolated) change in the thoracic EI signal. This is illustrated in the top panel of figure 2, which presents an example of a measured thoracic EI signal. Furthermore, ρ_{bl} (Ωcm) is the resistivity of blood and L (cm) is the distance between the voltage pick-up electrodes. Equation (1.1) however is only valid if blood only flows into the cylinder representing the aorta and does not

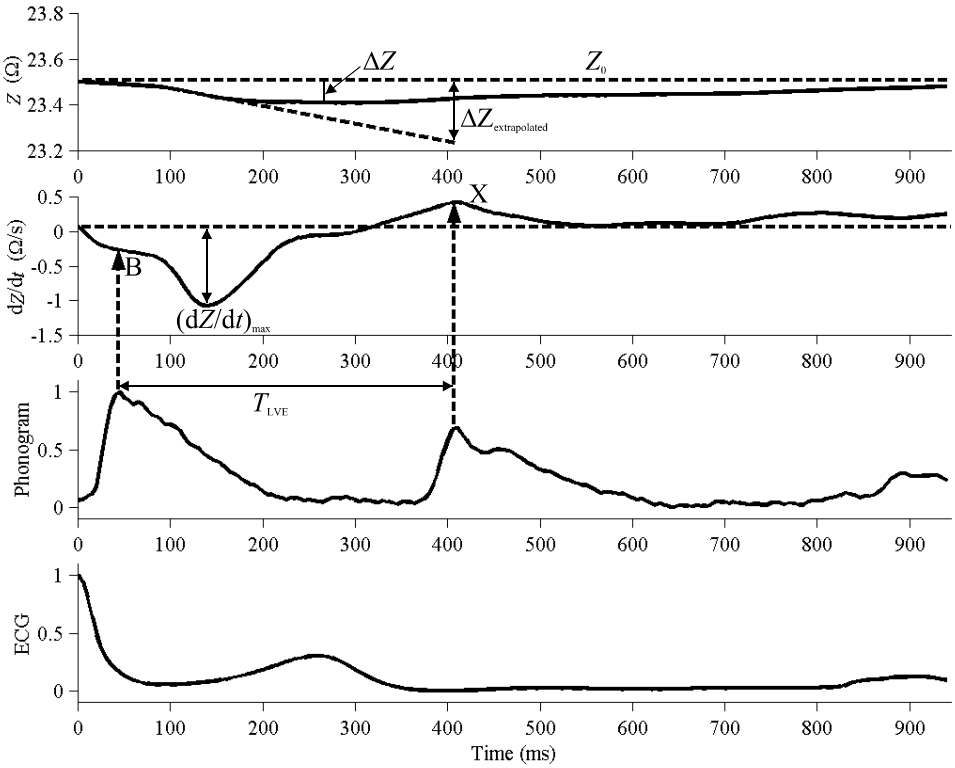

Figure 2. An example of a thoracic EI signal. From top to bottom are shown as function of time the thoracic impedance, the first time derivative of the thoracic impedance, a normalized envelope of a phonogram and a normalized ECG. The time range covers about 90% of a cardiac cycle.

leave this cylinder. Luckily in reality blood also leaves the aorta and the volume change of the aorta is, due to the law of conservation of mass for an incompressible fluid, the difference between inflow and outflow of blood. As a result, V_S in (1.1) is in fact not an estimation of SV, but of the difference between aortic inflow and aortic outflow of blood (see for details chapter 6). Estimations of SV should, therefore, be corrected for the outflow of blood from the aorta, cf. Yamakoshi, Togawa, & Ito (1977) and Faes et al. (1999a). This is sometimes called the outflow-problem. To solve this problem Nyboer suggested replacing ΔZ by $\Delta Z_{\text{extrapolated}}$. The rationale being that this latter variable represtents the impedance change had there been no outflow in the time interval of blood ejection into the aorta. According to Kubicek et al. and later Lababidi [e.g. Kubicek et al. (1966) and Lababidi et al. (1970)] this time interval, also called left ventricular ejection time, can be estimated from the EI

cardiogram by identifying the B-point (opening of aortic valve) and X-point (closing of aortic valve) as is illustrated in figure 2.

In the 1960's Kubicek et al. (1966) tried to solve the outflow-problem by introducing the following equation,

$$V_S = \rho_{bl} \frac{L^2}{Z_0^2} \left| \frac{dZ(t)}{dt} \right|_{MAX} T_{LVE} \qquad (1.2)$$

where $(dZ(t)/dt)_{MAX}$ is the maximum[1] deflection of the first derivative of the EI signal and T_{LVE} is the left ventricular ejection time (s). The difference with (1.1) is that the term ΔZ is replaced by the product of the absolute value of the maximum deflection of the first derivative of the EI signal during systole and the ventricular ejection time. In fact, this is equal to replacing ΔZ in (1.1) by $\Delta Z_{extrapolated}$. Lamberts et al. state without prove that this so-called forward extrapolation method to correct for the outflow is only correct if the slope of the inflow is constant, and if this slope is not influenced by the outflow, cf. [Lamberts, Visser, & Zijlstra (1984) page 19]. The validity of these assumptions is highly questionable.

Based on (1.2) first Sramek and later Bernstein [Sramek (1981); Sramek, Rose, & Miyamoto (1983) and Bernstein (1986)] developed a similar equation,

$$V_S = \frac{\delta}{4.25} \frac{(0.17H)^3}{Z_0} \left| \frac{dZ_0(t)}{dt} \right|_{MAX} T_{LVE} \qquad (1.3)$$

Where δ is a weight correction factor obtained from a nomogram and H is the total body height (cm). In this equation the outflow is corrected for with the same forward extrapolation procedure as in (1.2), the difference being that the much debated value of the blood resistivity ρ_B is
replaced by a term that estimates the electrically participating thorax volume from a truncated cone model instead of a cylinder model.

[1] Mathematically it would be more elegant to use the (negative) minimum value of the first derivative, but for now we will stay with the original notation.

Problems associated with Electrical Impedance Cardiography

The most fundamental point of critique is that the electrical representation of the thorax, the parallel cylinder model, is not adequate. Several studies have indicated that the measured thoracic EI is the result of multiple sources, see for example Sakamoto et al. (1979); Patterson et al. (1990); Wang & Patterson (1995); Kauppinen, Hyttinen, & Malmivuo (1998) and Wtorek (2000). Other possible origins of the thoracic EI change, apart from the aorta, are the other major blood vessels in the thorax (e.g. pulmonary artery, vena cava etc.), the heart, muscle tissue, the lungs, and possibly even the electrical resistivity change of blood due to blood flow. Under physiologically normal conditions the EI change has been hypothesized to be the result of [cf. Mohapatra (1981)]:

1. volume changes of the thoracic organs, especially the major blood vessels, the heart, and the lungs;
2. change in blood perfusion of organs like the lungs and muscle tissue;
3. the change of electrical resistivity of blood due to blood flow in the major blood vessels;
4. the movement of organs in the thorax.

More exotic sources of impedance change like movement of the voltage pickup electrode due to breathing have also been suggested, but their validity has been refuted through experiments. In order to calculate SV or CO from the measured thoracic EI change, the contribution of the aorta to the thoracic EI change should first of all be separable in time and location on the thorax from the contribution of the other sources. For example, the change of air volume in the lungs due to breathing is not synchronous with the heart rate, but with the breathing rate. As the breathing rate is normally lower than the heart rate, this contribution can presumably be removed by averaging the EI signal over a number of heart beats [see Raza, Patterson, & Wang (1992)] or filtering. The other origins of EI change, however, are directly or indirectly the result of heart activity and can not be removed by simply averaging or filtering. Consequently, to calculate SV or CO from the thoracic EI change, a time window during the

cardiac cycle in combination with a measurement location on the thorax should be found where the aorta is preferably the only (but probably at best the major) source of the EI signal.

Even if it is possible to isolate the contribution of the aorta, the problem of the electrical resistivity change of blood due to blood flow complicates matters considerably, see for example Edgerton (1974); Visser et al. (1976); Sakamoto & Kanai (1979); Shankar, Webster, & Shao (1985); Ninomiya et al. (1988); Visser (1989); Visser (1992); Raaijmakers et al. (1997b) and Fujii et al. (1999). Suppose the aorta can be represented by a conductor with fixed length l_{Ao} (cm), time varying electrical resistivity of blood $\rho_B(t)$ (Ωcm), and time varying cross-sectional surface area $A_{Ao}(t)$ (cm^2). According to Ohm's Law the time varying EI of the aorta can be written as

$$Z_{Ao}(t) = \frac{\rho_B(t) \cdot l_{Ao}}{A_{Ao}(t)} \tag{1.4}$$

If the heart pumps blood into the aorta, two different processes may cause a measurable EI change. On the one hand, the increase of cross-sectional surface area of the aorta will result in a decrease of the measured EI. On the other hand, in flowing blood shear stresses result in orientation and deformation of red blood cells. The orientation and deformation of red blood cells alters the pathway of the electrical current. As a consequence the electrical resistivity of blood decreases and this in turn will also produce a decrease of the measured EI. Therefore, the decrease in measured EI is possibly partly caused by a cross-sectional surface area change of the aorta that can be related to the inflow of blood (and consequently to SV or CO) and partly caused by the resistivity change of blood due to blood flow. This latter contribution to the EI change is related to the flow velocity of blood and thus indirectly to the inflow of blood. Consequently, if SV is to be obtained from a measured EI change, theoretical knowledge about the relation between inflow of blood into the aorta, cross-sectional surface area change of the aorta and blood resistivity change is of eminent importance.

Suppose that the measured thoracic EI change can be related only to the cross-sectional surface area change (or equivalently to the volume change) of

the aorta, still another problem remains. How can SV or CO be calculated from the volume change of the aorta? Theoretical studies of the forward extrapolation model developed by Kubicek et al. (1966) have shown that this method does not properly take into account the outflow of blood from the aorta and consequently leads to an overestimation of stroke volume, see Yamakoshi, Togawa, & Ito (1977) and Faes et al. (1999a). Therefore, the outflow-problem still remains unsolved and as a consequence a theoretically founded estimator of SV from thoracic EI changes is still not available.

Aims of this thesis

The previous section has demonstrated that several fundamental problems concerning EI Cardiography still remain unsolved. This thesis, as a continuation of earlier research that was reported in Raaijmakers (1998), focuses on these problems by answering the following fundamental questions:

1. Can the contribution of the aorta to the thoracic EI signal be separated from the contribution of other possible sources?
2. Can the contribution of the blood resistivity change due to blood flow to the thoracic EI change be quantified?
3. Can the outflow-problem be solved?

To begin with, **chapter 2** will introduce a mapping method to study the origins of the thoracic EI signal and compare the results to Magnetic Resonance (MR) images of cross-sections of the thorax. With an 'Woltjer-like' electrode array the EI signal of small slices of the thorax is measured and volume changes in the slices are calculated. These volume changes will be compared to volume changes of organs in the thorax measured with MRI. The aim is to answer the question whether the contribution of the aorta can be separated from the other sources. This chapter was published under the same title in IEEE Transactions on Medical Imaging, vol. 21, no. 6, June 2002 and presented orally at the XI ICEBI 17-21 June 2001 Oslo, Norway.

In **chapter 3** different electrode arrangements for measuring the thoracic EI signal will be investigated. Reducing the number of electrodes needed for EI

cardiography is more comfortable for the patient and more practical for medical personnel, especially in the Intensive Care Unit and after extensive surgery. The idea is that if the aorta is the only source of the thoracic EI change, the parallel cylinder model is a valid representation of the thorax and aorta. A consequence of the parallel cylinder model is that, due to axis-symmetry, the equipotential lines are perpendicular to the axis of the cylinders and therefore, voltage pickup electrodes on the left-hand side, right-hand side, and both sides of the thorax should give equal results. This chapter was published under the same title in Physiological Measurements 23 (2002) and presented at the XI ICEBI 17-21 June 2001 Oslo, Norway. Additionally, an international patent based on chapter 3 has been obtained: US 44866/VB, “Method for the in-vivo non-invasive measurement of a biological parameter”.

In **chapter 4**, as an intermezzo, a theory is presented that allows calculation of the blood resistivity change due to blood flow. The theory proposed by Fricke (1924) that gives the electrical conductivity (which is the reciprocal of the electrical resistivity) of a suspension of ellipsoidal particles in an electrolyte, is extended to the case of stationary and laminar flow. This chapter has been accepted for publication under the same title in IEEE Transaction on Biomedical Engineering and is currently in press.

The theory presented in **chapter 4** will be used in **chapter 5**, where we return to the problem of separating the different sources of the thoracic EI signal. Again mappings of the thoracic EI signal are made that are compared to MR images, but now the results of **chapter 4** will be used to quantify the contribution of the blood resistivity change due to blood flow to the thoracic EI change. Additionally, the ‘Woltjer-like’ electrode array is replaced by an electrode array that measures the EI signal on the left-hand side, right-hand side of the thorax and sternal line separately. **Chapter 5** has been submitted to IEEE Transactions on Biomedical Engineering.

Before summarizing and drawing conclusions in **chapter 7**, **chapter 6** will investigate the possibility of correcting for the outflow of blood. A theoretically founded estimator of SV will be developed that will be tested in a simulation study. **Chapter 6** has been submitted to Medical & Biological Engineering & Computing.

Chapter 2 Imaging of Thoracic Blood Volume changes during the Heart Cycle with Electrical Impedance using a LinearSpot-Electrode Array

A.E. Hoetink; Th.J.C. Faes; J.T. Marcus; H.J.J. Kerkkamp; R.M. Heethaar

IEEE Transactions on Medical Imaging, Vol. 21, No. 6, June 2002, pp. 653-661

Summary

Electrical Impedance measurements conducted on the thorax contain useful information about the changes in blood volume that occur in the thorax during the heart cycle. The aim of this study is to present a new (tomographic-like) method to obtain this relevant information with electrical impedance measurements, using a linear electrode array. This method is tested on three subjects and the results are compared to results obtained from MR cine-images showing the cross-sectional surface area changes of the aorta, the vena cava, the carotid arteries and the heart. This study shows that the different sources of the thoracic EI waveform may be separated in time and location on the thoracic surface and that aortic volume changes may be estimated accurately.

Introduction

In the last two decades, the thoracic electrical impedance (EI) signal has been the subject of several studies trying to determine its source, e.g. Sakamoto et al. (1979); Kim et al. (1988); Wang & Patterson (1995); Patterson et al. (1990); Kauppinen, Hyttinen, & Malmivuo (1998); Wtorek (2000) and Wang, Haynor, & Kim (2001). These studies show that the EI waveforms, measured on the front surface of the thorax, are not only affected by changes in blood volume in the aorta, but also by changes in other organs such as the heart, the large veins and the lungs. The change of blood resistivity with flow is likewise suggested to be a possible source of the EI signal. These results indicate that the EI signal contains useful information about the changes in blood volume that occur in the thorax during a heart cycle. To obtain this relevant information, the different sources have to be separated both in time and location on the thoracic surface.

Currently, several tomographic methods are available to reconstruct conductivity changes in the thorax. For example, Mueller, Isaacson, & Newell (2001) demonstrated that conductivity changes caused by ventilation and perfusion in a human subject can be reconstructed from EI tomography data, using a rectangular array of electrodes placed on a subject's chest. To obtain EI tomography data, currents are applied on some electrodes of the array and the resulting voltages on the other electrodes of the array are measured. Data are collected for all possible combinations of current injecting and voltage pickup electrodes. For traditional EI cardiographic measurements, on the other hand, the electrical current is applied on electrodes generally located in the neck (or on the forehead) and below the xiphoid level. The direction of this current is approximately parallel to the body axis, as opposed to the current's direction in tomographic measurements. The resulting potential difference across the thorax is measured with a different set of electrodes than the current injecting electrodes. Several different electrode arrays have been compared by Kauppinen, Hyttinen, & Malmivuo (1998) and Woltjer et al. (1996a). All these electrode arrays use voltage pickup electrodes that are separated by a relatively large distance (the voltage pickup electrodes are generally located at the level of the xiphoid process and in the neck). Numerous model studies [e.g.

Sakamoto et al. (1979); Kim et al. (1988); Wang & Patterson (1995); Kauppinen, Hyttinen, & Malmivuo (1998); Wtorek (2000) and Wang, Haynor, & Kim (2001)] indicate that due to the multiple sources and therefore complexity of the traditional EI cardiographic signal, clinical appliciation of this method is problematic. Sakamoto et al. (1979) suggested that the EI signal measured by a similar set-up, but with a pair of small voltage pickup electrodes separated by a short distance, gives useful information about the region in the vicinity of the electrodes. Consequently, using such localized measurements, the different sources of the thoracic EI signal might be separated in time and location.

We designed a method to image the thoracic blood volume changes during the heart cycle from regional thoracic EI measurements, using a newly developed estimator that calculates segmental surface area changes of the organs in the thorax. To collect the EI data, a linear electrode array was used. To test this imaging method, we compared images obtained from EI measurements to images of the surface area changes of the thoracic organs obtained from MRI measurements. These latter images included contributions of the aorta, the vena cava, the carotid arteries and the heart. Furthermore, we calculated thoracic blood volume changes from the EI images and the MRI images. These measurements could possibly help to understand the model based results presented in the literature. The aim of this study is to present this new (tomographic-like) method to image the changes in thoracic blood volume using EI measurements.

Theory

Consider a small transversal slice of the upper portion of the body with thickness *l* (cm). Injection of an alternating current[2] into the body, using electrodes located on the forehead and the upper part of the legs, will result in a potential difference across this slice. If this potential difference is measured with spot electrodes at certain locations on the circumference of the slice, then using Ohms law will yield the impedance of the slice in the vicinity of the electrodes. This impedance, say $Z_{slice}(t)$, can be represented by a lumped circuit element.

[2] Consider a current of constant amplitude and of a frequency such that the impedances of all tissues are essentially resistive.

Furthermore, this element can be considered to be a parallel connection of a time-dependent impedance, say $Z_{source}(t)$, and a time-independent[3] impedance, say Z_{tissue}. Now suppose that $Z_{source}(t)$ represents the impedance of all the organs (sources) inside the slice that cause the potential distribution to be time-dependent and Z_{tissue} represents the impedance of all tissues with constant electrical properties and cross-sectional surface area. Consequently, the total time-dependent impedance of the small slice can be written as

$$Z_{slice}(t) = \frac{Z_{source}(t) \cdot Z_{tissue}}{Z_{source}(t) + Z_{tissue}} \tag{2.1}$$

Furthermore, suppose that for this small slice we may take together all sources into an equivalent lumped circuit element. The time-dependent impedance of this element with fixed length l, time-dependent resistivity $\rho(t)$ and time-dependent cross-sectional surface area $A(t)$, can then be written as

$$Z_{source}(t) = \frac{\rho(t) \cdot l}{A(t)} \tag{2.2}$$

Differentiating (2.1) and (2.2) with respect to t and substituting the time derivative of (2.2) together with (2.1) into the time derivative of (2.1), we obtain an estimator of the rate of change of cross-sectional surface area of all the sources in the small slice considered, i.e.

$$\frac{dA(t)}{dt} = -\frac{\rho(t) \cdot l}{Z_{slice}^2(t)} \frac{dZ_{slice}(t)}{dt} + A(t) \frac{d \ln\{\rho(t)\}}{dt} \tag{2.3}$$

where ln denotes the natural logarithm. We now assume that the resistivity of this lumped circuit element is independent of time or that the rate of change of the resistivity is small enough that the second term on the right-hand side of (2.3) can be neglected. Now, integrating with respect to t, yields an estimator of

[3] Time-independent with respect to the heart cycle.

the cumulative cross-sectional surface area change (SAC) of all the sources in the small slice, i.e.

$$\Delta A(t) = A(t) - A(t_0) = -\rho \cdot I \int_{t_0}^{t} \frac{1}{Z_{slice}^2(t)} \frac{dZ_{slice}(t)}{dt} dt \qquad (2.4)$$

where ρ is the time-independent resistivity. Finally, consider the thorax to be divided into N of these small slices. For each slice the cross-sectional surface area change is given by (2.4), say $\Delta A(z_i,t)$ for the ith slice at location z_i with respect to the body axis (say z-axis). Consequently, the total volume change of all the sources in the thorax is simply obtained by integrating $\Delta A(z_i,t)$ over the total number of slices (N), i.e.

$$\Delta V_{total}(t) = \int_{z_{i=1}}^{z_{i=N}} \Delta A(z_i, t) dz \qquad (2.5)$$

Experiment

The experiment was conducted on 3 healthy adult male subjects in supine rest. On all subjects first EI measurements were conducted, immediately followed by MRI measurements. Before the EI - and MRI measurements, the subjects were in supine rest for a period of approximately 30 minutes, to assure physiological stabilization.

EI measurements

Current injecting spot electrodes (Nutrode-P20M0) were placed on the forehead (one) and on the upper legs (two on each leg). Voltage pickup electrode pairs were placed, approximately 5 (cm) apart in the z-direction, in the mid-clavicular lines (in lines through the midpoints of the clavicles and parallel to the z-axis) and mid-axillary lines (at the lateral side of the thorax in lines through the center of the axils and parallel to the z-axis) from below the xiphoid process up to the neck (see figure 1). The minimum distance between current injecting and voltage pickup electrodes exceeded 15 (cm). The EI signals were recorded

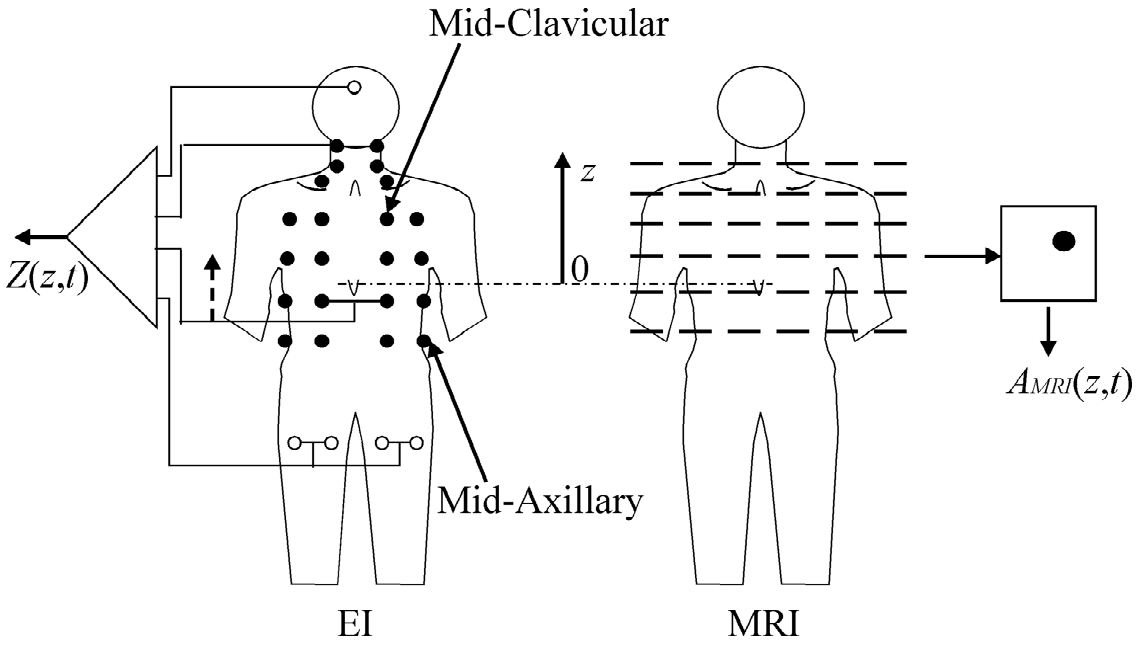

Figure 1. EI measurement setup (left) and MRI measurement-setup (right).

between the upper voltage pickup electrode pair in the neck and all other electrode pairs, until the upper electrode pair in the neck was reached. The signals were collected, for one minute, using a system developed in our laboratory [for details see Goovaerts, Raaijmakers, & Heethaar (1995)] at 64 kHz and at a sample frequency of 200 Hz, resulting in a temporal resolution of 5 ms. The registrations were ensemble averaged (approximately 60 heartbeats) to remove the affects of respiration. The variable obtained from the EI signal was the impedance between the voltage pickup electrodes as a function of time and z_i-coordinate, say $Z(z_i,t)$ (Ω). From $Z(z_i,t)$ the impedances of each slice between different voltage pickup electrode pairs were calculated by subtraction, i.e.

$$Z^{i}_{slice}(t) = Z(z_i, t) - Z(z_{i+1}, t) \qquad (2.6)$$

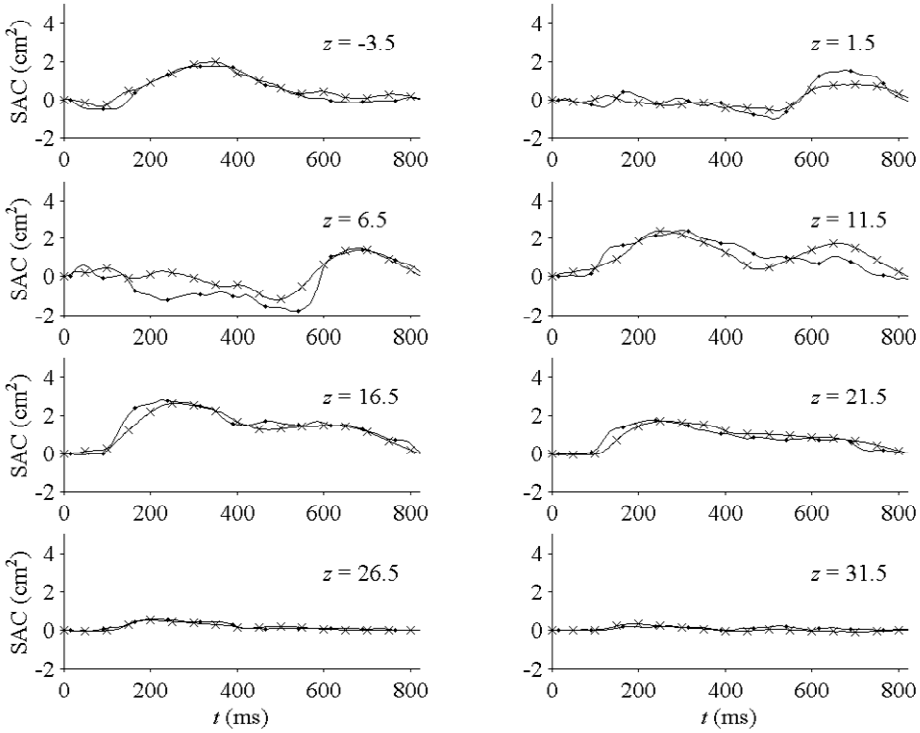

Figure 2. Estimated SAC (cm^2) from mid-clavicular EI measurements (crosses) and MR cine-images (dots) including contributions from the aorta, the vena cava, the carotid arteries and the heart for each slice against time (ms). The position (cm) of each slice relative to the level of the xiphoid process is given as the *z*-coordinate. See text for a discussion.

The slice impedances were inserted into (2.4) to obtain the SAC of the sources in the slices. For the resistivity a constant value of the resistivity of blood was used, ρ = 135 (Ωcm). For the slice thickness the distance between the voltage pickup electrode pairs was inserted, i.e. *l* = 5 (cm), consequently the spatial resolution in the direction of the *z*-axis was 5 (cm). Since the EI signals were measured simultaneously on the left - and right side of the thorax, it is not sensible to use the term spatial resolution in the other directions.

MRI measurements

MR cine-images (see appendix for details) were recorded in transverse planes, reaching from the neck to below the xiphoid process. The distance between each image plane was 5 (cm). The R-wave of the ECG was used to trigger the image acquisition. The temporal resolution was 15 ms, and the number of temporal phases that were acquired, were chosen in such a way that 90% of the heart cycle, of the individual subject, was covered. In each slice and for

each phase of the heart cycle contours were drawn manually around the aorta, the vena cava (inferior and superior), the carotid arteries and the circumference of the heart. The cross-sectional surface area of each organ was calculated as a function of time. The total cross-sectional surface area of a slice was taken as the sum[4] of the cross-sectional surface areas of the organs in that slice, yielding $A_{MRI}(z_i,t)$ (cm^2). The resulting total cross-sectional surface area for each slice was then differentiated with respect to time. The resulting differential area changes were then integrated with respect to time (with the integration constant set to zero), to obtain the SAC, say $\Delta A_{MRI}(z_i,t)$, for each slice.

Results

As an example, figure 2 shows for each slice the SAC (cm^2) obtained from EI measurements (crosses) with the electrode array located at the mid-clavicular lines and the SAC calculated from the MR cine-images (dots). The latter includes, contributions of the aorta, the vena cava (all slices except the slices located at z = 25.6 (cm) and 31.5 (cm)), the carotid arteries (slices located at z = 26.5 (cm) and z =31.5 (cm)), and the total cross-sectional surface area change of the heart (slices located at z = 1.5 (cm) and z = 6.5 (cm)).

The SAC for each slice were used to obtain SAC images by means of interpolation. Using the interpolation function provided by the software package MATLAB version 6, a spline was fitted to the data and this resulted in a time resolution of 2.5 ms and a spatial resolution of approximately 0.10 (cm). This interpolated data was used to obtain the images presented in figures 3 and 4. These figures show the interpolated SAC (cm^2) in one hart cycle coded in color-scale against time (horizontal axis) and position on the thorax (vertical axis) for the EI measurements (top left) and MRI measurements (top right). Thus, the color of each pixel in the images represents the value of the interpolated SAC at a specific moment in the heart cycle and at a specific location on the z-axis of the thorax. The zero level of the z-axis coincides with the level of the xiphoid process. The SAC image obtained from EI measurements with the linear electrode array located on the mid-clavicular lines and the SAC obtained from

[4] The organs are considered to be conductors in parallel connection.

MRI including the aorta, the vena cava, the carotid arteries and the heart are shown in the figure 3. Figure 4 gives the SAC image obtained from the EI measurements with the electrode array located on the mid-axillary lines, together with the image of the SAC calculated from MRI measurements including the aorta, the vena cava and the carotid arteries, but without the heart contribution. Furthermore, the contour maps obtained from the SAC images are displayed below each SAC image in figures 3 and 4, respectively. The levels of the contours were set at –1, 0, 1 and 2 (cm^2). This way of representing the interpolated data suppresses the finer details and shows more clearly the location in time and space of the observed SAC.

Using (2.5), the total volume change of all the sources in the thorax was calculated from the EI SAC images and compared to the total volume change calculated form the MRI SAC images. The top left panel in figure 5 shows these volume changes as a function of time obtained from the mid-clavicular EI SAC image (crosses) and from the MRI SAC image including the contribution of the heart (dots). The top right panel in figure 5 shows these results from the mid-axillary EI SAC image (crosses) and the MRI SAC image without the heart contribution. For each moment in time the total volume change is obtained by integrating with respect to the z-coordinate over the whole region shown in the images, i.e. for each moment in the heart cycle the numerical values, represented by the color coding, are integrated with respect to the vertical axis in figures 3 and 4. The normalized recorded ECG signals are included as a reference. Furthermore, the correlation coefficients of the EI - and MRI results were also determined and read r = 0.930 for the mid-clavicular EI measurements and r = 0.911 for the mid-axillary EI measurements, respectively.

To determine whether the contribution of the aorta to the thoracic EI signal can be separated from the other sources, we calculated the total volume change of the ascending aorta, aortic arch and upper part of the descending aorta from the MRI measurements. These results were compared to the total volume changes obtained from the EI SAC images. Figure 6 shows the results for the three subjects, when the aortic volume changes calculated from MRI SAC images are compared to the volume changes of all the sources in the thorax estimated from mid-clavicular EI SAC images (left side in figure 6) and

mid-axillary EI SAC images (right side in figure 6). The volume changes are given as a function of normalized[5] time and the region, over which the SAC images were integrated was reduced to the region of the ascending aorta, aortic arch, and upper part of the descending aorta, e.g. approximately from z = 10 (cm) to z = 20 (cm) for subject 1 in figures 3 and 4. Note that in figure 6, the calculated total volume changes are smaller than in figure 5, due to the smaller region of integration. Again normalized recorded ECG signals are included as a reference. The correlation coefficients of the EI results and the results obtained from MRI range from r = 0.794 to r = 0.925. Furthermore, the correlation coefficients of the volume changes obtained from the mid-clavicular EI SAC images and mid-axillary EI SAC images in figure 6, were found to be r = 0.987 for subject 1, r = 0.986 for subject 2 and r = 0.932 for subject 3, respectively.

Discussion

When comparing the EI SAC images to the MRI SAC images (see figures 3 and 4), a promising similarity is found. On inspection it can be seen that in the systolic part of the heart cycle, roughly between t = 0 and t = 400 ms, and located in the region between 10 (cm) and 20 (cm) above the xiphoid process, both in the EI SAC images and MRI SAC images, a large positive SAC occurs. Just below this region, a negative SAC occurs in the mid-clavicular EI SAC image and corresponding MRI SAC image that includes the contribution of the heart (see figure 3), while this negative SAC is absent in the mid-axillary EI SAC image and the corresponding MRI SAC image without the contribution of the heart (see figure 4). The mid-clavicular EI measurements place the electrode array close to the heart. For the mid-axillary EI measurements, on the other hand, the electrode array is applied on the lateral sides of the body at a relatively large distance from the heart. Therefore, the negative SAC observed in figure 3 may well be the result of the decrease of the total cross-sectional surface area of the heart during systole when blood is rapidly ejected from the heart into the aorta and pulmonary artery before atrial filling occurs. The distance between the aorta and the electrode array located on the mid-

[5] Normalized to the time length of the heart cycle that was covered by the MR cine-images

clavicular lines is comparable to the distance between the aorta and the electrode array located on the mid-axillary lines. This indicates that the large positive SAC just above the region of the heart, found in both EI SAC images and both MRI SAC images (see figures 3 and 4), is mainly caused by the rapid expansion of the aorta during systole. The contribution of the pulmonary artery is probably much smaller, since it branches off to the sides just above the heart and the direction of the electrical current is perpendicular to these branches.

The calculated volume changes obtained from the EI SAC images and MRI SAC images (see figure 5) show a high correlation of the EI - and MRI measurements. Note that the total volume changes calculated from the mid-clavicular EI SAC images and corresponding MRI SAC images are smaller than those calculated from the mid-axillary EI SAC images and corresponding MRI SAC images. This is due to the negative SAC of the heart in the region of the heart, i.e. approximately between z = 0 and z = 10 (cm) (see figure 3). Furthermore, the total volume change calculated from the MRI SAC image without the contribution of the heart shows no diastolic volume increase, as opposed to the total volume change calculated from the MRI SAC image including the heart contribution (figure 5). This indicates that this diastolic volume increase is the result of an increase in cross-sectional surface area of the heart during diastole.

Figure 6 presents the results when the volume changes of only the ascending aorta, aortic arch and descending aorta calculated from the MRI measurements are compared to the volume changes calculated from the EI measurements in the corresponding region [roughly between z = 10 (cm) and z = 20 (cm)]. These latter volume changes include contributions from all possible sources. All three subjects show a high correlation (ranging from r = 0.794 to r = 0.925) of the volume changes calculated from EI SAC images and MRI SAC images, substantiating our statement that the large positive SAC just above the region of the heart, found in both EI SAC images and both MRI SAC images (see figures 3 and 4), is mainly caused by the rapid expansion of the aorta during systole. Furthermore, the two sets of EI measurements show a very high correlation coefficients (r > 0.93) for all three subjects. This indicates that in the region above the heart the EI measurements are highly insensitive to a change in electrode position from mid-clavicular to mid-axillary.

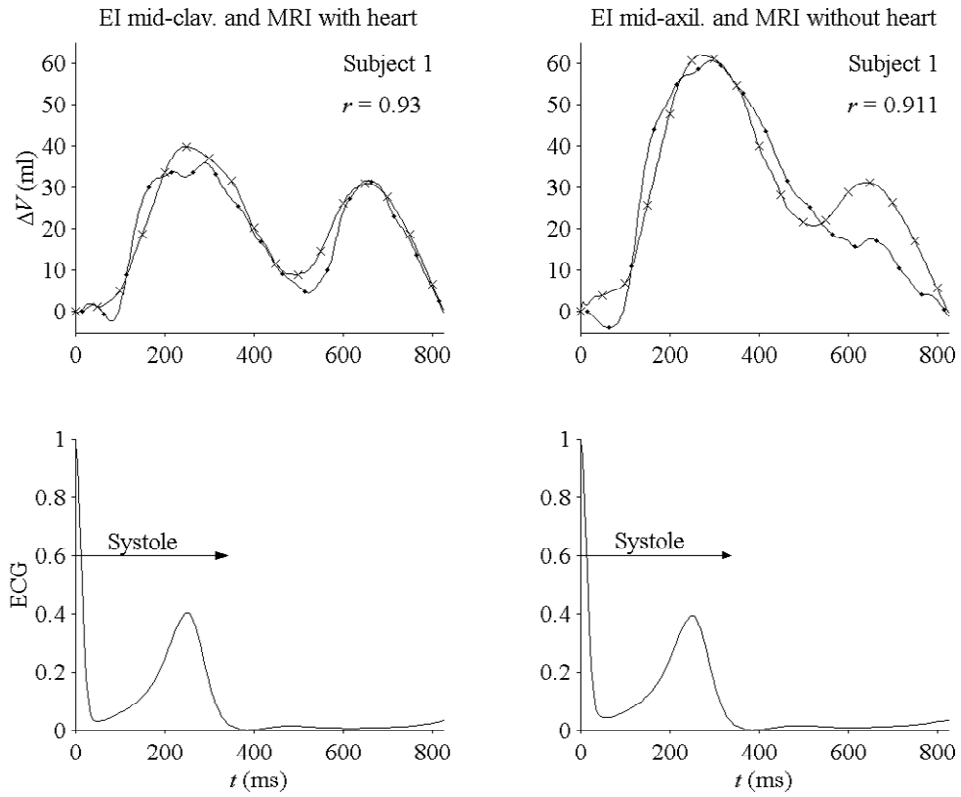

Figure 5. (top left) Total volume changes, ΔV (ml), estimated from mid-clavicular EI SAC images (crosses) and MRI SAC images including contributions from the aorta, the vena cava, the carotid arteries and the heart (dots); (top right) Total volume changes (ml) estimated from mid-axillary EI SAC images (crosses) and MRI SAC images including contributions from the aorta, the vena cava and the carotid arteries, but without the contribution of the heart (dots); (bottom left and right) Normalized ECG registration (top R-wave at $t = 0$). Correlation coefficiens, r, of the EI and MRI measurements are given.

To understand the results presented in this paper it is useful to look at the problem from the perspective of the lead field theory as presented by Geselowitz (1971) and used in model studies by Kauppinen, Hyttinen, & Malmivuo (1998) and Wtorek (2000). The lead field theory relates regional conductivity changes inside a volume conductor to an impedance change measured on the surface of that volume conductor. If a current is injected by means of a pair of electrodes and the resulting potential difference is measured between a different pair of electrodes, then the measured impedance change (say ΔZ) on the surface of the volume conductor can be written as a volume integral of the regional conductivity change (say $\Delta\sigma$) and the dot product of two lead fields called the sensitivity field (say S). One lead field results from the current field when the current is injected by means of the current electrodes. The other lead field results from a hypothetical current field that would have

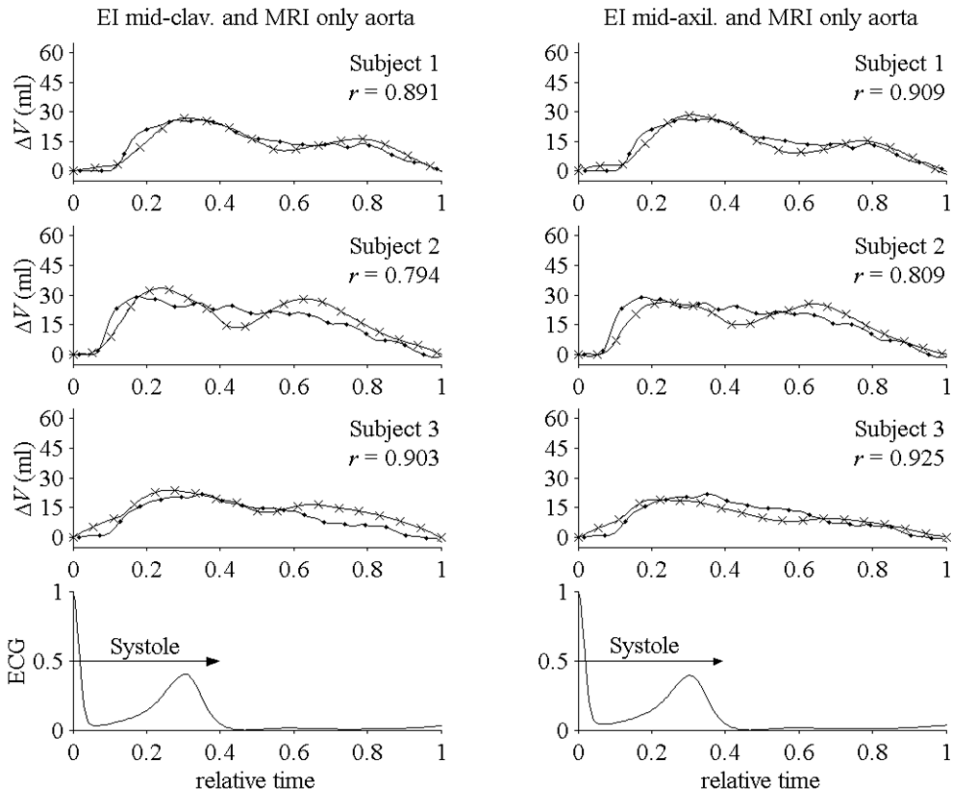

Figure 6. (left) Total volume changes estimated from mid-clavicular EI SAC images (crosses) and MRI SAC images including only contributions of the aorta (dots); (right) Total volume changes estimated from mid-axillary EI SAC images (crosses) and MRI SAC images including only the contribution of the aorta (dots); The region of integration was reduced to the region of the ascending aorta, aortic arch, and upper part of the descending aorta in the SAC images (see text). Correlation coefficiens, *r*, of the EI and MRI measurements are given.

resulted if the current had been injected by means of the voltage pickup electrodes. The integration is done over the region where the conductivity change is nonzero. Wtorek [cf. Wtorek (2000)] gives an equation that relates the impedance change measured on the surface of the volume conductor to conductivity changes inside that volume conductor, i.e.

$$\Delta Z = \sum_{s=1}^{M} K_s \Delta\sigma_s \qquad \text{with} \qquad K_s = \iiint_{V_s} S dV \tag{2.7}$$

Where M is the number of regions that have a nonzero conductivity change (the sources) and V_s is the volume of the sth region with nonzero conductivity change. Different locations of the voltage pickup electrodes may result in different hypothetical current fields and therefore in different sensitivity fields.

Consequently, a specific location of the voltage pickup electrodes may result in a higher sensitivity for a specific source. This is demonstrated in figure 3 when the voltage pickup electrodes are located close to the heart, i.e. in the region between z = 0 (cm) and z = 10 (cm). Comparing the EI SAC image in figure 3 with the EI SAC image in figure 4 it can be seen that placing the electrodes at the same z-coordinates but on the mid-axillary lines, the influence of the heart disappears and thus the mid-axillary measurement is clearly less sensitive for that particular organ. If we now compare the EI SAC images in figures 3 and 4 with the voltage pickup electrodes located in the region of the aortic arch, i.e. between z = 10 (cm) and z = 20 (cm), it can be seen that the two sets of measurements are almost identical. This is substantiated by comparing the volume changes obtained from the mid-clavicular EI measurements to the volume changes obtained from the mid-axillary EI measurements (see figure 6). The high correlation coefficients (r = 0.987 for subject 1, r = 0.986 for subject 2 and r = 0.932 for subject 3) of the two sets of EI measurements indicate that these measurements are sensitive for one particular organ (the aorta) only and that the sensitivity field is not greatly changed in this region. Although it might be argued that the assumptions used to derive (2.3) do not hold in the region of the heart, it seems that they do hold in the region of the aortic arch.

Sakamoto et al. [cf. Sakamoto et al. (1979)] used a simplified 3-D FEM model of the human thorax containing the heart, the lungs, the aorta and the vena cava. They found that, on the front surface of the thorax, the greatest change of the potential gradient caused by the heart is in the region of the heart, a result that was recently confirmed by Wang, Haynor, & Kim (2001). Furthermore, Sakamoto et al. (1979) showed that the changes of the potential gradient, originating from the aortic arch, are significantly larger than the contribution of other parts of the aorta. When the influence of both the heart and the aorta were combined, they found that the potential gradient in the vicinity of the aortic arch and the heart, changes much more than at other locations on the thorax. The potential changes due to impedance changes of the lungs were found to be very small, relative to the changes caused by the heart and the aorta. They also concluded that the EI signals measured by a pair of small electrodes separated by a short distance give useful information about the

region in the vicinity of the electrodes. These model based results agree very well with our experimental results.

Kim et al. [see Kim et al. (1988)] used anatomical maps to construct a 3-D FEM model of the thorax. They found that the impedance change is nearly linearly related to the blood volume change in the aorta. Apart from the aorta, the heart (ventricles) and other organs, the change of blood resistivity with flow was added as a possible source of the EI signal. The contribution of blood perfusing the lungs was found to be much smaller than the effects of the aorta and the heart. Wang & Patterson [cf. Wang & Patterson (1995)] constructed 3-D Finite Difference models of the human thorax, based upon MR-images taken at end diastole and end systole. They concluded that the most significant influences on the EI waveform are the blood resistivity change due to flow and the lung resistivity change. However, in a similar study Wtorek (2000) showed graphs which show the contribution of different organs to the measured impedance changes under varying conditions. Careful reading of these graphs learns that the aorta is a major source of impedance changes under varying conditions. This model-based finding is in close correspondence with our experimental finding. All these model studies, however, only presented results for an electrode array that applies voltage pickup band electrodes located at the level of the xiphoid process and the lower part of the neck. The contribution of the different organs to the EI waveform were expressed as percentages of the impedance change measured with such an electrode array, without giving the relative contribution of the different origins for other locations on the thorax. Therefore, the results of our study may contribute to understand how the EI waveforms, measured at different locations on the thorax, are affected by the contribution of the different organs.

Many authors have studied the dependence of the resistivity of blood on blood flow, e.g. Edgerton (1974); Sakamoto & Kanai (1979); Shankar, Webster, & Shao (1985); Ninomiya et al. (1988); Visser (1989); Visser (1992); Raaijmakers et al. (1997b) and Fujii et al. (1999). Although there is a general consensus that this dependence is caused by deaggregation, orientation and deformation of erythrocytes, there is still debate on the magnitude of this effect in-vivo. Visser [see Visser (1992)] demonstrated in in-vitro experiments that the magnitude of the decrease of blood resistivity due to blood flow may be as large

as 20%, relative to blood with undeformed and randomly orientated erythrocytes. Both Shankar, Webster, & Shao (1985) and Raaijmakers et al. (1997b) argued that this is an overestimation of the so-called resistivity effect, since in-vivo it is questionable whether a state of complete deorientation exists before the onset of blood flow. The magnitude of the resistivity change due to pulsatile blood flow, they found, was about 5%. More recently Kornet et al. (1999) found, in in-vivo experiments in pigs, that no sudden decrease in blood resistivity occurred in the aorta at the onset of blood flow, probably because most erythrocytes remain deaggregated, orientated and deformed throughout the heart cycle. In our study we used a constant value of ρ = 135 (Ωcm) for the resistivity of blood, although (2.3) remains valid if this resistivity is assumed to be time-dependent. This value of the resistivity of blood was not selected to achieve a match between the two sets of measurements a posteriori, but the rationale of this choice was that in-vivo a mean resistivity decrease of approximately 10% can be expected for flowing blood compared with blood at rest, see for example Wang & Patterson (1995). Since for male subjects generally a value of 150 (Ωcm) for the resistivity of blood at rest is assumed, a 10% decrease would result in a value of 135 (Ωcm) for the resistivity of flowing blood in male subjects. More research is needed, however, to determine the magnitude of the contribution of the resistivity effect.

Conclusion

To obtain the relevant information contained by the thoracic EI signal, the different sources have to be separated in time and location on the thorax. To do so, we designed a method, based on a very simple model of the thorax, that calculates volume changes from thoracic EI measurements. To test this method we compared the EI results to MRI measurements of volume changes of the aorta, the vena cava, the carotid arteries and the heart. The basis of our reasoning is that if our method is incorrect, the EI results and the MRI results will not be similar. The results presented in this study show that the volume changes obtained from the EI measurements and the MRI measurements are very similar both as a function of time in the cardiac cycle and as a function of location on the thorax. Consequently, although the assumptions underlying this

method are quite simple, the measurement results show that, as a first order approximation, they seem to be justifiable and the method can not be rejected as being incorrect. Therefore, we conclude that thoracic EI measurements using a linear electrode-array may provide a non-invasive method to obtain images of the cross-sectional surface area changes of thoracic organs during the heart cycle. With such a method the effects of the multiple sources on the EI waveform may be separated both in time and in location on the thorax. Furthermore, regional measurements seem to allow aortic volume changes to be estimated accurately. This offers the possibility to obtain, in combination with model studies, a better understanding of the origins of the thoracic EI waveform.

Appendix

Specifications of the MRI method used for cine imaging:
The MRI scanner was a 1.5 Tesla Siemens 'Vision' whole body system (Siemens Medical Systems, Erlangen, Germany). A phased-array body coil was used as receiver. Image acquisition was prospectively triggered by the R wave of the ECG.
The pulse sequence was a 2-dimensional gradient-echo sequence:

Flip angle	30 deg
Echo time	4.8 ms
Temporal resolution	15 ms
Phase-encoding direction	anterior-posterior
Field of view	240 x 320 mm
Acquisition matrix	96 x 256 pixels
Acquisition pixelsize	2.5 x 1.25 mm
Slice thickness	6mm.

Chapter 3 Comparing Spot Electrode Arrangements for Electrical Impedance Cardiography

A.E. Hoetink; Th.J.C. Faes; E.H. Schuur†; R. Gorkink;
H.G. Goovaerts; J.H. Meijer; R.M. Heethaar

Physiological Measurement, 23 (2002), pp. 457-467

Summary

This study investigates whether an arrangement with 9 spot electrodes, for thoracic electrical impedance cardiography, can be replaced by an arrangement with 5 spot electrodes. The study was conducted on 15 healthy subjects, 6 females and 9 males, in supine rest. The variables obtained from the measurements were the mean of the impedance of the thorax segment between the recording electrodes, the maximum negative deflection of the first derivative of the thoracic impedance, the left ventricular ejection time and an estimate of stroke volume. An analysis of variance for a Randomized Complete Block Design was used to determine whether significant differences exist in the group means of the observed variables between 6 different electrode arrangements. If no statistically significant differences were found in these group means between pairs of arrangements, Bland-and-Altman analyses were used to determine the differences in the observed variables between pairs of arrangements for individual subjects. This study concludes that reducing the number of spot electrodes from 9 to 5, does not yield significant differences in the group means of the observed variables, but it could result in large differences in the values of these variables for individual subjects.

Introduction

The thoracic electrical impedance (EI) signal contains useful information about the heart function and systemic blood circulation. To record this signal, electrodes must be applied onto the thorax. A wide range of different electrode arrangements have been proposed in the literature, for an overview of different arrangements the reader is referred to e.g. Sherwood et al. (1990) and Kauppinen, Hyttinen, & Malmivuo (1998). Woltjer et al. (1995) and Woltjer et al. (1996a) proposed an arrangement with 9 spot electrodes (5 current injecting electrodes and 4 voltage pickup electrodes) which yields similar results compared to an arrangement with band electrodes, introduced by Kubicek et al. (1966) and further evaluated by Patterson, Wang, & Raza (1991). Reducing the number of electrodes needed for this Woltjer-arrangement is more comfortable for the patient and more practical for medical personnel, especially in the Intensive Care Unit and after extensive surgery.

To determine whether different electrode arrangements, used for thoracic EI measurements, yield similar results, generally an analysis of variance is used to determine whether statistically significant differences exist between the group means of the measured variables. However, if the group means do not differ significantly, there still may be large differences between the obtained variables for individual subjects. Therefore, apart from an analysis of variance, an analysis as proposed by Bland and Altman, cf. Bland & Altman (1986), should be used to determine the differences between the observed variables for individual subjects.

The aim of this study is to investigate whether a 9 spot electrode arrangement, proposed by Woltjer et al. (1996a), can be replaced by an arrangement with 5 spot electrodes, by determining whether statistically significant differences exist between group means of the observed variables and by assessment of the differences in observed variables for individual subjects.

Methods

The study was conducted on 15 healthy subjects, 6 females and 9 males, in supine rest. Six tetra-polar electrode (Nutrode-P20M0) arrangements were used to obtain the thoracic EI signal (see figure 1). All arrangements place the upper current injecting spot electrode on the forehead. The lower current injecting electrodes are placed at least 15 cm below the lower voltage pickup electrodes. Arrangement A places the upper voltage pickup electrodes in the neck, at least 5 cm above the clavicle. All other arrangements place the upper voltage pickup electrodes as close as possible to the clavicles at the lateral aspect of the base of the neck. The lower voltage pickup electrodes are placed at the crossing of the transverse plane at the xiphoid process and the mid-axillary line. The arrangements were specifically chosen for the following reasons:

- Arrangement A was proposed by Raaijmakers et al. (1998) and is a modification of the Woltjer arrangement. It has been used until recently in our laboratory.
- Arrangement B is the arrangement advocated by Woltjer et al. (1996a),
- Arrangements C and F differ from arrangement B only in the number of the current injecting electrodes. Thus, comparing arrangement C and arrangement B, and comparing arrangement F and arrangement B will indicate whether the lower current injecting electrodes can be reduced from four to two,
- Arrangement D differs from arrangement C in the number of voltage pickup electrodes, while the current injecting electrodes are the same. Likewise, arrangement E differs from arrangement F only in the number of voltage pickup electrodes, but now the voltage pickup and current injecting electrodes are located at the right-hand side of the thorax. Consequently, comparing arrangement D and arrangement B, and comparing arrangement E and arrangement B will indicate whether the 9 spot electrode Woltjer-arrangement can be replaced by an arrangement with 5 spot electrodes.

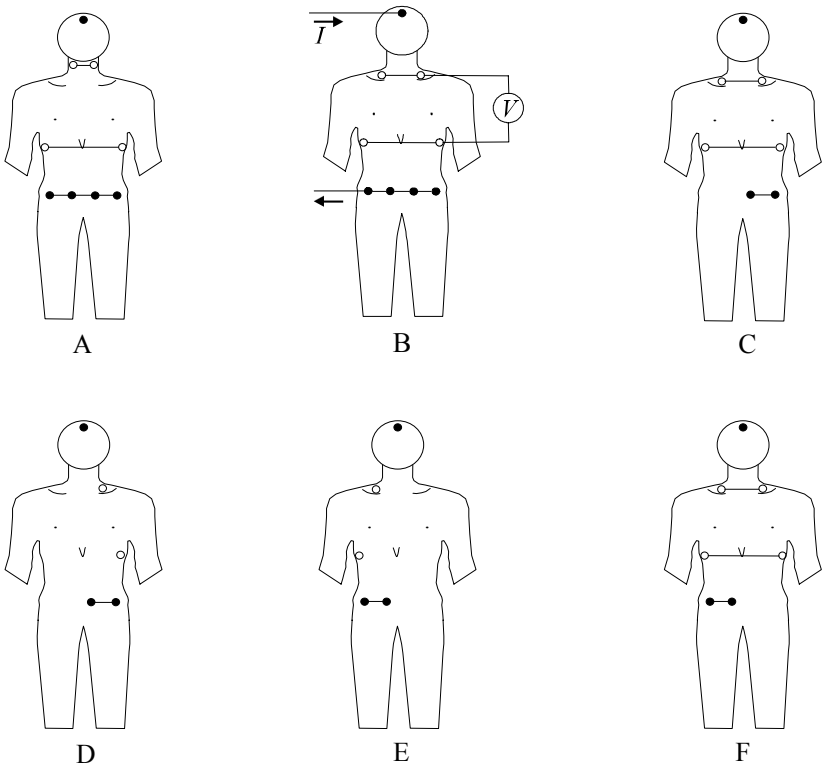

Figure 1. Investigated electrode arrangements: the open circles denote the voltage pickup spot electrodes and the black dots the current injecting spot electrodes.

The data were collected in supine rest, during two minutes, using the Hemologic® Hemodynamograph model HL-4 at a frequency of the injected current of 64 kHz. The signals were recorded using a sample frequency of 500 Hz. These recordings were subsampled, resulting in a sample frequency of 100 Hz. The electrode arrangements were measured in order of increasing arrangement number (see figure 1). The variables obtained from the EI signal were:

Z_0 mean of the measured impedance between the voltage pickup electrodes (Ω),

dZ/dt_{min} peak value of negative deflection of the first derivative of the measured impedance between the voltage pickup electrodes (Ω/s),

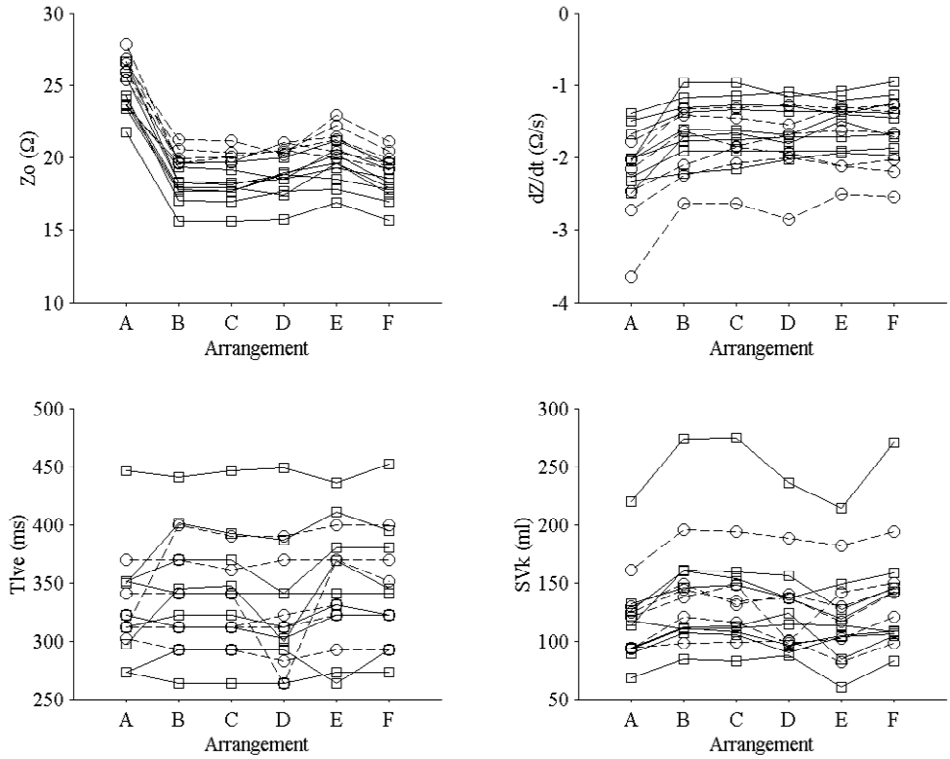

Figure 2. For each individual subject the observed values for Z_0, dZ/dt_{min}, T_{LVE} and calculated SV_K are given for each electrode arrangement (- -O- - = female; –□– = male).

T_{LVE} left ventricular ejection time (s), i.e. the time interval between B-point and X-point in the dZ/dt_{min} signal, e.g. Kubicek et al (1966), Lababidi et al (1970).

The signals were ensemble averaged with reference to dZ/dt_{min} (at least 30 heart beats) to remove the affects of respiration, e.g. Kim, Song, & Lee (1992). To determine the influence of variations of the observed variables on a stroke volume estimator, the estimator proposed by Kubicek et al. (1966) was used:

$$SV_K = -\frac{\rho l_e^2}{Z_0^2}\left(\frac{dZ}{dt}\right)_{\min} T_{LVE} \qquad (3.1)$$

Where SV_K (ml) is the stroke volume, ρ is the resistivity of blood (and taken as 135 Ωcm) and l_e (cm) is the distance between the voltage pickup electrodes.

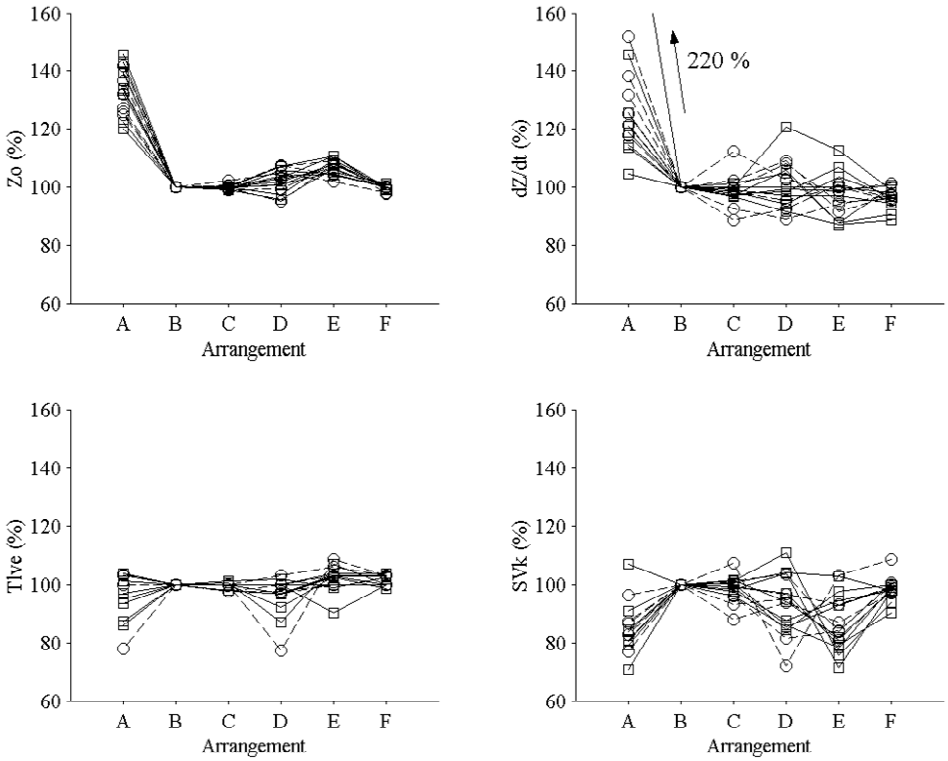

Figure 3. For each individual subject the observed values for Z_0, dZ/dt_{min}, T_{LVE} and calculated SV_K are given for each electrode arrangement expressed as a percentage of the values of arrangement B (- -O- - = female; –□– = male).

The values of Z_0, dZ/dt_{min}, T_{LVE} and SV_K, using the different arrangements, were compared. To this end an analysis of variance for a Randomized Complete Block Design was used, see Montgomery (1997). The electrode arrangements were considered to be the different treatments (fixed factors) and the blocks represented the different subjects (random factors). Only main effects were considered. The Tukey procedure for Post Hoc testing was used to determine whether statistically significant differences (type I error: α = 0.01) exist in the group means of the observed variables between various pairs of arrangements. If no statistically significant differences were found in the group means of these variables between certain pairs of arrangements, a Bland-and-Altman analysis was used to determine the differences for individual subjects between the variables.

Results

Figure 2 shows the observed values of Z_0, dZ/dt_{min}, T_{LVE} and SV_K in all subjects against electrode arrangement. The circles and broken lines represent the results of the female subjects and the squares and full lines represent the data of the male subjects. Figure 3 presents the same data, but now the values of Z_0, dZ/dt_{min}, T_{LVE} and SV_K are expressed as percentages of their values for arrangement B. From figure 2 it is clear that females differ from males only in the somewhat higher value of Z_0, due to the generally smaller cross-sectional area of the female thorax and possibly somewhat higher percentage of fat tissue. Figure 3, however, shows no differences between females and males, when the results of the different electrode arrangements are expressed as percentages of their values obtained with arrangement B. Therefore, the means and standard deviations presented in this study were calculated over all subjects. Table 1 gives the mean $\pm$ standard deviation of the observed values over all subjects for each arrangement. Table 2 summarizes the results of the post hoc Tukey-test for the different group means of Z_0, dZ/dt_{min}, T_{LVE} and SV_K, respectively. The first column gives the arrangements that were compared. Columns two, three, four and five present the differences between the values of the group means of these variables for the compared arrangements, respectively. For example, the estimated value of the group mean of Z_0 for arrangement A is 6.2 Ω higher than the estimated value of the group mean of Z_0 for arrangement B. Note that the value of the group mean of dZ/dt_{min} for arrangement A is 0.47 Ω/s more negative than the value of the group mean of dZ/dt_{min} for arrangement B (see figure 2) and therefore, for dZ/dt_{min} a negative difference in group means should be interpreted as a positive difference in absolute values of these group means.

Arrangement A yields significantly different results compared with all other arrangements for the values of the group means of Z_0, dZ/dt_{min} and SV_K, but not for the value of the group mean of T_{LVE}. Comparing arrangements E and B shows that significant differences exist between the values of the group means of Z_0 and SV_K. Comparing arrangements C-B, D-B, and F-B, no significant differences are found in the values of the group means of Z_0,

Table 1. Mean ± standard deviation over all subjects of the variables for each electrode arrangement.

El. Arr.	Z_0 (Ω)	dZ/dt_{min} (Ωs^{-1})	T_{LVE} (ms)	SV_K (ml)
A	25.0 ± 1.7	-2.17 ± 0.55	329 ± 43	118 ± 36
B	18.8 ± 1.5	-1.69 ± 0.46	341 ± 48	141 ± 47
C	18.8 ± 1.5	-1.67 ± 0.44	340 ± 47	138 ± 47
D	19.2 ± 1.5	-1.69 ± 0.44	328 ± 52	129 ± 41
E	20.1 ± 1.6	-1.63 ± 0.40	347 ± 50	122 ± 39
F	18.7 ± 1.4	-1.63 ± 0.43	345 ± 48	138 ± 47

dZ/dt_{min}, T_{LVE} and SV_K. Therefore, these results indicate that reducing the lower current injecting electrodes from 4 to 2 (compare arrangements C-B, and F-B), and reducing the lower current injecting and voltage pickup electrodes from 4 to 2 (compare arrangements D-B), do not yield statistically significant differences in *group* means of the values of Z_0, dZ/dt_{min}, T_{LVE} and SV_K.

For a comparison of these arrangements for individual subjects, Bland-and-Altman analyses were used to determine the differences in Z_0, dZ/dt_{min}, T_{LVE} and SV_K, say ΔZ_0, $\Delta dZ/dt_{min}$, ΔT_{LVE} and ΔSV_K. Figures 4, 5 and 6 present for arrangements C-B, F-B and D-B, ΔZ_0, $\Delta dZ/dt_{min}$, ΔT_{LVE} and ΔSV_K plotted against the mean for each subject, respectively. Again the circles represent the results for the female subjects and the squares for the male subjects. A full line denotes the mean of the differences, and the upper and lower limits of agreement (mean difference ± 2 x standard deviation) are given by the broken lines, respectively. Thus, 95% of all observed differences in the variables between a certain pair of arrangements are expected to lie between the upper and lower limits of agreement. Table 3 gives the means and standard deviations of ΔZ_0, $\Delta dZ/dt_{min}$, ΔT_{LVE} and ΔSV_K between the considered pairs of arrangements. The numbers in brackets give the variances of ΔZ_0, $\Delta dZ/dt_{min}$, ΔT_{LVE} and ΔSV_K, for the considered pairs of arrangements, as a percentage of the variances of Z_0, dZ/dt_{min}, T_{LVE} and SV_K obtained with arrangement B (see

Table 2. Post Hoc Tukey-test for pair wise comparisons of arrangements. Presented are the differences between arrangements in group means of the variables.

El. Arr.	ΔZ_0 (Ω)	$\Delta dZ/dt_{min}$ (Ωs^{-1})	ΔT_{LVE} (ms)	ΔSV_K (ml)	Bland & Altman analysis required?
A-B	**6.2***	**-0.47***	-12	**-22***	No
C-B	0.0	0.03	-1.4	-2.1	Yes
F-B	0.1	0.06	4.2	-2.3	Yes
D-B	0.4	0.00	-12	-11	Yes
E-B	**1.3***	0.06	6.5	**-19***	No

* = significant.

table 1), respectively. For example, the variance of ΔZ_0, when arrangements C and B are compared, is 1.8 % of the variance of Z_0, when arrangement B is used on all subjects.

Discussion

The limitation of the number of electrodes in EI cardiography is important for patients in critical situations where many parameters are monitored. Therefore, we compared in 6 electrode arrangements, the basic determinants for a stroke volume estimator found in the literature: Z_0, dZ/dt_{min} and T_{LVE}. As an example the Kubicek estimator was included, which is known, see e.g. Faes et al. (1999a) and Yamakoshi, Togawa, & Ito (1977), to overestimate stroke volume, hence the relatively large stroke volume values presented in this study.

The results show no significant differences between the values of the group means of T_{LVE} for all arrangements. Placing the voltage pickup electrodes in the neck (arrangement A), yields significant differences in the values of the group means of Z_0, dZ/dt_{min} and SV_K, compared with all other arrangements. The higher value of the group mean of Z_0, for arrangement A, is the result of the contibution of the neck, which can be represented as a cylindrical conductor with relatively small radius in series with the thorax, as was shown by Raaijmakers et al. (1997a). Furthermore, the value of the group mean of

Table 3. Mean ± standard deviation of the (within subject) differences in the variables for the different arrangements. The numbers in the brackets are the normalized variances, see text for a discussion.

El. Arr.	ΔZ_0 (Ω)	$\Delta dZ/dt_{min}$ (Ωs^{-1})	ΔT_{LVE} (ms)	ΔSV_K (ml)
F-B	0.1 ± 0.2 (1.8 %)	0.06 ± 0.07 (2.3%)	4.3 ± 5.8 (1.5%)	-2.2 ± 5.5 (1.4 %)
C-B	0.0 ± 0.2 (1.8%)	0.03 ± 0.10 (4.7%)	-1.4 ± 4.3 (0.8%)	-2.1 ± 6.2 (1.7 %)
D-B	0.4 ± 0.8 (28%)	± 0.13 (8.0%)	-12 ± 23 (23 %)	-11 ± 15 (10 %)

dZ/dt_{min}, for arrangement A, is somewhat more negative than those for all other arrangements (representing a larger amplitude), due to the contribution of the carotid arteries in the neck, see Patterson et al. (1990). However, the value of the group mean of SV_K, for arrangement A, is much smaller than those for the other arrangements. This can be understood by considering the Kubicek equation, where SV_K is a linear funtion of dZ/dt_{min}, but is not a linear function of Z_0.

The Kubicek stroke volume estimator is based upon the assumption of homogenous parallel cylinders. Hence, if the upper voltage pickup electrodes are located in the neck, the validity of this model is questionable. Therefore, the upper voltage pickup electrodes should not be located in the neck. Woltjer et al. [cf. Woltjer et al. (1996b)] showed that stroke volume values obtained with arrangement B correlate well (r = 0.9) with thermodilution stroke volume values. Since, to our knowledge, arrangements C, D and F have not yet been compared to any reference method, arrangement B will serve as a reference for comparison with the other arrangements.

The results show that reducing the number of lower current injecting spot electrodes from 4 to 2 (arrangements C and F) does not give significant differences in the values of the *group* means of Z_0, dZ/dt_{min}, T_{LVE} and SV_K. Likewise, reducing both the lower current injecting and the voltage pickup spot electrodes from 4 to 2 electrodes (arrangement D) does not give significant differences in the values of the *group* means of Z_0, dZ/dt_{min}, T_{LVE} and SV_K,

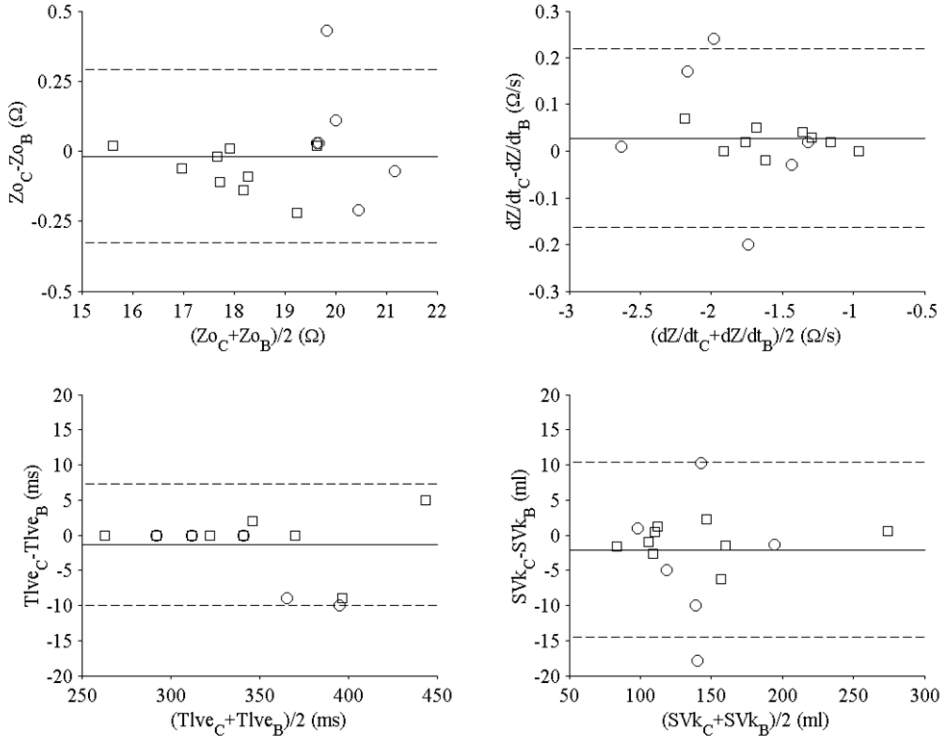

Figure 4. Bland-and-Altman plots of comparison of arrangements C and B for Z_0 (top left), dZ/dt_{min} (top right), T_{LVE} (bottom left) and SV_K (bottom right). The broken lines denote the limits of agreement and the full line the mean of the differences (O = female; □ = male).

provided that the electrodes are placed on the left-hand side of the thorax. Therefore, Bland-and-Altman analyses will have to indicate the magnitude of the differences between these arrangements for individual subjects. If, on the other hand, the reduced number of current injecting and voltage pickup electrodes are located at the right-hand side of the thorax (arrangement E), significant differences are found in the values of the group means of Z_0 and SV_K and further analysis is not necessary. The significant difference found in the value of the group mean of SV_K for arrangement E is the result of the larger observed values of Z_0 (see figures 2 and 3). Possibly the fact that the heart is located at the left-hand side of the thorax results in significantly higher values of Z_0 measured on the right-hand side of the thorax, due to the somewhat larger lung volume on that side.

Bland-and-Altman analyses to compare the differences between arrangements in the values of Z_0, dZ/dt_{min}, T_{LVE} and SV_K for individual subjects shows that the means of ΔZ_0, $\Delta dZ/dt_{min}$, ΔT_{LVE} and ΔSV_K are relatively small

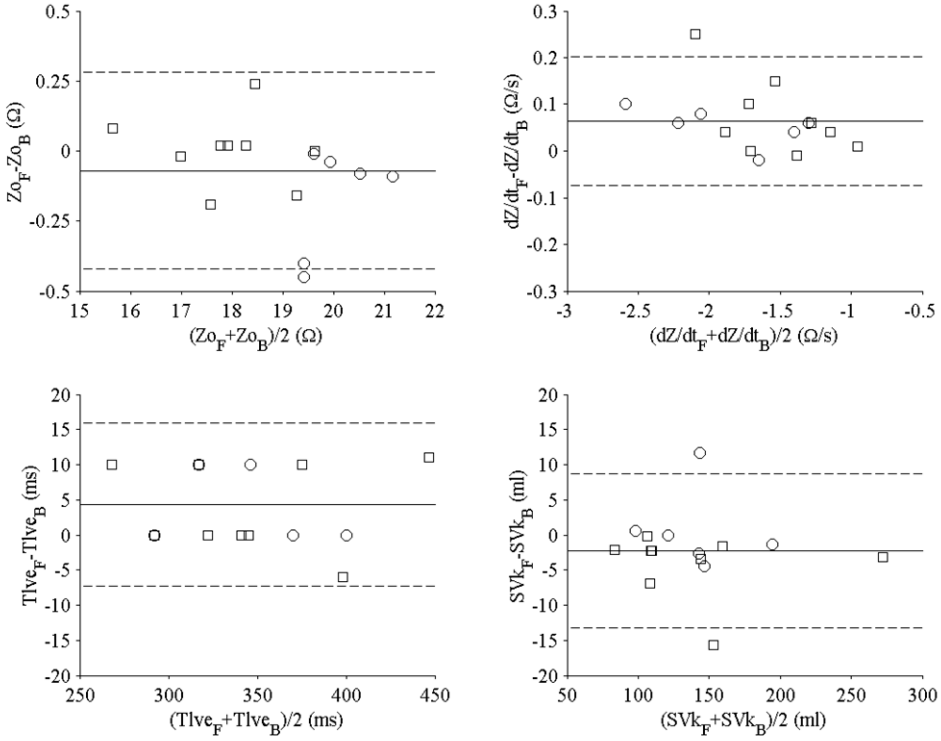

Figure 5. Bland-and-Altman plots of comparison of arrangements F and B for Z_0 (top left), dZ/dt_{min} (top right), T_{LVE} (bottom left) and SV_K (bottom right). The broken lines denote the limits of agreement and the full line the mean of the differences (O = female; □ = male).

compared to the standard deviations of these differences (see Table 3). Therefore, when group means were compared, no statistically significant differences were found when comparing arrangement C, D and F with arrangement B, although for arrangement D large differences were found in the values of Z_0, dZ/dt_{min}, T_{LVE} and SV_K for individual subjects, see figure 6. The differences in the values of SV_K for individual subjects, between arrangement D and B, can be as large as –40 ml. The differences in SV_K between arrangements C-B (see figure 4) and F-B (see figure 5) are relatively small and range roughly from –15 ml to 10 ml. To be able to compare the variances of ΔZ_0, $\Delta dZ/dt_{min}$, ΔT_{LVE} and ΔSV_K among each other, these variances are normalized to the variance obtained when arrangement B is used on all subjects. For example, the variance of ΔZ_0 is expressed as a percentage of the variance of Z_0 when arrangement B is used on all subjects. Likewise, the variances in $\Delta dZ/dt_{min}$, ΔT_{LVE} and ΔSV_K are normalized to the variances of dZ/dt_{min}, T_{LVE} and SV_K for arrangement B. These normalized variances are

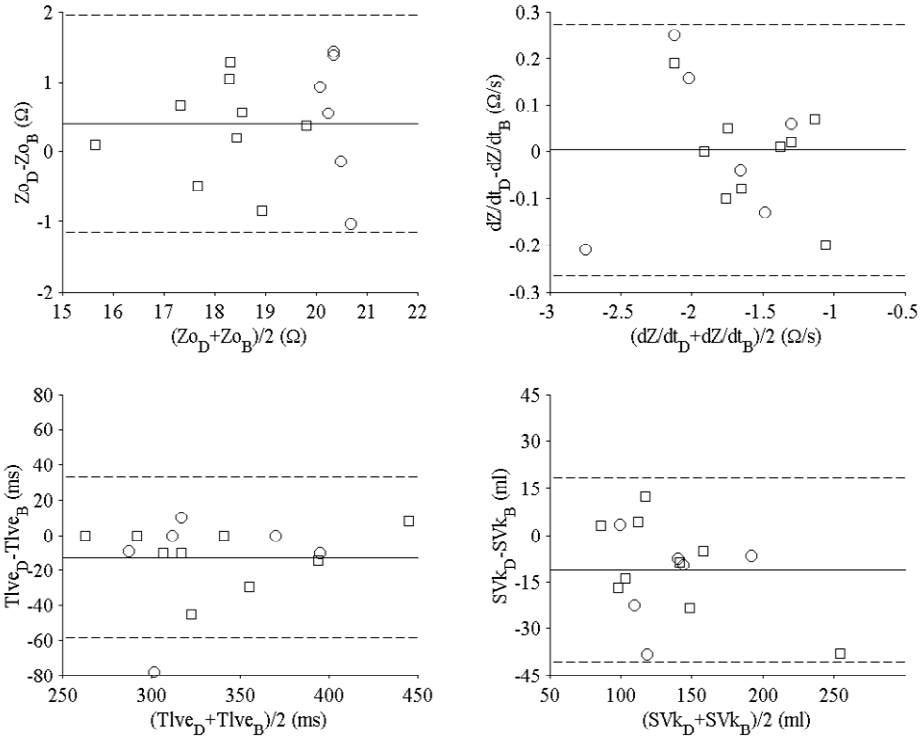

Figure 6. Bland-and-Altman plots of comparison of arrangements D and B for Z0 (top left), dZ/dtmin (top right), TLVE (bottom left) and SVK (bottom right). The broken lines denote the limits of agreement and the full line the mean of the differences (O = female; □ = male).

given in brackets in Table 3 and express the variance due to using different arrangements as a percentage of the variance due to differences between individuals when arrangement B is used.

From Table 3, it can be seen that the following holds. Reducing the number of current injecting electrodes from 4 to 2 (compare arrangements C-B and F-B), results in small normalized variances for ΔZ_0 (1.8 %). For $\Delta dZ/dt_{min}$, the normalized variance of C-B (4.7 %) is twice the normalized variance obtained when comparing arrangements F-B (2.3 %). For ΔT_{LVE}, on the other hand, the normalized variance of F-B (1.5 %) is about twice that of C-B (0.8 %). The normalized variance of ΔSV_K for C-B (1.7 %) is almost the same as that of F-B (1.4 %). If we now compare the values of the normalized variances of ΔZ_0, $\Delta dZ/dt_{min}$ and ΔT_{LVE} for D-B (reduction of both voltage pickup - and lower current injecting electrodes), to those obtained for C-B and F-B, we find that these values are much larger, ranging from 8.0 % for $\Delta dZ/dt_{min}$ to 28 % for ΔZ_0. The resulting normalized variance of ΔSV_K (10 %) is about six times that of

arrangements C-B (1.7 %). The main contributors are the increased normalized variances of ΔZ_0 and ΔT_{LVE}. However, some form of compensation occurs, since the normalized variance of ΔSV_K is only about one half the normalized variances of ΔZ_0 and ΔT_{LVE}. In other words, ΔZ_0, $\Delta dZ/dt_{min}$ and ΔT_{LVE} are not independent variables. Apparently a smaller value of, for example, ΔZ_0 is compensated by smaller values of $\Delta dZ/dt_{min}$ and ΔT_{LVE}.

Kauppinen et al. [see Kauppinen, Hyttinen, & Malmivuo (1998)] compared different electrode arrangements, among others the band electrode arrangement devoloped by Kubicek et al. and the arrangement proposed by Woltjer et al. (1996a), using sensitivity distributions analyzed by a three-dimensional computer model. The authors compared the contribution of different thoracic organs and tissues to the mean impedance, Z_0, measured between the voltage pickup electrodes for the different electrode arrangements. Their results indicate that the 9 spot electrode arrangement has slightly different sensitivity properties than the band electrode arrangement, the first having larger contributions from the aorta, the vena cava, the carotid arteries and the jugular veins and a smaller contribution from the lungs. Where Kauppinen, Hyttinen, & Malmivuo (1998) did not specifically look at impedance changes, Wtorek (2000) conducted a similar study, but calculated the contribution of different thoracic organs to the total impedance change measured with the band electrode arrangement developed by Kubicek. In his work, Wtorek presents graphs that give the relative contribution of different thoracic organs to the measured impedance change under varying conditions. Careful inspection of these graphs learns that the volume change of the aorta is a major source (its relative contribution is about 80% or more) of the impedance signal. If, as Kauppinen, Hyttinen, & Malmivuo (1998) indicated, the 9 spot electrode arrangement is more sensitive to the contribution of the large vessels, then the contribution of the aorta to the measured impedance change possibly increases. The changes in measurement sensitivity, when the number of spot electrodes is reduced from 9 to 5 could be investigated by means of model studies using sensitivity distributions.

Conclusion

In answering the question whether a 9 spot-electrode arrangement (arrangement B) for the measurement of stroke volume can be replaced by a 5 spot-electrode arrangement (arrangement D), the following should be considered. The two arrangements under consideration are said to be equivalent if the stroke volume values obtained with these arrangements:

1. do not differ statistically significantly in their group means, and
2. yield small differences in obtained stroke volume values for individual subjects.

The results show that, when arrangement D is compared with arrangement B, the differences in group means of Z_0, dZ/dt_{min}, T_{LVE} and SV_K are not statistically significant. However, the results also show that the differences in Z_0, dZ/dt_{min}, T_{LVE} and SV_K between arrangements D and B for individual subjects can be considerable. Since 95% of all observed values are expected to fall between the limits of agreement, it can be expected that for approximately 47.5% of the subjects, the value of SV_K measured with arrangement D is between 11 ml to 41 ml lower than the value measured with arrangement B (see figure 6). Thus these arrangements are clearly not equivalent. Furthermore it can be concluded from this study, that the observed difference between arrangements D and B is mainly caused by the reduction of the number of voltage pickup electrodes from 4 to 2. All these conclusions, however, are based on results found in healthy subjects in supine rest and the question whether these findings remain valid in critically ill patients, especially patients with thoracic oedema, needs further investigation. When investigating such patients, additional or different sources may contribute to the signal, hence leading to larger differences between electrode arrangements.

Whether the 5 spot electrode arrangement yields better results in estimating stroke volume than the 9 spot electrode arrangement, can not be decided from this study, alone. To answer this question, the stroke volume estimations, using these arrangements, should be compared, in one way or

another, to stroke volume values obtained with a reference method, e.g. MRI or thermo-dilution. Possibly, such a study should include changes in subject position (for example from supine to sitting), since this causes changes in cardiac output and organ position, which may result in significant differences between different electrode arrangements. The subjects could also be asked to perform an exercise, which would result in changes in only the cardiac output.

Chapter 4 On the Flow-dependency of the Electrical Conductivity of Blood

A.E. Hoetink; Th.J.C. Faes; K.R. Visser; R.M. Heethaar

IEEE Transactions on Biomedical Engineering (in press)

Summary

Experiments presented in the literature show that the electrical conductivity of flowing blood depends on flow velocity. The aim of this study is to extend the Maxwell-Fricke theory, developed for a dilute suspension of ellipsoidal particles in an electrolyte, to explain this flow-dependency of the conductivity of blood for stationary laminar flow in a rigid cylindrical tube. Furthermore, these theoretical results are compared to earlier published measurement results. To develop the theory, we assumed that blood is a Newtonian-fluid and that red blood cells can be represented by oblate ellipsoids. If blood flows through a cylindrical tube, shear stresses will deform and align the red blood cells with one of their long axes aligned parallel to the stream-lines. The pathway of a low frequency (< 1 Mhz) alternating electrical current will be altered by this orientation and deformation of the red blood cells. Consequently, the electrical conductivity in the flow direction of blood increases. The theoretically predicted flow-dependency of the conductivity of blood corresponds well with experimental results. This theoretical study shows that red blood cell orientation and deformation can explain quantitatively the flow-dependency of blood conductivity.

Introduction

The change of the electrical conductivity of blood due to flow, has been examined in many studies, e.g. Sigman et al. (1937);Coulter & Pappenheimer (1949); Edgerton (1974); Frewer (1974); Dellimore & Gosling (1975); Visser et al. (1976); Sakamoto & Kanai (1979); Shankar, Webster, & Shao (1985); Ninomiya et al. (1988); Visser (1989); Visser (1992) and Fujii et al. (1999). For stagnant blood, the electrical conductivity depends on the volume fraction (the hematocrit) of red blood cells and the conductivity of plasma which is dependent on e.g. the temperature, osmolarity, ionic content, etc. The electrical conductivity of flowing blood, however, also depends on the flow velocity of blood. As early as 1937, it was observed Sigman et al. (1937) that the conductivity of flowing blood, measured longitudinally to the flow direction, increases in comparison to the conductivity of stagnant blood. This effect was confirmed experimentally in other studies: Edgerton (1974); Frewer (1974); Dellimore & Gosling (1975); Visser et al. (1976); Sakamoto & Kanai (1979); Shankar, Webster, & Shao (1985); Ninomiya et al. (1988); Visser (1989); Visser (1992) and Fujii et al. (1999). Several explanations have been proposed for this conductivity increase: Sigman et al. (1937); Frewer (1974) and more recently Fujii et al. (1999), pointed out that deformation of RBCs is an important cause, whereas others focused on the orientation of the non-spherical RBCs Edgerton (1974); Dellimore & Gosling (1975); Visser et al. (1976); Sakamoto & Kanai (1979); Shankar, Webster, & Shao (1985); Ninomiya et al. (1988); Visser (1989) and Visser (1992). These ideas were only elaborated into a quantitative theory for Couette flow, see Edgerton (1974). For a stationary and laminar flow in a rigid cylindrical tube (Poiseuille flow), Visser (1992) presented an empirical function that was fitted to experimentally measured results.

The aim of this study is to develop and test a quantitative theory to explain the flow-dependency of the conductivity of blood in Poiseuille flow. Since for low frequency (< 1 Mhz) alternating currents the conductivity of RBCs is generally considered to be much lower than the conductivity of plasma, the disintegration of rouleaux (chains of RBCs) at very low flow velocities as well as the orientation and deformation of RBCs results in a change of the current

pathway in the plasma, and consequently in a change of the conductivity. Therefore, we hypothesize that both orientation and deformation of RBCs contribute to the flow-dependency of the conductivity of blood.

To develop the theory, we first employ the Maxwell-Fricke equation to determine the conductivity of a suspension of RBCs in a low frequency alternating electrical field. Secondly, the deformation of RBCs in shear flow is related to the resulting shear stress in the fluid. Thirdly, the shear stress profile in blood, in Poiseuille flow, is related to the rate of blood-flow in the tube. In addition, a relation between shear stress and experimentally measured reduced average velocity is presented. Finally, the theoretical results are combined and compared to experimental results published earlier in Visser (1992).

Theory

To determine the conductivity of a suspension of RBCs in a low frequency (< 1 Mhz) alternating electrical field we use the theory originally developed in Maxwell (1954) for a dilute suspension of spherical particles and extended in Fricke (1924), for application to a dilute suspension of ellipsoidal particles. Apart from assuming that blood is a dilute suspension, it is assumed that the RBC's are ordered in a cubic arrangement. Fricke states that it seems difficult theoretically to decide whether these assumptions are adequate to describe the case of a random distribution of the suspended particles. That they are adequate, he argues, is supported by the fact that there is usually a very close agreement between theoretical results and experimental results, see e.g. Fricke (1924); Edgerton (1974); Visser (1992) and many others. Like Fricke, to develop our theory, we consider the RBCs and surrounding plasma to form a regular grid of control volumes with small dimensions compared to the dimensions of the tube. One control volume consists of a RBC in the center that is surrounded by plasma. A blood-filled tube can now be considered to consist of a large number of control volumes. Additionally, it is assumed that the hematocrit has the same value at any location in the tube. That is, the slight shear rate induced accumulation of RBCs at the tube axis is considered to be negligible. This assumption is supported by calculations, presented in

Sakamoto & Kanai (1979), showing that this effect is negligible when the tube diameter is larger than 1 mm.

The Maxwell-Fricke Equation

Consider blood to be a suspension of homogeneous ellipsoidal particles with one symmetry axis of length 2*a* and two axes of equal length 2*b* (*a* < *b*). Furthermore, assuming that the conductivity of the RBC is negligible compared to the plasma conductivity, the Maxwell-Fricke equation [see Fricke (1924)] for the conductivity of one control volume reads

$$\frac{\sigma_c}{\sigma_p} = \frac{1-H}{1+(C-1)H} \tag{4.1}$$

where σ_c and σ_p are the conductivities of the control volume and the plasma, respectively, H is the hematocrit expressed as the volume fraction of RBCs relative to the total blood volume and C is a factor that depends on the geometry and orientation of the RBC, i.e.

$$C_a = \frac{1}{M} \tag{4.2}$$

$$C_b = \frac{2}{2-M} \tag{4.3}$$

Where C_a and C_b are the values of C with either the *a*-axis or *b*-axes parallel to the electrical field, respectively. Additionally, M is given for RBCs in the shape of oblate ellipsoids (*a* < *b*) by

$$M(a<b) = \frac{\varphi - \frac{1}{2}\sin(2\varphi)}{\sin^3(\varphi)}\cos(\varphi) \tag{4.4}$$

where

$$\cos(\varphi) = \frac{a}{b} \tag{4.5}$$

In case of random orientation a value of $C = C_r$ is proposed in Fricke (1924), corresponding to taking the mean of the values when a RBC is aligned with the *a*-axis parallel or with the two *b*-axes parallel to the electrical field. That is

$$C_r = \frac{1}{3}\left(C_a + 2C_b\right) \tag{4.6}$$

Equations (4.1)-(4.6) give the dependence of the electrical conductivity of blood on hematocrit, orientation and deformation according to the Maxwell-Fricke theory. Orientation effects may be studied by comparing the results of (4.1) with $C = C_r$ to the results of (4.1) with $C = C_a$ or $C = C_b$, whereas deformation effects may be studied by changing the short-to-long axis ratio a/b in (4.5).

Red Blood Cell Deformation

A full treatment of the theory of deformation of membranes is beyond the scope of this text. Here only some main results will be mentioned, partly based on Evans & Skalak (1979a) and Evans & Skalak (1979b). Although RBCs are generally considered to be shaped like biconcave disks, this is only true for situations where no external forces work on the membrane surface. For the purpose of describing the mechanical characteristics of RBCs in blood flow, the RBCs are considered to be ellipsoids with one symmetry-axis of length *a* and two axes of length *b* ($a < b$). The cell membrane encloses the internal fluid of the cell, which is assumed to be a Newtonian fluid. Also, the fluid pressure within the cell equals the fluid pressure outside the cell.

Consider a RBC located at tube-coordinates (r, α, z) with initial axis lengths a_0 and b_0. Due to the flow induced shear stress profile, the RBC membrane supports the shear stress $\tau(r)$ existing at distance r from the tube axis. As a result, the RBC will be deformed with new axis lengths a_d and b_d. According to Skalak, Keller, & Secomb (1981), for most situations of in-vivo

blood flow, it is an accurate approximation to regard the RBC membrane as having a constant surface area and constant enclosed volume, but allowing very large extensions of the RBC. Using the property of constant enclosed volume, together with the equation of the volume of an ellipsoid, we can write

$$\frac{4\pi}{3} a_d b_d^2 = \frac{4\pi}{3} a_0 b_0^2 \tag{4.7}$$

Furthermore, defining

$$a_d \equiv a_0 + \Delta a = a_0 \left(1 + \frac{\Delta a}{a_0} \right) \tag{4.8}$$

and

$$b_d \equiv b_0 + \Delta b = b_0 \left(1 + \frac{\Delta b}{b_0} \right) \tag{4.9}$$

and inserting (4.8) and (4.9) into (4.7) we can write

$$\left(a_0 + \Delta a \right) \left(b_0 + \Delta b \right)^2 = a_0 b_0^2 \tag{4.10}$$

Solving this algebraic equation, Δa can be written as a function of a_0, b_0 and Δb as follows

$$\Delta a = -a_0 \cdot \frac{2\frac{\Delta b}{b_0} + \left(\frac{\Delta b}{b_0} \right)^2}{\left(1 + \frac{\Delta b}{b_0} \right)^2} \tag{4.11}$$

Inserting (4.11) into (4.8) results in

$$a_d = a_0 \left\{ 1 - \frac{2\frac{\Delta b}{b_0} + \left(\frac{\Delta b}{b_0}\right)^2}{\left(1 + \frac{\Delta b}{b_0}\right)^2} \right\} = a_0 \cdot \left(1 + \frac{\Delta b}{b_0}\right)^{-2} \tag{4.12}$$

Dividing (4.12) by (4.9) gives the short-to-long axis ratio after deformation (a_d/b_d) in terms of the short-to-long axis ratio before deformation (a_0/b_0), b_0 and Δb

$$\frac{a_d}{b_d} = \frac{a_0}{b_0} \cdot \left(1 + \frac{\Delta b}{b_0}\right)^{-3} \tag{4.13}$$

In order to obtain the strain $\varepsilon_b = \Delta b/b_0$, we will assume [partly based on Evans (1973)] that the relation between extension ratio λ_b in the direction of the b-axis and shear stress $\tau(r)$ for a RBC membrane with elastic behavior, can be written as

$$\left(\lambda_b^2 - \lambda_b^{-2}\right) = \frac{\tau(r) b_d}{\mu} \tag{4.14}$$

With $b_d = \lambda_b b_0$ we can write for (4.14)

$$\left(\lambda_b - \lambda_b^{-3}\right) = \frac{\tau(r) b_0}{\mu} \tag{4.15}$$

where μ is the membrane or surface shear modulus[6] and according to Evans (1973) has a value of the order of 10^{-5} Nm^{-1}. Using the relation between strain ε_b and extension ratio λ_b given by Evans (1973), we can write

$$\varepsilon_b = \frac{1}{2}\left(\lambda_d^2 - 1\right) \tag{4.16}$$

[6] According to Evans & Skalak (1979a) biological membranes are only continuous in the two dimensions of the surface and therefore the surface shear modulus has a unit of force per unit length.

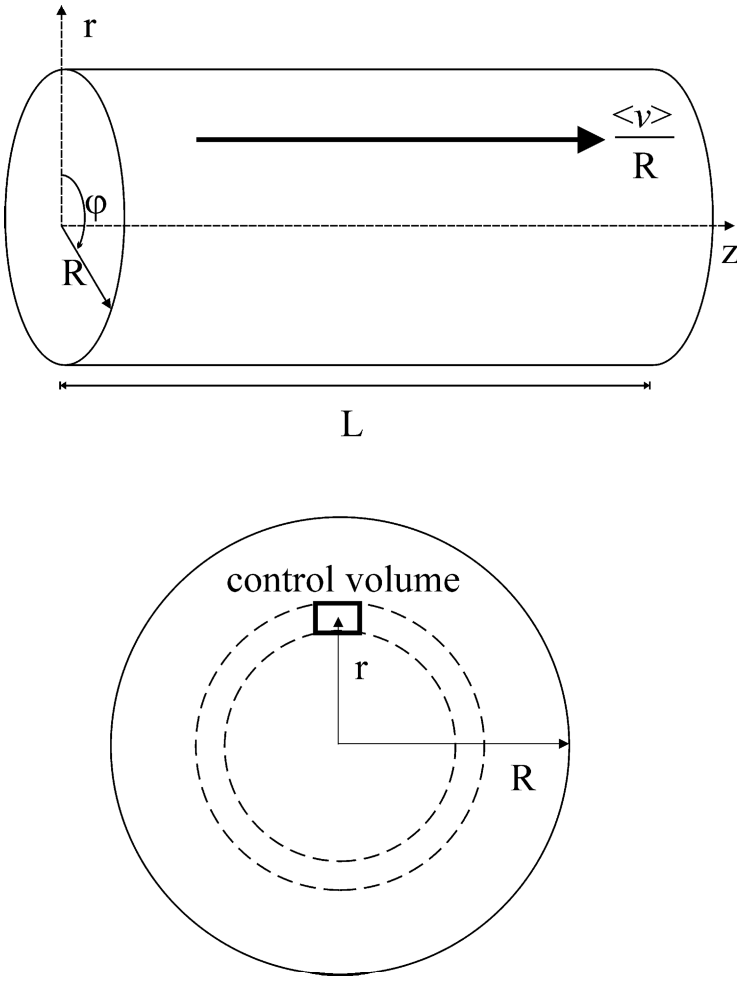

Figure 1. Blood-filled tube with radius *R* (top) and a cross-section with a control volume located at a distance *r* from the center (bottom).

Hence,

$$\lambda_b = (1 + 2\varepsilon_b)^{1/2} \approx 1 + \varepsilon_b \tag{4.17}$$

and

$$\lambda_b^{-3} = (1 + 2\varepsilon_b)^{-3/2} \approx 1 - 3\varepsilon_b \tag{4.18}$$

Where the approximations are due to binomial series expansion and hold for ε_b << 1.

After substitution of (4.17) and (4.18) into (4.15), the strain in the direction of the *b*-axis is found to be

$$\varepsilon_b = \frac{\Delta b}{b_0} = \frac{\tau(r) b_0}{4\mu} \tag{4.19}$$

Finally, inserting (4.19) into (4.13) gives the relation between shear stress, short-to-long axis ratio after deformation and this ratio before deformation

$$\frac{a_d(r)}{b_d(r)} = \frac{a_0}{b_0} \cdot \left(1 + \frac{\tau(r) b_0}{4\mu}\right)^{-3} \tag{4.20}$$

The notation of the short-to-long axis ratio on the left-hand side of (4.20) expresses the dependence on *r* (for a definition of *r* see figure 1) of both a_d and b_d. We will use this result to calculate the change of the axis ratio due to RBC deformation under shear stress.

Hemodynamics and Shear Stress

We will now briefly discuss a well-known result, e.g. Merrill (1969) or Bird, Steward, & Lightfoot (1966), for the shear stress profile of a fully developed stationary laminar flow of a viscous fluid in a horizontal rigid cylindrical tube under influence of a pressure difference across the tube. Let the physical dimensions of the tube be defined with the radius *R* and the length *L*. Define a cylindrical coordinate system *(r, α, z)* such that the origin of the coordinate system coincides with the center of the left side of the cylinder, see figure 1. In this coordinate system, the shear stress is independent of the *z*-coordinate because at a certain distance[7] from the tube entrance, the flow is stationary and laminar, and independent of α because of circle-symmetry. Hence, the shear stress τ is only dependent on *r*, i.e.

[7] for distances larger than 1 m for a tube with a radius of 4 mm, see Visser (1989)

$$\tau = \tau(r) \tag{4.21}$$

The external driving force of the fluid flow is a pressure difference ΔP across the length of the tube times the surface area perpendicular to the tube-axis *z*. It can be shown that the shear stress profile can be written as [see for example Merrill (1969) or Bird, Steward, & Lightfoot (1966)],

$$\tau(r) = -\frac{1}{2}\left(\frac{\Delta P}{L}\right) r = \frac{1}{2}\left|\frac{\Delta P}{L}\right| r \tag{4.22}$$

and

$$\tau_{\max} = \tau(R) = \frac{1}{2}\left|\frac{\Delta P}{L}\right| R \tag{4.23}$$

Having determined the shear stress profile, the velocity profile, say $v(r)$, of a fluid can be calculated using the relationship between shear stress and shear rate. For blood, we will use the relationship for a Newtonian-fluid, i.e.

$$\tau(r) = -\eta_{bl}\left(\frac{dv(r)}{dr}\right) \tag{4.24}$$

where η_{bl} is the dynamic viscosity coefficient of blood. Together with the boundary condition that the fluid velocity is zero at the tube wall, the result is the following velocity profile,

$$v(r) = \frac{1}{4\eta_{bl}}\left|\frac{\Delta P}{L}\right|\left(R^2 - r^2\right) \tag{4.25}$$

The shear stress and the velocity profile are not easy to measure. Therefore, these quantities will be obtained indirectly through the spatial average velocity, which (for an incompressible fluid) is the volume rate of flow divided by the cross-sectional surface area of the tube, see also Lih (1975).

Because of circle-symmetry, this definition of the spatial average velocity can be written as

$$\langle v \rangle = \frac{\int_0^R v(r) r dr}{\int_0^R r dr} \tag{4.26}$$

yielding with (4.25) for the spatial average velocity

$$\langle v \rangle = \frac{R^2}{8\eta_{bl}} \left| \frac{\Delta P}{L} \right| \tag{4.27}$$

Finally, the reduced average velocity is defined as the ratio of <*v*> to the tube radius *R*, i.e.

$$\frac{\langle v \rangle}{R} = \frac{R}{8\eta_{bl}} \left| \frac{\Delta P}{L} \right| = \frac{\tau_{\max}}{4\eta_{bl}} \tag{4.28}$$

To calculate the shear stress profile when average velocities or reduced average velocities have been measured experimentally, (4.22) and (4.23) are rewritten to give

$$\tau(r) = \frac{1}{2} \left| \frac{\Delta P}{L} \right| R \cdot \frac{r}{R} = \tau_{\max} \cdot \frac{r}{R} \tag{4.29}$$

Using (4.28) and (4.29), the shear stress profile can be written as

$$\tau(r) = 4\eta_{bl} \frac{\langle v \rangle}{R} \frac{r}{R} \tag{4.30}$$

in terms of blood viscosity and tube radius and experimentally measured reduced average velocity.

The Bulk Conductivity of Flowing Blood

Now that the shear stress profile has been related to the reduced average velocity an expression for the bulk conductivity of flowing blood can be deduced, which takes into account the orientation and deformation of the RBCs. The conductivity of a control volume depends on the magnitude of the shear stress at the location of the control volume. Because of circle-symmetry, this shear stress is a function of the radial distance only. Therefore, control volumes forming a ring at a certain radial distance r have equal conductivities, say $\sigma_c(r)$ (see figure 1). Assuming a rectangular geometry of a control volume, its conductance [say $Y_c(r)$] can be obtained with Ohms law, i.e.

$$Y_c(r) = \sigma_c(r) \cdot \frac{W_c H_c}{L_c} \tag{4.31}$$

Where W_c, H_c and L_c are the width, height and length of the control volume, respectively. Hence, the total conductance of such a ring at a radial distance r is simply the sum of the equal conductances of all control volumes in that ring, i.e.

$$Y_{ring}(r) = \sum_{n=1}^{N_c} Y_c(r) = N_c \cdot Y_c(r) \tag{4.32}$$

where N_c is the number of all control volumes in the ring. This number equals

$$N_c = \frac{2\pi r \Delta r}{W_c H_c} \tag{4.33}$$

where Δr is the thickness of the ring (i.e. the radial distance between the dashed circles in figure 2).
Thus using (4.31)-(4.33), the conductance of a ring can be written as

$$Y_{ring}(r) = \frac{2\pi}{L_c} \sigma_c(r) r \Delta r \tag{4.34}$$

The conductance of a cross-section with length L_c of a blood-filled tube is now simply the series summation of the conductances of all the rings in that cross-section, i.e.

$$Y_{CS} = \sum_{i=1}^{N_r} Y_{ring}(r_i) \tag{4.35}$$

where Y_{CS} is the conductance of the cross-section, N_r is the number of rings in the cross-section, i denotes the ith ring and r_i is the radial distance of the ith ring to the tube axis. Since the dimensions of the control volumes where considered to be small compared to the dimensions of the tube, the series summation can be replaced by an integration. Thus (4.34) together with (4.35) yields

$$Y_{CS} = \frac{2\pi}{L_c} \int_0^R \sigma_c(r) r dr \tag{4.36}$$

Since, with Ohm's law we can write

$$Y_{CS} = \frac{\pi R^2}{L_c} \sigma_{bl} \tag{4.37}$$

where σ_{bl} is the bulk conductivity of blood, it follows that

$$\sigma_{bl} = \frac{2}{R^2} \int_0^R \sigma_c(r) r dr \tag{4.38}$$

In summary, (4.38) relates the bulk conductivity of blood, σ_{bl}, to the r-dependent conductivity of the control volumes, $\sigma_c(r)$. The Maxwell-Fricke equations (4.1)-(4.6) relate the conductivity of these control volumes to hematocrit and geometry of the RBCs. The RBC deformation under shear stress in flowing blood can be calculated with (4.20) and (4.30). All these equations together, enable the theoretical studie of the conductivity of flowing blood.

In the following paragraphs we will derive expressions for $\sigma_c(r)$ for different ranges of the shear stress $\tau(r)$. First we will derive an expression for low values of the shear stress ($\tau(r)$ < 0.03 Nm^{-2}). Then we will derive an expression for fully aligned and deformed RBCs ($\tau(r)$ > 0.1 Nm^{-2}). Finally an expression for the transition region will be obtained.

According to Goldsmith (1999), for shear stresses $\tau(r)$ < 0.03 Nm^{-2}, RBCs are rotating with periodically varying angular velocity. At any moment in time, approximately 50% of the RBCs are found with their major axes (i.e. *b*-axes) within an angle of $\pm$ 20^{o} of the direction of flow. This fraction of RBCs is considered to be fully aligned with a *b*-axis in the flow direction. The remaining RBCs will have any other angle between the their major axes and the direction of flow. Therefore, these RBCs can be considered to have randomly distributed angles between their major axis and the direction of flow. Consequently, to account for this behavior we will assume that these RBCs have random orientation. Thus, the conductivity of a control volume for τ < 0.03 Nm^{-2} is given by

$$\sigma_{<} = \sigma_p \frac{1-H}{1+\{C_{<}-1\}H} \tag{4.39}$$

Analogously to the case of random orientation the constant $C_<$ is taken as the mean of the values of *C* for aligned and randomly oriented RBCs, that is

$$C_{<} = \frac{1}{2}\{C_b + C_r\} \tag{4.40}$$

where C_b and C_r are given by (4.3) and (4.6), respectively. Furthermore, it is assumed that in this regime the RBCs are not yet deformed. Therefore, the axis ratio of undeformed RBCs is used to determine the values of C_b and C_r

According to Goldsmith (1999), at shear stresses $\tau(r)$ > 0.1 Nm^{-2} RBCs progressively align themselves with the *b*-axis parallel to the flow direction without rotating. Additionally, they are deformed with an increase of length of the *b*-axis. At a certain value of the shear stress, say $\tau(r_2)$ > 0.1 Nm^{-2}, all the

RBCs will be fully aligned and (partly) deformed. In this case, the conductivity of a control volume is given by

$$\sigma_{>}(r) = \sigma_p \frac{1-H}{1+\{C_{>}(r)-1\}H} \tag{4.41}$$

where $C_{>}(r) = C_b(r)$ is given by (4.3). Additionally, (4.20) is used to determine the axis ratio of the deformed RBC, i.e.

$$\cos\{\varphi(r)\} = \frac{a_d(r)}{b_d(r)} = \left\{1 + \frac{b_0}{4\mu}\tau(r)\right\}^{-3} \frac{a_0}{b_0} \tag{4.42}$$

For $\tau(r_1) = 0.03$ Nm^{-2}, (4.39) is still valid, whereas for $\tau(r_2) > 0.1$ Nm^{-2}, (4.41) becomes valid. For in between values of the shear stress, the RBCs progressively move from a rotating state to an aligned state. To account for this behavior we will approximate the conductivity of a control volume by

$$\sigma_{<>}(r) = \sigma_p \frac{1-H}{1+\{C_{<>}(r)-1\}H} \tag{4.43}$$

for $r_1 \le r \le r_2$ and with

$$C_{<>}(r) = \frac{\{C_b(r) + f(r)C_r(r)\}}{1+f(r)} \tag{4.44}$$

Here we use (4.42) to calculate the deformed short-to-long axis ratio. In (4.44), $f(r)$ is a linear weighting function given by

$$\begin{aligned} f(r) &= 1 && \text{for } r < r_1 \\ f(r) &= \frac{\tau(r)-\tau(r_2)}{\tau(r_1)-\tau(r_2)} && \text{for } r_1 \le r \le r_2 \\ f(r) &= 0 && \text{for } r > r_2 \end{aligned} \tag{4.45}$$

that expresses that the fraction of randomly oriented RBCs linearly decreases as a function of $\tau(r)$. On inspection it can be seen that inserting $\tau(r) = \tau(r_1)$ into (4.45), together with (4.43) and (4.44), yields (4.39). Likewise, inserting $\tau(r) = \tau(r_2)$ yields (4.41).

Finally, the conductivity of flowing blood can be written as

$$\sigma_{bl} = \frac{2}{R^2}\left\{\int_0^{r_1} \sigma_< r dr + \int_{r_1}^{r_2} \sigma_{<>}(r) r dr + \int_{r_2}^{R} \sigma_>(r) r dr\right\} \tag{4.46}$$

where r_1 and r_2 follow from the conditions $\tau(r_1) = 0.03$ Nm^{-2} and $\tau(r_2) > 0.1$ Nm^{-2}. Since Goldsmith (1999) did not give an exact value for $\tau(r_2)$, this value will be determined by fitting the results of (4.46) to the measurement results. With (4.30) and (4.39)-(4.46), the conductivity change due to orientation and deformation in flowing blood can be calculated. Starting with the measured reduced average velocity, the shear stress profile in the tube can be calculated with (4.30). With this shear stress profile, the level of orientation of the RBCs is given by (4.45). Likewise, the level of deformation of the RBCs is given by (4.42). As a result, the conductivity of flowing blood is obtained with (4.39), (4.41), (4.43) and (4.46). In the next section, the theoretical results will be compared with measurement data published earlier in Visser (1992).

Results

Experimental Results

Reference Visser (1992) presents measurement results of the conductivity of stagnant human blood with randomly oriented RBCs and of the conductivity change of flowing human blood. For the measurements on stagnant and flowing blood two different measuring cells were constructed, both containing 4 Pt-electrodes. Two outer electrodes injected a constant alternating current (100 kHz) into the measurement cells and by means of the two inner electrodes the resulting potential difference was measured, yielding the conductivity of the blood sample in the cells. Both cells were calibrated with KCl solutions of known

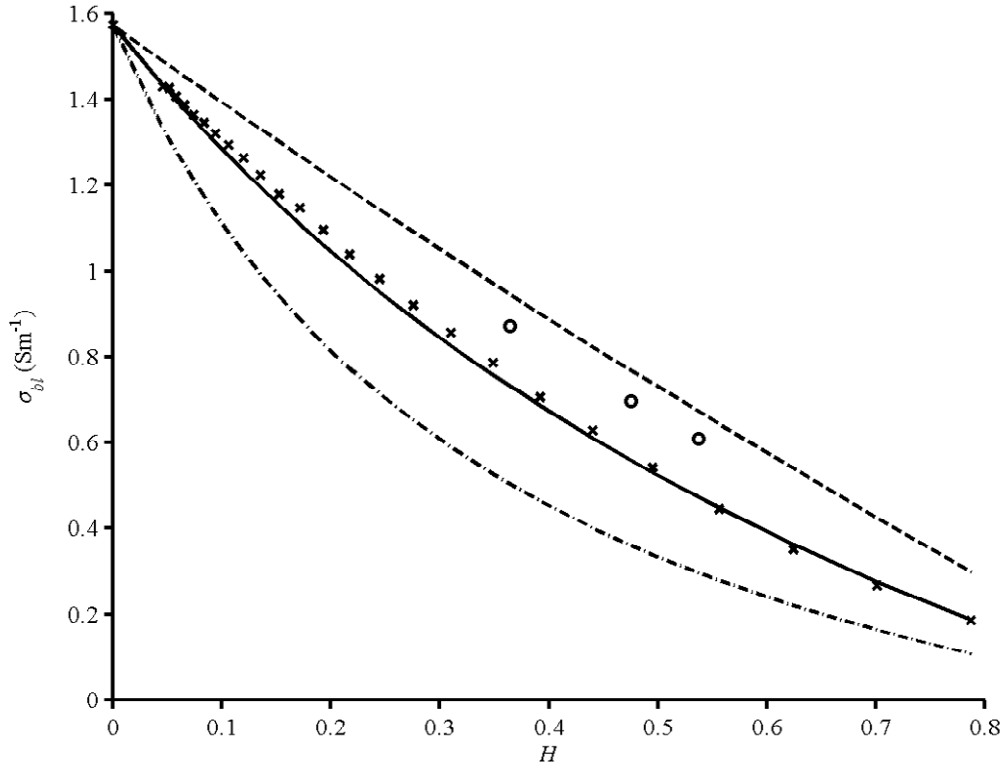

Figure 2. Hematocrit dependency of the conductivity of blood. The crosses denote the experimentally measured conductivity for random orientation of the RBCs. The solid line gives the result of the Maxwell-Fricke equations [(4.1)-(4.6)] for random orientation of the RBCs with $C = C_r$ and a/b = 0.22. The upper - and lower line give the results of the Maxwell-Fricke equation for parallel alignment of the *b*-axis with the electrical field ($C = C_b$ and a/b = 0.22*)* and the for parallel alignment of the a-axis ($C = C_a$ and a/b = 0.22), respectively. The circles give the conductivity of blood obtained from the measurements on flowing blood for an average reduced velocity of $\langle v \rangle / R$ = 477 s^{-1}. At this level the RBCs are assumed to be fully aligned and maximally deformed.

conductivity. For the measurements, blood obtained from healthy human donors was anticoagulated with heparin, and plasma was separated from the RBCs by centrifugation at 4 ^{o}C. Plasma and RBCs where then mixed in different proportions giving samples with different hematocrit values.

To obtain the conductivity of stagnant blood 25 samples with different hematocrit values (ranging from 0.046 up to 0.787) where measured in a cell. This cell was surrounded by water at 37 ^{o}C and was vibrated to maintain random orientation. The random orientation of the RBCs was checked by comparing the conductivity in the horizontal and vertical directions. A value was accepted only when these two measurements gave equal results. From the measurement results an axis ratio of the RBCs of a_0/b_0 = 0.22 was estimated. Figure 2 shows the results of measurements of the conductivity of blood for

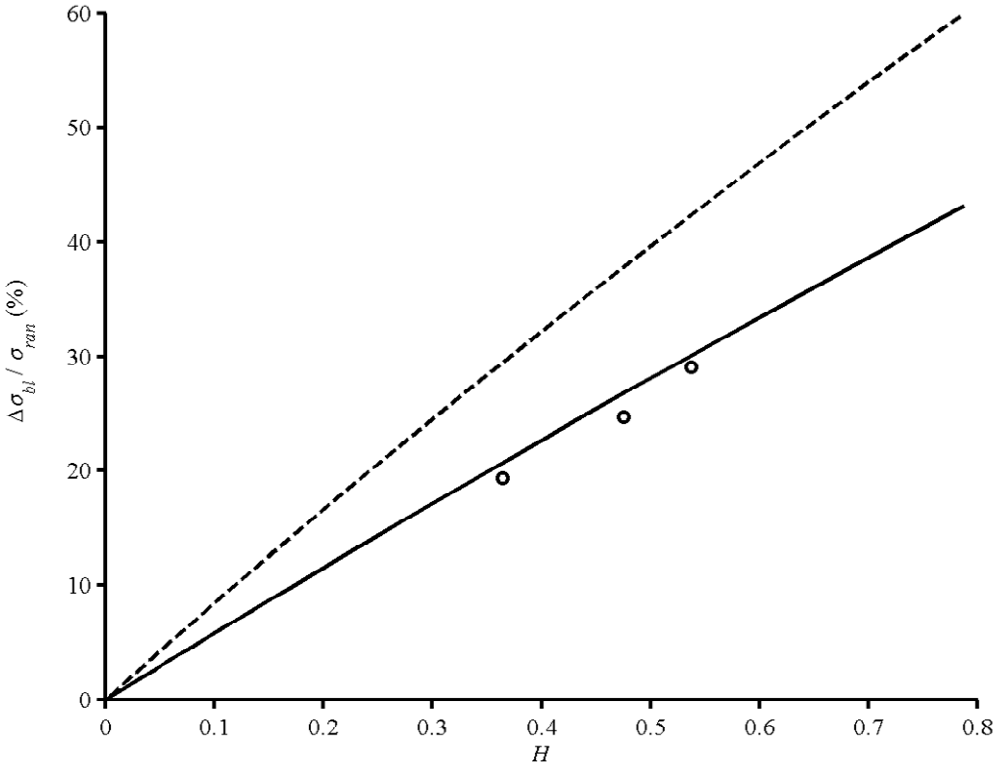

Figure 3. Hematocrit dependency of the relative conductivity change of blood for parallel orientation of the *b*-axis compared ($C = C_b$) to random orientation ($C = C_r$). The dashed line and solid line show the results of the Maxwell-Fricke equation with $a/b = 0.22$ and $a/b = 0.11$, respectively. The circles give the relative conductivity change obtained from the measurements on flowing blood for $\langle v \rangle / R = 477\ s^{-1}$.

random orientation of the RBCs (crosses). Additionally, the theoretical results are presented of the conductivity of blood using the Maxwell-Fricke equations [(4.1)-(4.6)], with $a/b = a_0/b_0 = 0.22$ for random orientation (solid line), orientation with the *b*-axis parallel to the electrical field (upper line) and parallel alignment of the a-axis (lower line).

For the measurement of the conductivity change parallel to the flow direction of blood[8] flowing through a cylindrical tube a different cell was used with an internal diameter of 4 mm. The conductivity changes of three blood samples (at 37 ^oC) with different hematocrit levels (0.364, 0.475 and 0.537) were measured in stationary and laminar blood flow for ten different constant reduced average velocities ($3.15\ s^{-1} \leq \langle v \rangle / R \leq 477\ s^{-1}$). From these measurements were obtained the relative blood conductivity changes[9]

[8] The direction of blood flow coincides with the direction of the electrical field.
[9] Relative to the conductivity of blood with random orientation of the RBCs.

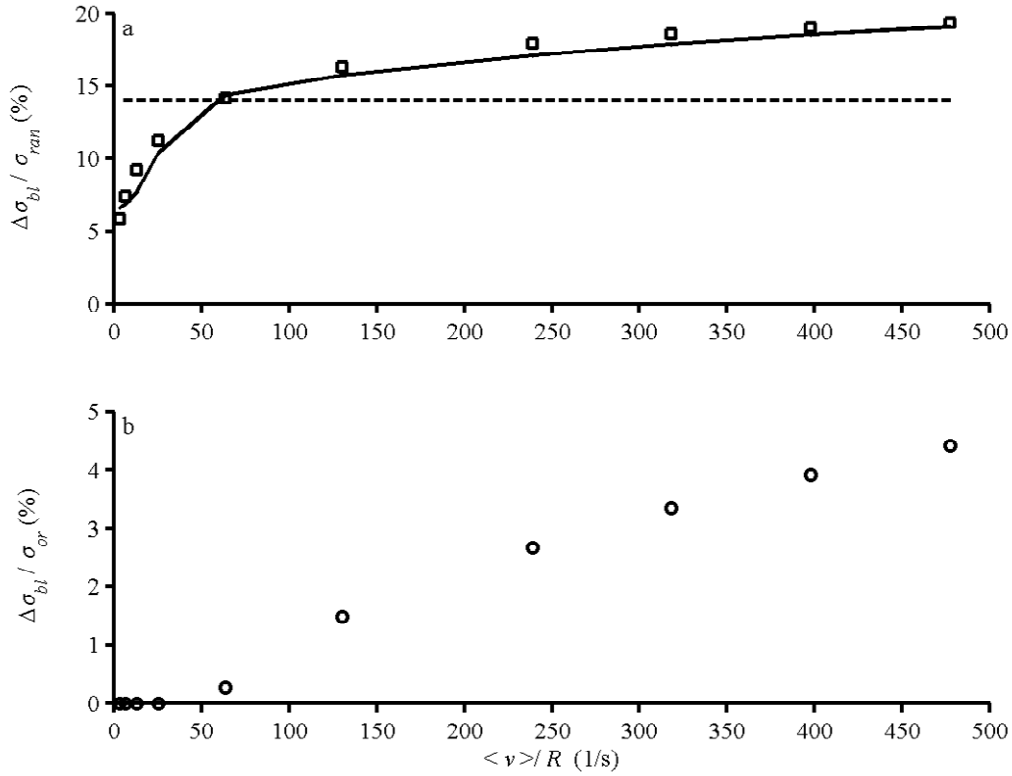

Figure 4. a) The relative conductivity change of blood compared to the conductivity of blood with random orientation as a function of reduced average velocity for a hematocrit level of H = 0.364. See text for a discussion; b) The relative conductivity change of blood due to deformation compared to the conductivity of blood with parallel orientation of the RBCs.

expressed as percentages. The circles in figure 2 show the measurement results of the conductivity of blood for a reduced average velocity of 477 s^{-1}.

Figure 3 compares the estimated hematocrit dependency of the relative conductivity change obtained, using the Maxwell-Fricke equation for fully aligned RBCs and a_0/b_0 = 0.22 (dashed line) with the measured relative conductivity changes for $<v>/R$ = 477 s^{-1} (circles). Note that to calculate the relative conductivity change predicted by the Maxwell-Fricke theory, the axis ratio of undeformed RBCs is used and thus, only orientation of the RBCs is assumed and deformation is neglected. This figure shows that neglecting deformation results in an overestimation of the relative conductivity change.

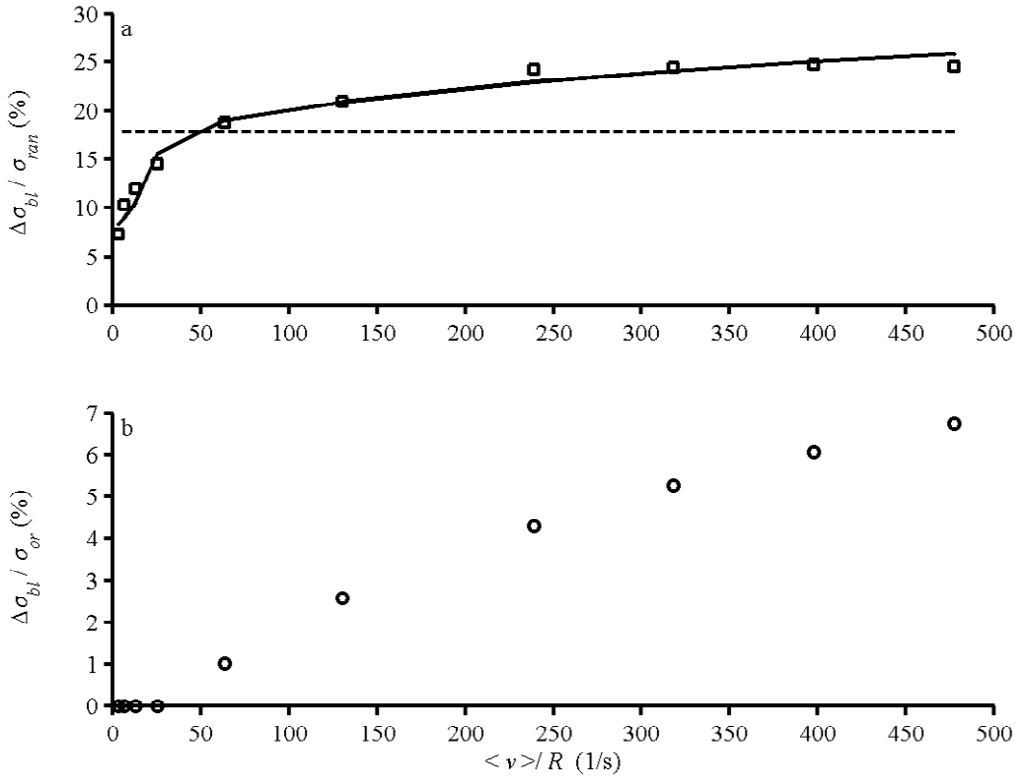

Figure 5. a) The relative conductivity change of blood compared to the conductivity of blood with random orientation as a function of reduced average velocity for a hematocrit level of H = 0.475. See text for a discussion; b) The relative conductivity change of blood due to deformation compared to the conductivity of blood with parallel orientation of the RBCs.

Theoretical Results

The original major axis length of the RBC was taken as $2b_0$ = 8 μm. Additionally, a value of μ = 1,5 x 10^{-5} Nm^{-1} was taken for the dynamic viscosity coefficient μ in (4.42). The value of μ, given in Evans (1973), is of the order 10^{-5} $N{\cdot}m^{-1}$. For the viscosity of blood, say η_{bl}, we used an expression given in Merrill (1969), which reads

$$\eta_{bl} = \eta_{pl}\left\{1 + 2.5H + 7.37\times10^{-2}H\right\} \qquad (4.47)$$

where η_{pl} is the viscosity of plasma which was taken as 1.35 x 10^{-3} Pas. For the initial axis ratio a_0/b_0 a value of 0.38 was taken from Goldsmith (1999). The integral expression in (4.46) was approximated with the trapezodial numerical integration method.

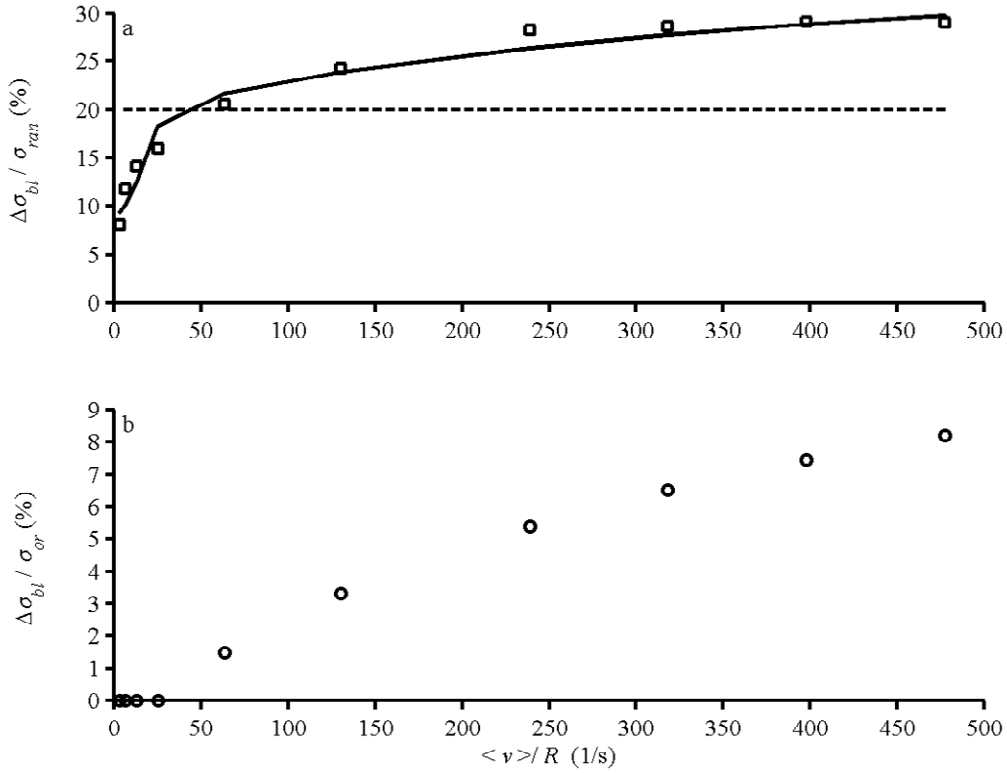

Figure 6. a) The relative conductivity change of blood compared to the conductivity of blood with random orientation as a function of reduced average velocity for a hematocrit level of H = 0.537. See text for a discussion; b) The relative conductivity change of blood due to deformation compared to the conductivity of blood with parallel orientation of the RBCs.

For the maximum average reduced velocity ($\langle v \rangle / R$ = 477 s^{-1}), the axis ratio calculated with (4.20) and (4.30) was approximately 0.11. The solid line in figure 3 demonstrates that using this axis ratio in the Maxwell-Fricke equation to estimate the hematocrit dependency of the relative conductivity change, accounting for both orientation and deformation of the RBCs, shows much better agreement with the measurement results than using an axis ratio of 0.22 (dashed line).

The top panels in figures 4-6 show the relative conductivity change of flowing blood relative to blood with randomly oriented RBCs (a_0/b_0 = 0.38) as a function of the reduced average velocity for three levels of the hematocrit. The squares give the experimental measurement results and the solid lines represent our results, i.e. (4.46). The dashed lines give the conductivity change predicted by the Maxwell-Fricke theory for parallel orientation of RBCs without deformation, i.e. (4.1) with $C = C_b$ and $a/b = a_o/b_o$ = 0.38 in (4.5). These figures

show good agreement between the measurement data and our theoretical results. To obtain this good fit the we used $\tau(r_2) = 0.4$ Nm^{-2} in (4.45) and (4.46). For lower values of $\tau(r_2)$ the relative conductivity change is overestimated for $\langle v \rangle / R < 50$ s^{-1}. This indicates that for $\tau(r_2) < 0.4$ Nm^{-2} not all RBCs are aligned, whereas in the model they are assumed to be. Likewise, for higher values of $\tau(r_2)$ the relative conductivity change will be underestimated. The value of $\tau(r_2)$ does not influence the results significantly for $\langle v \rangle / R > 50$ s^{-1}.

The bottom panels in figures 4-6 present the relative changes of blood conductivity due to deformation relative to the conductivity of blood without deformation of the RBCs (but with parallel orientation) as a function of reduced average velocity for the three different hematocrit levels. This is the difference between the solid lines and the dashed lines in the top panels of figure 4-6. For low values of the reduced average velocity (< 50 s^{-1}) and thus of the shear stress, the RBCs are not yet fully aligned in the flow direction. Therefore, for this range the relative conductivity change was set to zero. Inspection of figure 4-6 shows that after the RBCs are fully aligned in the flow direction, our theory predicts that the additional conductivity change due to deformation of the RBCs is only 4-9% of the conductivity at full alignment.

Discussion

Whole blood consists mainly of a suspension of RBCs in blood plasma. The hematocrit, under physiologically normal conditions, has a value of around 45%. It is generally assumed that the physical properties of whole blood, such as the viscosity and the electrical conductivity, are mainly determined by the properties of the RBCs and the surrounding blood plasma. In order to explain the hematocrit dependency of the electrical conductivity of blood in Fricke (1924) a theory was extended, originally developed in Maxwell (1954) for a dilute suspension of spherical particles in an electrolyte, to the case of a dilute suspension of ellipsoidal particles. This Maxwell-Fricke theory allows accurate calculation of the conductivity of stagnant blood with randomly oriented RBCs as a function of hematocrit.

In Edgerton (1974), the Maxwell-Fricke theory was elaborated into a quantitative theory on the change of blood conductivity in Couette flow, adding probability distributions for the orientation angles of the RBCs. Additionally, measurement results were presented of the viscosity and conductivity change in Couette flow and Poiseuille flow. These results show that in Couette flow, the distribution of orientation angles is a function of shear rate, and consequently of shear stress, until an equilibrium distribution is reached. This equilibrium distribution is reached at lower shear stresses for higher concentrations of RBCs in plasma. From viscosity measurements in Couette flow, Edgerton (1974) concludes that after an equilibrium distribution is reached the viscosity continues to decrease due to deformation of the RBCs. The author also states that the viscosity variation with shear stress is consistent with the speculation that at very low shear stresses the break up of rouleaux accounts for the viscosity change. From the measurements of the blood conductivity change in Poiseuille flow, Edgerton (1974) concluded that orientation of RBCs is an important factor.

Visser [Visser (1992)] applied Fricke's theory to the change of blood conductivity in Poiseuille flow. This experimental study concluded that orientation is the dominant origin of the conductivity change of blood, although large deformation of the RBCs occured. However, Sakamoto & Kanai (1979) and Fujii et al. (1999) showed that the conductivity change due to only orientation, measured in an experiment with hardened RBCs, does not depend on the shear stress for higher hematocrit levels ($Ht > 0.20$). This is consistent with the idea that for higher concentrations of RBCs in plasma the equilibrium distribution of orientation angles is already reached at very low shear stresses, which also follows from our theoretical results (for shear stresses of $\tau(r) = 0.4$ Nm^{-1} the RBCs are already fully aligned). Consequently, for higher shear stresses (or equivalently for higher average flow velocities) the variation of the conductivity of blood with shear stress must be the result of deformation of the RBCs.

Our theoretical prediction of the conductivity change of blood due to blood flow, i.e. (4.30) together with (4.39)-(4.46), shows good agreement with the measurement results (see figures 3-6). However, we used a higher axis ratio ($a_0/b_0 = 0.38$) than was obtained originally from the measurements on

stagnant blood (a_0/b_0 = 0.22), see Visser (1992). This difference may be explained by observations made in Fujii et al. (1999). The results of Couette flow experiments show that the axis ratio of RBCs rapidly increases at very low shear rates of less than 10 s^{-1}. For the flow measurements used in this study, blood in the reservoirs was continuously stirred and since stirring results in a shear stress profile somewhat similar to that of a Couette flow, this might have caused the axis ratio to increase. Furthermore, the change of the axis ratio a/b from 0.22 to 0.38-0.42, estimated originally in Visser (1992), would imply a shortening of the b-axis and an increase of the a-axis of the deformed RBCs. Our results, on the other hand, predict a decrease of the axis ratio a/b, corresponding to an increase of the b-axis and a decrease of the a-axis. Under conditions of Poiseuille flow, the RBCs are aligned with their long axis parallel to the flow direction. Deformation results in elongation of the long axis (b-axis) and shortening of the short axis (a-axis). Consequently, under these flow conditions the ratio a/b must decrease, which is in line with our findings. We hypothesize that the observed differences between our results and the original results, reported in Visser (1992), can be explained as follows: stirring blood in the reservoirs, might have caused a rapid increase in axis ratio. Then, when blood is pumped through the cylindrical tube, the RBCs are eventually fully aligned and the axis ratio decreases as a result of deformation.

Looking closer at (4.46) it can be observed that from our model it follows that depending on the value of the maximum shear stress[10] either of the following situations can occur, see figure 7[11]:

For τ_{max} < 0.03 Nm^{-2} all the RBCs are rotating with varying angular velocities. At any moment in time approximately 50% of the RBCs are aligned with their major axis in the flow direction. The remaining RBCs can be considered to be randomly oriented. As a result the conductivity of blood is given by (4.39)-(4.40) and is independent of the radial distance r, because the RBCs are not yet deformed.

[10] In the case of a Newtonian fluid is the maximum shear stress related linearly to the reduced average velocity

[11] Figure 7 is obtained by expressing the surface areas corresponding to $0 \le r \le r_1$, $r_1 < r \le r_2$, and $r_2 < r \le R$ relative to the total surface area of the tube as a function of reduced average velocity.

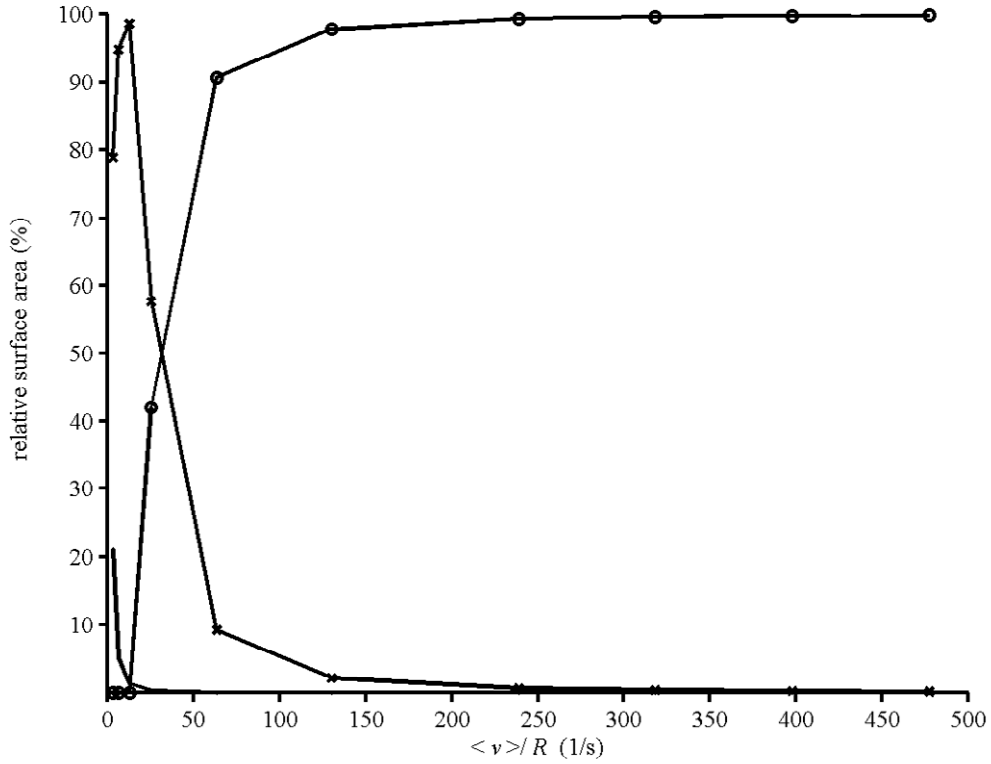

Figure 7. The surface area of the three regions that exist in the tube expressed as percentage of the total surface area of the tube; $0 \leq \tau(r) < 0.03$ Nm^{-2} where the RBCs are rotating and undeformed (solid line), $0.03 \leq \tau(r) \leq 0.4$ Nm^{-2} the transition region (line with squares), 0.4 Nm^{-2} $< \tau(r) \leq \tau_{max}$ where the RBCs are fully aligned and deformed (line with circles).

If $0.03 \leq \tau_{max} \leq 0.4$ Nm^{-2} the cross-section of the tube can be divided into two regions. The inner region ($0 \leq \tau(r) < 0.03$ Nm^{-2}) where the RBCs are rotating and an outer region (0.03 Nm^{-2} $\leq \tau(r) \leq \tau_{max}$) where a gradual transition occurs from a rotating state to a state of alignment together with (small) deformation of the RBCs. A tube with flowing blood can now be considered to consist of two parallel conductors. The inner conductor with the *r*-independent conductivity given by (4.39)-(4.40) and the outer conductor with an *r*-dependent conductivity given by (4.42)-(4.45). For increasing flow velocities and thus increasing maximum shear stresses, the surface area of the inner region decreases rapidly, while the surface area of the outer region increases. We have assumed that the transition from rotating to aligned state can be modeled with a linear function of the shear rate. Furthermore, we have assumed blood to be a Newtonian-fluid, which is a good approximation for shear rates of 100 s^{-1} or higher [see Merrill (1969)], corresponding in our case to reduced average

velocities above approximately 25 s^{-1}. Possibly these simplifications explain the slight deviation of the calculated from the observed relative conductivity change for $\langle v \rangle / R < 25\ s^{-1}$.

When $\tau_{max} > 0.4\ Nm^{-2}$ three regions can be thought to exist in the tube. The inner region ($0 \leq \tau(r) < 0.03\ Nm^{-2}$) where the RBCs are rotating and undeformed, the transition region ($0.03\ Nm^{-2} \leq \tau(r) \leq 0.4\ Nm^{-2}$) and the outer region ($0.4\ Nm^{-2} < \tau(r) \leq \tau_{max}$) where the RBCs are fully aligned and deformed. In this case, the blood-filled tube can be considered to exist of three conductors in parallel with the outer conductor having an *r*-dependent conductivity given by (4.41) and (4.42). For increasing flow velocities, the surface area of the outer region increases, while the surface areas of the other two regions rapidly decrease and are eventually negligible. For reduced average velocities above $\langle v \rangle / R > 50\ s^{-1}$, the conductivity of flowing blood is entirely dominated by the conductivity of the region with fully aligned and deformed RBCs, as is demonstrated in figure 7.

For low shear stresses, Brownian motion plays a role in deorientation of the RBCs. Especially when time varying flow is considered, for example in the human arterial system. The work in Visser (1989) demonstrates that the times involved with orientation and deorientation differ largely. In accelerating flow the conductivity changes synchronously with change of flow rate, whereas in decreasing flow the conductivity change shows an exponential-like decay. The relaxation time, taken as a measure of the exponential decay, was found to be in the order of 0.21-0.29 s, depending on the hematocrit. This possibly implies that at the end of the diastolic part of a heart cycle, when the flow in the aorta is (close to) zero, the RBCs are not yet completely randomly orientated. Possibly, in-vivo the relative conductivity change due to blood flow is smaller than the 25-30% conductivity change relative to random orientation measured in stationary laminar flow. If only shear stress induced deformation of RBCs is the cause of the conductivity to change in-vivo, then only a change of 4-9% should be expected (see the bottom panels in figures 4-6). The work in Kornet et al. (1999) found, in in-vivo experiments in pigs, that no sudden increase in blood conductivity occurred in the aorta at the onset of blood flow, probably because most erythrocytes remain disaggregated, orientated and deformed throughout

the heart cycle. Our results substantiate these findings to some extent. Although the results of in-vitro measurements can not be translated directly to the case of pulsatile blood flow in-vivo, due to the unsteady hemodynamic regime in-vivo, it may be reasonable to assume that in-vitro measurements give an upper limit of the resistivity change that can be expected in-vivo. This seems to indicate that the conductivity change of blood due to blood flow in the human arterial system is not as large as is sometimes assumed [e.g., Wang & Patterson (1995)].

We have only presented results for the conductivity change of blood in the direction of blood flow for the following reasons. First, the conductivity change was only measured in that direction. Secondly, the geometry of a cylindrical tube does not allow the conductivity of blood, in the direction perpendicular to the tube axis, to be calculated easily. Thirdly, studies that present results of measurements of the conductivity in directions perpendicular to the flow direction either use rectangular ducts or measure the conductivity change in Couette flow. In both cases, the shear stress profiles are different from those in cylindrical tubes.

The applications of the results presented in this study may include several areas. In non-medical areas the results may be used for studying particle properties in flowing suspensions, while in the field of medicine the conductivity change of blood due to extra corporal blood circulation can be used to indicate changes in RBC properties due to mechanical blood handling in heart-lung machines or during hemodialysis. In such applications the parameters temperature, electrolyte concentration, frequency and amplitude of the excitation current will play an important role.

Changes in blood temperature will affect blood conductivity. For increasing temperature the conductivity of blood at rest, like that of most electrolytes, also increases. Reference Mohapatra & Hill (1975) gives an expression of blood resistivity (which is the inverse of the conductivity) in the absence of flow as a function of hematocrit and temperature. This expression could be used as a reference value for blood at rest at different temperatures and hematocrit values, if relative conductivity changes due to blood flow are of interest. Alternatively, if absolute values of the conductivity of blood at different flow rates are of interest, an expression for the temperature dependence of the conductivity of blood plasma is given in Visser (1992). Insertion of this result

into (4.39), (4.41) and (4.43) yields an expression in which the temperature dependence of blood conductivity is incorporated into the model.

Plasma electrolyte concentration affects not only the conductivity of plasma but also RBC volume. Reference Troutman & Newbower (1983) presents an expression for the dependence of plasma conductivity on plasma protein concentration that can be inserted into (4.39), (4.41) and (4.43). Changes of RBC volume can be accounted for by changing the initial axis ratio a_0/b_0. In future research our model may help to determine more accurately the dependence of RBC properties on hematocrit, temperature and electrolyte concentration. With an expression that gives plasma conductivity and blood viscosity in terms of the parameters hematocrit, temperature, and electrolyte concentration, blood conductivity changes due to blood flow can provide information on both the initial axis ratio a_0/b_0 and the membrane shear modulus μ in terms of these parameters.

With regard to the frequency of the excitation current, the following consideration is important. For frequencies below several hundred kHz the impedance of blood can be considered purely resistive, because the charging time of the RBC membranes is small enough to charge and discharge the membrane completely during a single cycle (cf. Duck (1990) Hoetink et al. (2002)Chpt. 6). Furthermore, the conductivity of the RBC is much smaller than that of blood plasma and therefore RBCs can be considered as insulating particles. It should be noted, however, that the original equation presented in Fricke (1924) allows the calculation of the conductivity of suspension with non-insulating particles and therefore the model presented in this paper could be extended to this case. For higher frequencies the impedance of the RBC membrane decreases because of its large capacitance. For frequencies above roughly 3 MHz the conductivity of RBCs increases rapidly and eventually approaches the value of plasma, i.e. the electrical current passes through the RBC virtually undisturbed. Reference Ninomiya et al. (1988) has shown that the relative conductivity change of flowing blood is independent of the frequency of the excitation current up to several hundred kHz, then it increases slightly and finally decreases sharply above 2-3 MHz.

Regarding the amplitude of the excitation current, it is important that the amplitude is within the “limit of linearity” (cf. Geddes & Baker (1989) p. 332).

Above a certain threshold current density, the resistance of a saline solution decreases and the capacitance increases as a function of current density. For lower excitation current frequencies, this threshold occurs at progressively lower current density values. Calibration of our measurement cells with KCl solutions of known conductivity, insured that the current density did not pass the threshold value. If blood conductivity is to be measured with the patient as a part of the electrical circuit, amplitudes of the excitation current should be used such that the patient safety is ensured. A safe level of the excitation current amplitude depends on the frequency of this current [see for example Geddes & Baker (1989)]. In this case and in the case of flow produced by a roller pump that is also part of the electrical circuit, the excitation current will not only pass through the measurement cell, but a certain fraction will also pass through the patient or roller pump, respectively. This will affect the measurement of blood conductivity, but a correction method may be designed to compensate the effects.

Conclusion

This study shows that the conductivity change of blood due to blood flow can be understood and described quantitatively. Our model based results show a close agreement with measurement data reported in Visser (1992). A set of expressions has been obtained, based on the Maxwell-Fricke theory, which gives this conductivity change as a function of the average reduced velocity.

The theory presented in this study accounts for both orientation and deformation of RBCs as origins of the conductivity change of blood due to blood flow. In our opinion, this leads to a more complete understanding of this phenomenon and may lead to more insight in the magnitude of blood conductivity change in in-vivo blood flow. Additionally, measurement of the conductivity change of blood due to extra corporal blood circulation can be used to indicate changes in RBC properties, due to mechanical blood handling in heart-lung machines or during hemodialysis.

Chapter 5 An Experimental Study on the origins of the Thoracic Electrical Impedance Signal

A.E. Hoetink; Th.J.C. Faes; J.T. Marcus; R.M. Heethaar

IEEE Transactions on Biomedical Engineering (submitted)

Summary

The usablity of Electrical Impedance (EI) cardiography as a non-invasive technique to measure cardiac output has been the subject of debate for many years. Three major problems are the contribution of blood resistivity change and volume change of other blood vessels to the EI signal, and the choice of electrode location on the thorax. The aims of this study are: a) to estimate the accuracy of an aortic volume change estimator that neglects the conductivity change of blood; b) to determine the relative contribution of the aorta to the EI signal; c) to investigate the sensitivity of an electrode array to pick up the aorta as a major source. On four subjects EI measurements were conducted, followed by MRI measurements of aortic cross-sectional surface area and blood flow velocity. From the EI measurements the volume change of the aorta was estimated. These results were compared to the aortic volume change calculated from the MRI measurements of aortic cross-sectional surface areas and aortic blood flow velocity. The results show that: a) neglecting the conductivity change of blood introduces an error of at most 9% in volume change estimation; b) on most measurement locations on the thorax, the aorta is not the major source of the EI signal; c) it seems that the aorta is the major source of the thoracic EI signal that is measured at the left-hand side of the thorax.

Introduction

Accurate non-invasive assessment of cardiac output (CO) could benefit the treatment of patients greatly. Electrical impedance (EI) cardiography is a non-invasive technique to measure CO, cf. Hayes (1997), but its usability has been the subject of debate for many years.

The rationale underlying the method is quite simple. The heart ejects blood into the aorta and pulmonary artery during the systolic part of the cardiac cycle. This results in a volume increase of the these arteries. If an electrical current is injected into the body and the resulting voltage changes across the thorax are measured, the volume increase of mainly the aorta is assumed to cause a heart rate synchronous decrease in the thoracic EI (i.e. the magnitude of the measured voltage divided by the magnitude of the injected current). In fact it is assumed that the thorax can be represented electrically by two cylinders in parallel connection, often referred to as the parallel cylinder model. One cylinder (with time varying volume) represents the aorta and the other cylinder (with constant volume) represents the thorax tissue. Consequently, if this parallel cylinder model is a correct representation of the thorax, CO can be calculated from the measured EI decrease.

However, Sherwood et al. (1990), Raaijmakers et al. (1999) and others show that several methodological problems still remain to be solved before accurate non-invasive hemodynamic assessment of CO is within reach. Firstly, the aorta is not the only possible source of impedance change, which raises questions about the validity of the parallel cylinder model. Several other sources have been put forward that may contribute to the change in measured thoracic EI. To name a few: the heart, other major blood vessels, the lungs, and possibly even the change of blood conductivity due to blood flow. Secondly, different electrode configurations show differences in sensitivity for impedance changes due to different organs in the thorax, as was demonstrated by Kauppinen, Hyttinen, & Malmivuo (1998). Consequently, the accuracy of CO estimation from EI changes will depend on the electrode configuration that is used. Possibly an electrode configuration could be designed that is most sensitive for aortic volume changes. Thirdly, during systole blood is not only ejected into the

aorta, there is also outflow of blood from the aorta further into the arterial system. As a result, the volume change of the aorta is the difference between inflow and outflow of blood. Thus even if the aorta is the main source of EI signal, then a CO estimator should correct for the outflow of blood from the aorta [cf. Yamakoshi, Togawa, & Ito (1977) and Faes et al. (1999a)]. This study will deal with the first problem that is the multiple origins of the EI signal, although the second problem, the sensitivity of EI to electrode configurations, will be discussed as it is closely connected to the first problem.

The origin of the thoracic EI signal has been the subject of many studies. These studies can be divided into two categories. The first category comprises many experimental studies that have tried to relate the thoracic impedance signal to volume changes of the major blood vessels and other organs in the thorax, e.g. Bonjer, van den Berg, & Dirken (1952); Kubicek et al. (1966); Geddes & Baker (1972); Ito, Yamakoshi, & Yamada (1976); Mohapatra (1981); Lamberts, Visser, & Zijlstra (1984); Zhang et al. (1986); Patterson (1989); Patterson et al. (1990); Patterson, Wang, & Raza (1991); Patterson et al. (1993); Raaijmakers et al. (1997a) and van de Water et al. (2003). These studies vary largely in used methodology, ranging from experiments on animals (mostly dogs) to comparison of CO measured with EI and a reference method (mostly some kind of dilution method) in both healthy human subjects and patients. A problem associated with the latter approach is that differences between CO values obtained from the EI signal and the reference method can have many different causes. It may be possible that the aorta is not the (only) major source of the EI signal. However, differences may also be explained by for example the location of the measurement electrodes, the use of different and possibly incorrect equations to calculate CO from the EI signal or even the inaccuracy of the reference method. Generally it can be stated that these experimental studies are not conclusive about the possible sources of the thoracic EI signal.

To overcome the incapability of experimental studies to isolate the contribution of different sources to the thoracic EI signal, a second category of studies has used mathematical models, like e.g. finite element models, to determine theoretically the different contributions to the thoracic EI signal. These studies calculated volume changes of the major blood vessels, the heart,

the changes in volume and blood perfusion of the lungs, and the change of blood conductivity due to blood flow, e.g. Sakamoto et al. (1979); Kosicki et al. (1986); Kim et al. (1988); Wang & Patterson (1995); Wtorek & Polinski (1995); Kauppinen, Hyttinen, & Malmivuo (1998); Wtorek (2000) and Wang, Haynor, & Kim (2001). One major methodological problem with these studies, however, is that they require much a priori knowledge - concerning the geometry of the thoracic organs and their changes in the cardiac and respiratory cycle under normal and pathological conditions, and the electrical properties of the organs - while these modeling results are seldom verified in extensive experiments. As an example Wang & Patterson (1995) had to assume 93 values of the conductivities of 31 organs at both end diastole and end systole, whereas the outcome of the model was only verified with one experimental thoracic impedance measurement at end diastole and end systole. This example reveals another problem concerning these studies. That is, the impedance is only calculated at two moments in the heart cycle, at the end of diastole and at the end of systole. These objections notwithstanding these studies provide important information on the sources of the EI signal. Although some of these studies seem to confirm that the aorta is the major source of the EI signal, most of these model studies indicate that the thoracic EI signal is produced by multiple sources.

In chapter 2 an approach was introduced to map changes in blood volume in thoracic organs using a linear spot electrode array. This method was tested by comparing the results to Magnetic Resonance Imaging (MRI) measurements of volume changes of the aorta, vena cava, the carotid arteries, and the heart. The results showed that the volume changes of these organs are the main contributors to the EI signal. Furthermore the magnitude of the contribution of each organ to the EI signal changes, depending on the measurement location on the thorax. However, one possible source of the thoracic impedance change was not included: the change of the conductivity of blood due to blood flow. The estimator of blood volume changes of the thoracic organs, developed in chapter 2, assumed a constant value for the conductivity of blood during the heart cycle. Several studies have shown that in pulsatile flow the conductivity of blood changes with time, e.g. Gollan & Namon (1970); Liebman (1970); Visser et al. (1976); Sakamoto & Kanai (1979); Lamberts,

Visser, & Zijlstra (1984); Shankar, Webster, & Shao (1985); Ninomiya et al. (1988); Visser (1989). However, the magnitude of the contribution of the conductivity changes to the EI signal reported in these studies varies from 5% to roughly 50%. In chapter 4 we proposed a theoretical model that accurately predicts the conductivity change of blood in laminar and stationary flow. Although the flow pattern in-vivo is far from laminar and stationary, this theoretical model may be considered a worst case estimation of the blood conductivity change in-vivo. Consequently this theoretical model may help to estimate an upper bound of the error introduced when using a blood volume change estimator that neglects the change of blood conductivity.

In this present study both experiment and theory will be combined to investigate the accuracy of aortic volume change estimation from the EI signal. The experimental part consists of measurements of aortic volume changes and blood flow velocity in an MR-scanner. These experimentally measured aortic volume changes and blood flow velocity together with our theoretical model of blood conductivity change, allows the generation of a simulated EI signal. This simulated EI signal represents the EI signal that would be measured if the aorta is the major source of the EI-signal (i.e. the parallel cylinder model is a valid representation of the thorax), and if both aortic volume changes and blood conductivity changes due to blood flow contribute to the EI-signal. To investigate, subsequently, the importance of blood conductivity changes relative to aortic volume changes we estimate the aortic volume change from this simulated EI signal using the estimator developed in chapter 2. This estimator neglects the conductivity change of blood, and consequently, comparing the estimated volume change of the aorta with the experimentally measured volume change of the aorta, will give an indication of the error introduced by neglecting blood conductivity change. Finally, comparing the simulated EI signal to actually measured thoracic EI signals will indicate whether the parallel cylinder model is a correct representation of the thorax. Additionally, it allows quantification of the contribution of the aorta to the EI signal.

The aim of this study is threefold: a) to estimate the accuracy of an aortic volume change estimator that neglects the conductivity change of blood; b) to determine the relative contribution of the aorta to the thoracic EI signal; c) to investigate the sensitivity of a linear electrode array, in order to determine a

region on the thorax where the aorta as the major source may be picked up by the electrodes.

Theory

In chapter 2 a method was developed and tested to estimate the volume change of sources in small slices of the thorax from EI measurements. It will be more convenient here to consider the admittance, which is the reciprocal of the impedance. Suppose that the measured slice admittance, say $Y_{slice}(t)$, can be represented by a lumped circuit element that can be considered to be a series connection (this corresponds to a parallel connection in terms of impedances) of a time-dependent admittance, say $Y_{source}(t)$, and a admittance, say Y_{tissue}, which is time-independent with respect to the heart cycle. The time-dependent admittance represents the admittance of all the organs (sources) inside the slice that cause the potential distribution to be time-dependent. The time-independent admittance represents the admittance of all tissues with constant electrical properties and cross-sectional surface area. The total time-dependent admittance of the small slice can be written as

$$Y_{slice}(t) = Y_{source}(t) + Y_{tissue} \tag{5.1}$$

Differentiating (5.1) with respect to time yields

$$\frac{dY_{slice}(t)}{dt} = \frac{dY_{source}(t)}{dt} \tag{5.2}$$

which expresses the fact that the change in slice admittance is entirely determined by the change in source admittance. Furthermore, it was assumed that for this small slice all sources may be taken together into an equivalent lumped circuit element. The time-dependent admittance of this element with fixed length l, time-dependent conductivity $\sigma(t)$ and time-dependent cross-sectional surface area $A(t)$, can be written as

$$Y_{source}(t) = \frac{\sigma(t) \cdot A(t)}{l} \tag{5.3}$$

Differentiating (5.3) with respect to time gives

$$\frac{dY_{source}(t)}{dt} = \frac{\sigma(t)}{l}\frac{dA(t)}{dt} + \frac{A(t)}{l}\frac{d\sigma(t)}{dt} \tag{5.4}$$

Suppose that the aorta is the only source in the thorax. With MR cine-images the cross-sectional surface area of the aorta can be measured. With MR flow measurements the average flow velocity of blood in the aorta can be measured. In chapter 4 we have derived an equation that allows the conductivity change of blood due to flow to be calculated from measured average flow velocities, see Appendix B. With the measured cross-sectional surface area of the aorta, say $A_{MRI}(t)$, a time-varying conductivity of blood calculated from the flow measurements, say $\sigma_{bl}(t)$, and (5.2) and (5.4), the corresponding first derivative of the simulated slice admittance can be calculated with

$$\frac{dY_{SIM}(t)}{dt} = \frac{\sigma_{bl}(t)}{l}\frac{dA_{MRI}(t)}{dt} + \frac{A_{MRI}(t)}{l}\frac{d\sigma_{bl}(t)}{dt} \tag{5.5}$$

This simulated admittance represents the EI signal that would be measured if:

a) the thorax can be represented electrically by two cylinders connected in parallel, one representing the aorta and the other representing the other thorax tissue (parallel cylinder model);
b) both the cross-sectional surface area of the aorta and the electrical conductivity of blood vary with time.

Furthermore, an estimator of the total cross-sectional surface area changes (SAC) of all the sources in a slice was derived in chapter 2 that reads in terms of admittance

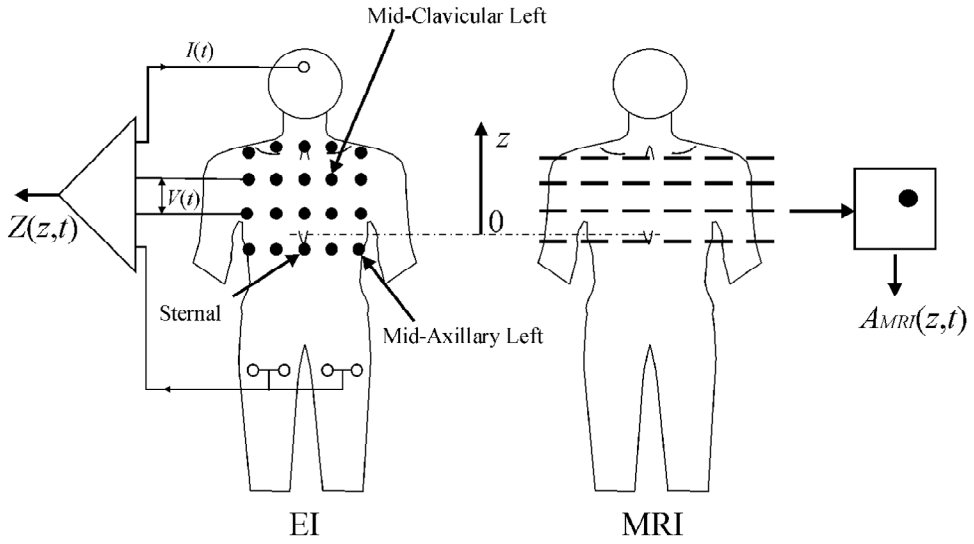

Figure 1. Electrical impedance measurement setup for a male subject (left) and MR measurements (right).

$$\Delta A(t) = A(t) - A(t_0) = \frac{I}{\sigma}\int_{t_0}^{t} \frac{dY_{slice}(t)}{dt}dt \qquad (5.6)$$

where σ is the time-independent conductivity of the lump circuit element representing all the sources and t_0 is a certain reference moment in time[12]. The time-independent conductivity was assumed to equal the time-independent conductivity of flowing blood. Inserting (5.5) into (5.6) gives an estimation of the simulated SACs, say $\Delta A_{SIM}(z_i,t)$, with the time-varying nature of the conductivity of blood deliberately neglected.

Let the thorax be made up of N of these slices. For each slice the SAC, say $\Delta A(z_i,t)$ for the ith slice at location z_i with respect to the body axis (see figure 1), is given by (5.6). The total volume change in the thorax can be obtained by integrating $\Delta A(z_i,t)$ over all slices (N), i.e.

$$\Delta V_{total}(t) = \int_{z_{i=1}}^{z_{i=N}} \Delta A(z_i,t)dz \qquad (5.7)$$

[12] The reference time moment t_0 is the moment of occurrence of the R-wave of the ECG.

Inserting the simulated SACs calculated with (5.6) for the *N* slices into (5.7) gives a simulated aortic volume change, say $\Delta V_{SIM}(t)$. Comparing this to the experimentally measured aortic volume change, say $\Delta V_{MRI}(t)$, gives an estimate of the error introduced by deliberately neglecting the time-varying nature of the conductivity of blood in (5.6), see figure 2 for a schematic representation of the data processing.

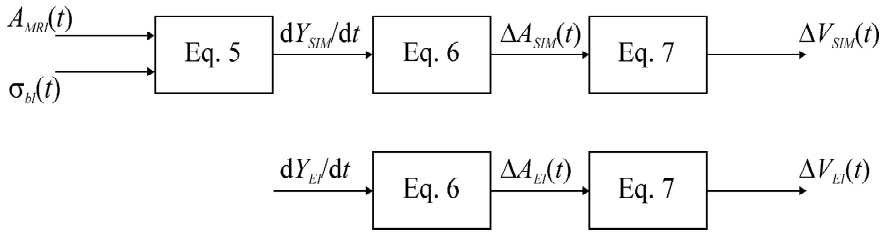

Figure 2. Schematic representation of the data processing, see text for a discussion.

Inserting thoracic slice admittances measured experimentally with EI into (5.6) yields EI SACs, say $\Delta A_{EI}(z_i,t)$. Inserting these EI SACs into (5.7) and comparing the result, say $\Delta V_{EI}(t)$, to the simulated aortic volume change or the measured aortic volume change will give an estimation of the magnitude of the contribution of the aorta to the EI signal. If $\Delta V_{EI}(t)$ corresponds well with $\Delta V_{MRI}(t)$, then this can be interpreted as evidence that the aorta is the major source of the EI signal (and thus the parallel conductor model is a valid representation of the thorax). Additionally it may be seen as evidence that the conductivity of blood changes during little the cardiac cycle. If, on the other hand, $\Delta V_{EI}(t)$ shows closer correspondence to $\Delta V_{SIM}(t)$, this may be interpreted as evidence that the aorta is the major source of the EI signal, but the conductivity of blood changes considerably during the heart cycle. Finally, if $\Delta V_{EI}(t)$ shows no correspondence to either $\Delta V_{MRI}(t)$ or $\Delta V_{SIM}(t)$, this must lead to the conclusion that the aorta is not the major source and consequently the parallel cylinder model does not correctly represent the thorax.

Experiment

The experiment was conducted on 4 healthy adult subjects in supine rest. Two males aged 69 (subject 1) and 26 (subject 2), and two females aged 24 (subject 3) and 27 (subject 4). On all subjects first EI measurements were conducted, followed by MRI measurements. Before the EI and MRI measurements the subjects were in supine rest for a period of approximately 30 minutes to assure physiological stabilization.

EI Measurements

Current injecting spot electrodes (Nutrode-P20M0) were placed on the forehead (one) and on the upper legs (two on each leg). Voltage pickup electrode pairs were placed approximately 2 (cm) apart in the *z*-direction on the mid-axillary lines and mid-sternal line for both the male and female subjects, and on the mid-clavicular lines for the male subjects only. See figure 1 for a schematic representation of the measurement setup for a male subject. The measurements were conducted starting at the xiphoid process up to the base of the neck. The minimum distance between current injecting and voltage pickup electrodes exceeded 15 (cm). The EI signals were recorded between adjacent pair of voltage pickup electrodes, with a system developed in our laboratory. The signals were collected for 30 seconds at 128 kHz and at a sample frequency of 200 Hz, resulting in a temporal resolution of 5 ms. The registrations were ensemble averaged (approximately 30 heartbeats) to remove the affects of respiration. The variable obtained from the EI signal was the impedance between the voltage pickup electrodes as a function of time and z_i-coordinate, say $Z_{EI}(z_i,t)$. Since the admittance is the reciprocal of the impedance it holds that

$$\frac{dY_{EI}(t)}{dt} = \frac{d}{dt}\frac{1}{Z_{EI}(t)} = -\frac{1}{Z_{EI}^2(t)}\frac{dZ_{EI}(t)}{dt} \tag{5.8}$$

The EI SACs, $\Delta A_{EI}(z_i,t)$, are obtained by inserting the measured slice impedances into (5.6) and using a value of the calculated conductivity of σ = 7.4 x 10^{-3} Scm^{-1} (this corresponds to a resistivity of blood of 135 Ωcm). For the slice thickness the distance between the voltage measuring electrode pairs was inserted, i.e. l = 2 (cm).

MRI Measurements

MRI cine imaging was performed with a 2-dimensional Steady State Free Precession pulse sequence, temporal resolution 13.8 ms and pixel size 1.8 x 1.4 mm (see appendix A). These cine images were recorded in transverse planes, reaching from the base of the neck to just below the xiphoid process. The distance between each image plane was 1 cm. The R-wave of the ECG was used to trigger the image acquisition. The number of temporal phases that were acquired, was chosen such that 90% of the heart cycle was covered. In each slice and for each phase of the heart cycle contours were drawn manually around the aorta. With these contours the cross-sectional surface area of the aorta was calculated as a function of time, yielding $A_{MRI}(z_i,t)$ in cm^2. The cross-sectional surface area for each slice was then differentiated with respect to time. The resulting differential area changes were then integrated with respect to time (with the integration constant set to zero) to obtain the MRI SACs, $\Delta A_{MRI}(z_i,t)$, for each slice. Additionally, MRI phase-contrast velocity quantification was performed by using a gradient-echo sequence, with a velocity sensitivity of 150 cm/s in the through-plane direction (see appendix A). The velocity was recorded at the beginning of the ascending aorta just above the aortic valve, and at the top of the descending aorta just below the aortic arch.

Results

Figure 3 shows the measured reduced average velocities (i.e. the average flow velocity divided by the radius of the aorta, c.f. chapter 4) for the four subjects in the ascending aorta (top left) and the descending aorta (top right). The corresponding estimated relative conductivity changes are shown in the bottom panels. The time-axis represents relative time, i.e. the time is for each subject normalized to the length of their heart cycle. The hematocrit of all subjects was assumed to equal H = 47.5%. On inspection it can be seen that the reduced average velocities in the ascending aorta are very similar for the three young subjects, the maximum values are in the range 30-40 s^{-1}. The maximum value of the reduced average velocity for the older male subject (crosses) is much smaller, due to a larger radius of the (less elastic) aorta and somewhat lower value of the average velocity. It is worth noticing that the reduced average velocities measured in the ascending aorta show less variation between subjects, than do the reduced average velocity measured in the descending aorta. This is mainly the result of large variations between subjects in average flow velocities measured in the descending aorta.

The bottom panels in figure 3 indicate that the relative conductivity change estimated in the ascending aorta is somewhat lower (roughly 9% for young subjects) than in the descending aorta (roughly 11 % for young subjects). The conductivity change for the older subject is much smaller than that for the younger subjects, as the average reduced velocity is much smaller for the older subject. Notice the difference in shape of the relative conductivity change between ascending and descending aorta. Where the relative conductivity change in the ascending aorta shows close resemblance to the shape of the reduced average velocity, the relative conductivity change in the descending aorta shows a somewhat different (smoother) form.

The estimated absolute conductivity change together with the measured aortic cross-sectional surface areas obtained from MR cine-images were inserted into (5.5) to obtain a simulated first derivative of the slice impedance signal, $dY_{SIM}(t)/dt$. This simulated signal represents the slice impedance that would be measured if the aorta is the only source of the EI signal and blood

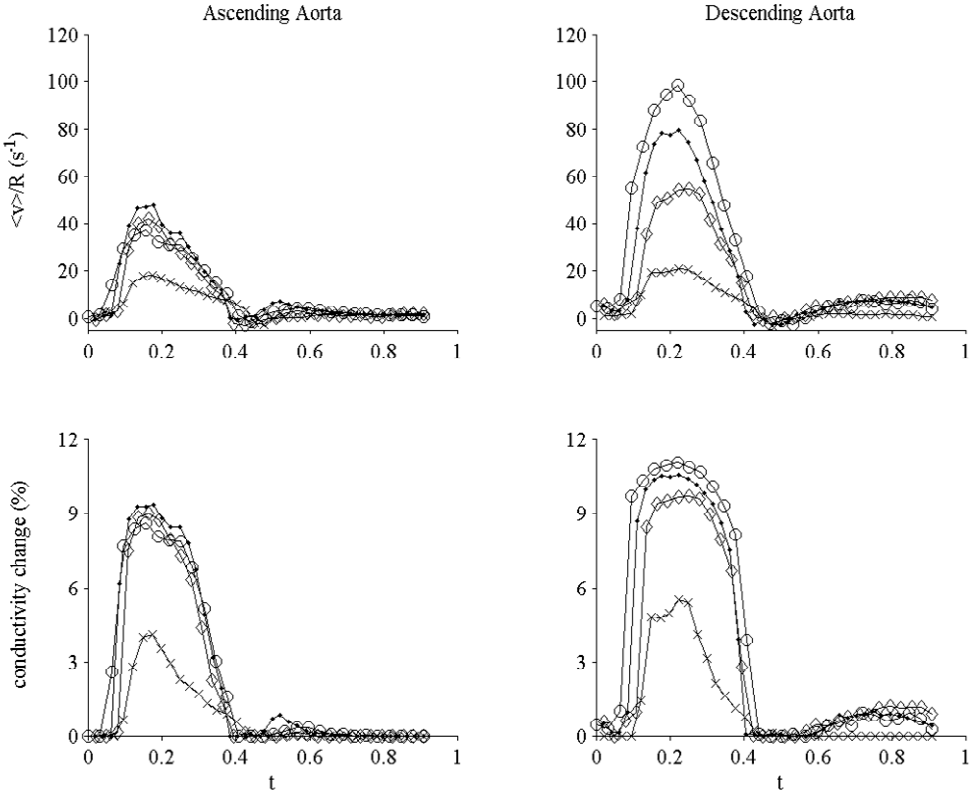

Figure 3. (Top Left) Measured reduced average flow velocity of blood in the ascending aorta for the four subjects. (Bottom Left) Estimated conductivity change in percentage relative to the conductivity at the onset of flow calculated with the measured reduced average velocity in the ascending aorta. (Top Right) Measured reduced average flow velocity of blood in the descending aorta for the four subjects. (Bottom Right) Estimated conductivity change in percentage relative to the conductivity at the onset of flow calculated with the measured reduced average velocity in the descending aorta. Subject 1: crosses; subject 2: diamonds; subject 3: circles; subject 4: dots.

conductivity changes due to blood flow. This simulated slice impedance, in turn, was used to calculate simulated SACs with (5.6). The value of the conductivity in (5.6) was taken as $\sigma = 7.41 \times 10^{-3}$ Scm^{-1}. This corresponds to a resistivity of blood of ρ = 135 Ωcm. This value was used in chapter 2 for the following reason. For male subjects the value of the resistivity[13] of blood in the absence of flow is generally taken as ρ = 150 Ωcm. However, we assumed that the resistivity of flowing blood decreases by about 10%, resulting in a value of the resistivity of blood of ρ = 135 Ωcm. With the simulated SACs we calculated aortic volume changes, $\Delta V_{SIM}(t)$, for the four subjects, which include the error

[13] For female subjects sometimes different values are given in the literature, implying different plasma conductivity values and axis-ratio values in the theory on blood conductivity. Visser used blood of healthy donors and we assume that this includes both male and female donors. Therefore the value of the blood conductivity calculated in Appendix B is considered to hold for female subjects also.

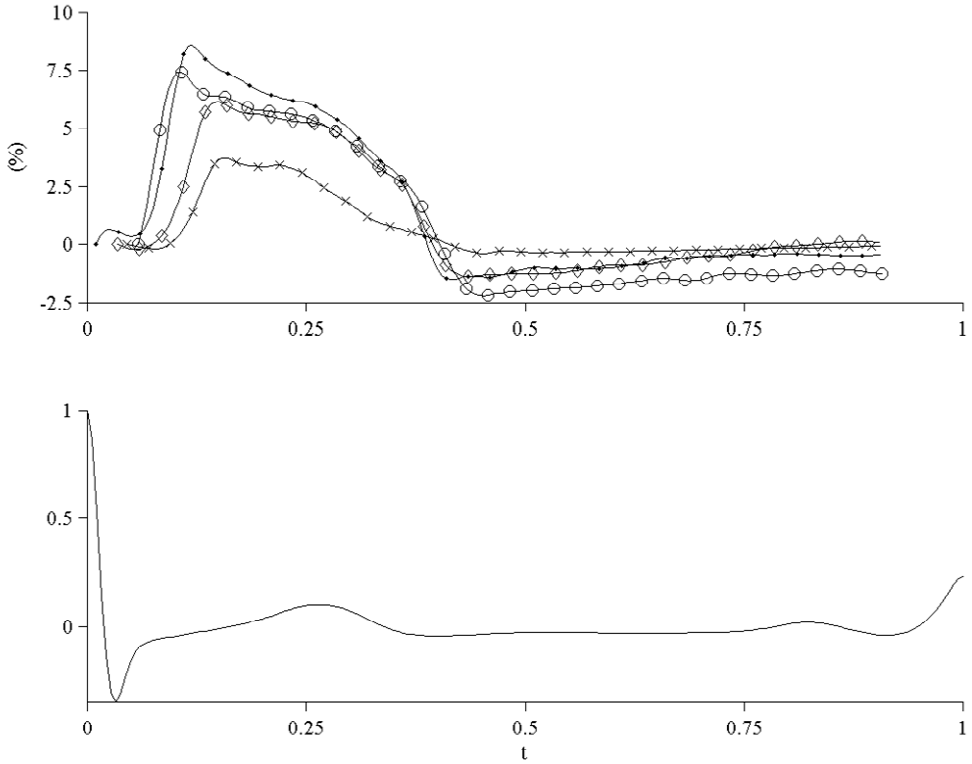

Figure 4. (Top) Relative difference between measured aortic volume changes with MR and simulated aortic volume change (subject 1: crosses; subject 2: diamonds; subject 3: circles; subject 4: dots). (Bottom) Normalized ECG recording.

introduced by disregarding the conductivity change of blood. Comparing $\Delta V_{SIM}(t)$ with the experimentally measured volume change of the aorta, $\Delta V_{MRI}(t)$, allows an estimation of this error. Figure 4 shows the estimation error in terms of percentage of the total volume of the aorta [i.e. $\{\Delta V_{SIM}(t)-\Delta V_{MRI}(t)\}/\{V_{MRI}(t_0)+\Delta V_{MRI}(t)\}$]. This figure shows that the maximum error in estimating the volume change of the aorta introduced by disregarding the conductivity change of blood ranges during systole from 3% for the older subject to 9% for the younger subjects, and is between -0.75% and -2.5% during diastole.

With the measured EI signals and (5.6), we calculated EI SACs [$\Delta A_{EI}(z_i,t)$] that can be compared to the simulated SACs [$\Delta A_{SIM}(z_i,t)$]. Figures 5 and 6 show these results for the male and female subjects, respectively. These maps were obtained by interpolating the SACs between slices using the spline interpolation function provided by the software package MATLAB. This resulted in a time resolution of 5 ms and a spatial resolution of 0.10 cm. The top row in

figure 5 shows the maps for subject 1 and second row for subject 2. The first column from the left presents the EI SACs measured at the mid-axillary line on the right-hand side (MAR), the second column for the mid-clavicular line on the right-hand side (MCR), the third column for the sternal line (STE), the fourth column for the mid-clavicular line on the left-hand side (MCL), and the fifth column for the mid-axillary line on the left-hand side (MAL). Finally the last column gives the maps of $\Delta A_{SIM}(z_i,t)$. In each figure the horizontal axis represents the time normalized to the length of the cardiac cycle. The vertical axis gives the location on the thorax, where the origin is at the level of the xiphoid process. The SACs are coded in color, with yellow and white representing large positive SACs, red representing small positive to no SACs, and black representing negative SACs. The bottom row shows, as an example, a (normalized) ECG recording of one subject. Likewise, figure 6 presents the mappings for the female subjects (top row for subject 3 and second row for subject 4). No measurements on the mid-clavicular lines were conducted on females for reasons of anatomy.

Comparing the EI results for the different subjects shows that on the sternal lines the maps are consistently very similar, apart from small differences between subjects in magnitude of the SACs. On the sternal line the influence of the heart is clearly present (a negative SAC) in the region z = 0 (cm) to z = 10 (cm), whereas above this region a large positive SAC occurs. The sternal map of the old male (top row in figure 5) differs somewhat in magnitude of the SACs, but still a positive SAC above the region of the heart can be observed and a small negative SAC on the mid-clavicular line on the left-hand side. The maps at both mid-axillary lines show rather large differences between male and female subjects. On the mid-axillary lines the largest positive SAC occurs above z = 15 (cm) for the young male (second row in figure 5), possibly due to the clavicular arteries. For the old male (top row in figure 5) the SACs are much smaller. For the female subjects (figure 6) the largest positive SAC measured at the mid-axillary lines occurs between z = 5 (cm) and z = 15 (cm). Furthermore, this SAC is most pronounced on the right-hand side of the thorax. As to the origin of this SAC we can only guess, but the difference between left and right might indicate that the vena cava might be responsible. The heart must be ruled out as a possible source, as the positive SAC occurs during systole when the

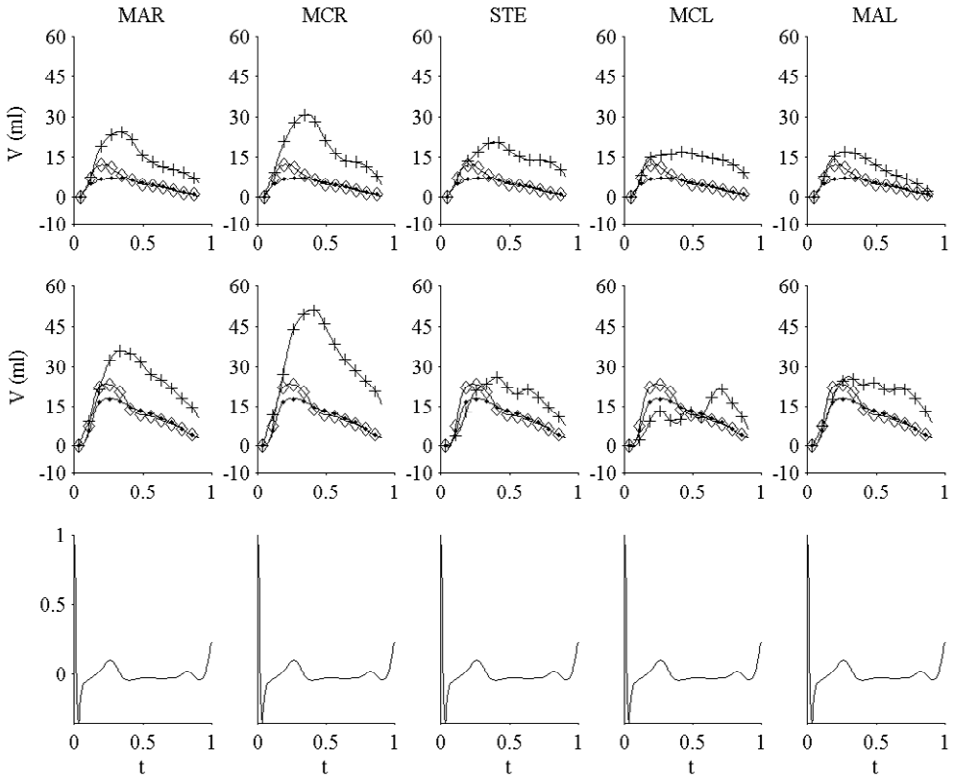

Figure 7. Volume changes for the male subjects. The top row gives the results for subject 1 and the second row for subject 2. $\Delta V_{MRI}(t)$: dots; $\Delta V_{SIM}(t)$: diamonds; $\Delta V_{EI}(t)$: crosses. The bottom row gives examples of an ECG.

heart contracts, which would have resulted in a negative SAC. The difference in the SACs measured at the mid-clavicular lines between the young male and old male, may only be a difference in magnitude of the SACs (probably due to less elasticity of the vessels because of age).

A comparison of the EI SAC mappings with the simulated SAC mappings shows generally no convincing resemblance between these mappings. This indicates that the aorta can not be considered to be the major source of the EI signal, when it is measured on the front of the thorax. This is confirmed when figures 7 and 8 are inspected. These figures show the results when for each moment in time the volume change are calculated with (5.7), i.e. integrating the data shown in figures 5 and 6 along the z-axis. For each subject the integration region was chosen to equal the full length of the aorta in the thorax, i.e. the length of the map showing $\Delta A_{SIM}(z_i,t)$. The results are presented in figures 7 and 8 for the male and female subjects, respectively. The lines with dots in these figures represent volume change of the aorta measured with MRI, $\Delta V_{MRI}(t)$. The

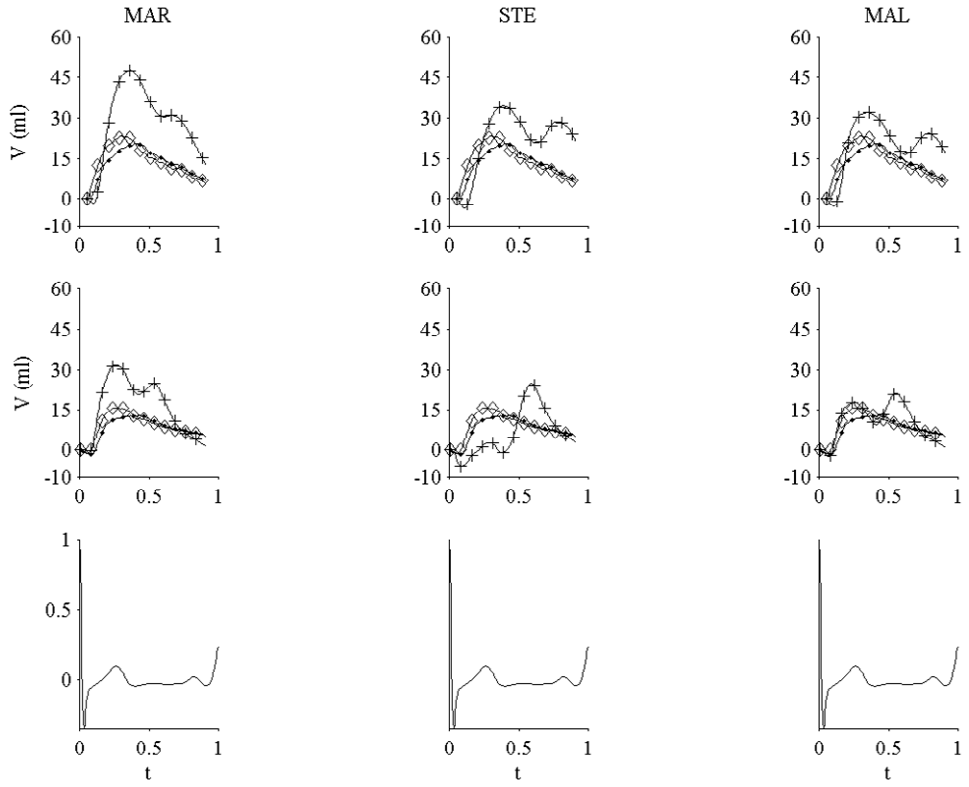

Figure 8. Volume changes for the female subjects. The top row gives the results for subject 3 and the second row for subject 4. $\Delta V_{MRI}(t)$: dots; $\Delta V_{SIM}(t)$: diamonds; $\Delta V_{EI}(t)$: crosses. The bottom row gives examples of an ECG.

lines with diamonds give the estimated aortic volume change obtained from the simulated SACs, $\Delta V_{SIM}(t)$. Finally, the lines with crosses show the volume change measured with EI, $\Delta V_{EI}(t)$.

Remember that in calculating the EI volume change, $\Delta V_{EI}(t)$, the blood conductivity is assumed to be time-independent. Consequently, if blood conductivity in reality does change with time, an error is introduced by disregarding this conductivity change. The simulated volume changes, $\Delta V_{EI}(t)$, estimate this error. If aortic volume change is the only source of the EI signal measured across the front of the thorax, the lines with crosses in figures 7 and 8 should coincide with the lines with dots. However, if both aortic volume change and blood conductivity change are the sources of the thoracic EI signal, the lines with crosses and the lines with diamonds should coincide. On inspection it can be seen that neither is true and this seems to indicate that the EI signal measured across the front of the thorax contains contributions from other sources, apart from aortic volume change and blood conductivity change.

Moreover, the contribution of other sources to the EI signal seems to differ greatly, depending on the location of the voltage pick-up electrodes. Measuring $\Delta V_{EI}(t)$ at the mid-axillary line on the left-hand side of the thorax (MAL), appears to show closest correspondence to $\Delta V_{SIM}(t)$, and thus might indicate that the aorta is a major source of the EI signal. This does not hold, however, for the other lines. Especially the lines at the right-hand side of the thorax (both the mid-axillary lines and the mid-clavicular lines) indicate that the aorta is only a minor source of the EI signal, even if the error due to assuming a constant conductivity of blood is accounted for. It seems that on these lines the aorta accounts for only 30%-50% of the EI signal. The results for the sternal lines and the mid-clavicular lines on the left hand side show great differences between the subjects. This can be understood by realizing that the total volume change is the sum of a negative SAC (for z = 0-10 cm) and a positive SAC (for z > 10 cm). Depending on the relative magnitude of these contributions, $\Delta V_{EI}(t)$ is either larger or smaller than $\Delta V_{MRI}(t)$ and $\Delta V_{SIM}(t)$. Consequently, any correspondence between $\Delta V_{EI}(t)$ and $\Delta V_{MRI}(t)$ or $\Delta V_{SIM}(t)$ in this region would be a matter of coincidence.

Discussion

The aim of this study was: a) to estimate the accuracy of an aortic volume change estimator that neglects the conductivity change of blood; b) to determine the relative contribution of the aorta to the thoracic EI signal; c) to investigate the sensitivity of a linear electrode array, in order to determine a region on the thorax where the aorta as the major source may be picked up by the electrodes.

To estimate the accuracy of the estimator developed in chapter 2, in four healthy subjects MR cine images of the aortic cross-sectional surface area were recorded and MRI measurements of the blood flow velocity in the ascending and descending aorta were conducted. These measurement results were combined with a theory on the conductivity change of blood that was developed in chapter 4. This theory was developed assuming a stationary and laminar flow profile in a rigid tube (Poiseuille flow). In-vivo, however, the flow profile is much

more erratic and surely not stationary. Still the theoretical model may be considered to give an upper bound of the conductivity change in-vivo. To understand this consider the following. If at a certain time t in the cardiac cycle the average flow velocity is $\langle v(t) \rangle$ and the radius of the aorta is $R(t)$, then inserting these values into the model gives the conductivity change, had the flow been a fully developed stationary and laminar flow. In this case the red blood cells would have been in an equilibrium state, either rotating, fully aligned or in a transition from rotating to aligned, cf. chapter 4. Additionally, they would have been deformed to some extent, depending on the magnitude of the average flow velocity. In-vivo the flow is not laminar and stationary and this deviation results in some red blood cells that are not fully aligned or less deformed. The less stationary and laminar the flow, the less aligned or deformed the red blood cells, which in turn will result in smaller conductivity changes, as an equilibrium state is never reached. Thus by calculating the theoretical conductivity change for each moment in the cardiac cycle, assuming a fully developed stationary and laminar flow[14], an upper bound of the conductivity change is established. Figure 3 shows that this quasi-stationary approach results in a maximum theoretical conductivity change for young subjects of roughly 9% in the ascending aorta, and 11% in the descending aorta. The conductivity change of blood for older subjects is much smaller (roughly one third of the conductivity change for young subjects). This is due to the smaller magnitude of the reduced average velocity. The resulting error in estimating the aortic volume with an estimator that neglects the conductivity change of flowing blood ranges from 3% for older subjects to 9% for younger subjects.

To determine the contribution of the volume changes of the aorta, both EI signals and MR cine-images were recorded at different locations on the thorax. From the measured MRI data the volume change of the aorta in the thorax was determined. Furthermore, together with the estimated conductivity change, the measured MRI data allowed simulation of EI signals that would have been produced, had the volume change of aorta and blood conductivity change been the only sources. From these simulated EI signals simulated SACs were

[14] This can be considered as a quasi-stationary approach.

calculated that can be compared to SACs obtained from EI signals measured on different lines on the thorax, as is done in figures 5 and 6. These figures show clearly that the aorta is not the only source of the thoracic EI signal. This was established earlier in chapter 2, where similar mappings where made showing that the EI signal also contains contributions of the vena cava and carotid arteries. Furthermore, contributions of the cross-sectional surface area change of the heart were found when measuring the EI signal on the mid-clavicular lines between z = 0 (cm) and z = 10 (cm). In that earlier study however, the EI signals were measured on the left-hand and right-hand side of the thorax simultaneously and therefore no distinction could be made between these sides. In the current study, on the other hand, EI signals were measured on both sides separately and on the sternal line in addition, showing that the contribution of the heart occurs at the sternal line and the mid-clavicular line on the left-hand side of the thorax only. This can be expected as the heart is located slightly left of the sternum. The SAC maps measured on the other lines show large differences between the subjects. No close correspondence is found with the maps showing the simulated SACs of the aorta, with the possible exception of the mid-axillary lines on the left-hand side. This latter correspondence, however, is very weak.

Figures 7 and 8 show for the male and female subjects, respectively, the total volume change of the aorta in the thorax measured with MRI (line with dots), calculated from the simulated SACs (lines with diamonds) and calculated with EI (lines with crosses). These figures show clearly that the volume change calculated with EI is generally of larger magnitude than that measured with MRI. This is especially true when EI is measured on the right side of the thorax at the mid-axillary line (MAR) and mid-clavicular line (MCR). This is mainly due to the contribution to the EI signal of other sources than the aorta. The assumption of time-independence of the blood conductivity introduces an error that leads to overestimation of the volume change in the thorax, but this error is not large enough to account for the difference between the aortic volume change measured with MRI and the volume changes measured with EI. For the right-hand side of the thorax, the magnitude of this latter volume change is about twice to thrice the magnitude of the volume change measured with MRI. The error due to disregarding conductivity change only accounts for an

overestimation of the volume change by at most 10%. It is worth noticing that for the male subjects (figure 5) at the mid-axillary lines, a relatively large positive SAC is found for z > 20 cm. This seems to confirm results reported in Patterson et al. (1990) that about 22% of the EI signal is contributed above the suprasternal notch. As the authors stated, this suggests contributions form the carotid arteries and the jugular veins.

For the sternal line (STE) and the left mid-clavicular line (MCL) the EI impedance signal is the sum of a positive and a negative SAC. Consequently the contribution of the heart (negative SAC) cancels part of the large positive SAC (probably due to aorta, vena cava and possibly also the pulmonary artery) above the heart. As a result, the volume change measured with EI is sometimes larger and sometimes smaller than the aortic volume change measured with MRI. Clearly any correspondence in this region does not reflect that the aorta is the major source. It only reflects that multiple sources cancel each other out and possibly as a coincidence the total EI volume change corresponds in some cases to the aortic volume change. These results may help to understand earlier findings, cf. Patterson et al. (1993). In that study an increase of CO measured with EI - using electrodes applied at the sternum - was observed when subjects changed their position from supine to sitting. This is opposite to the change that was expected (a decrease of CO of approximately 30%). The change of position may have resulted in a downward movement of the heart. This in turn could have resulted in a smaller relative contribution of the heart, such that it no longer dominated the contributions of the aorta, vena cava and possibly also the pulmonary artery.

The mid-axillary lines on the left side of the thorax (MAL), however, show close correspondence for two subjects between the EI volume change and the MRI volume change, whereas for the two other subjects the EI volume change is somewhat larger, but not as large as for the MAR and MCR lines. It would be tempting to conclude that at the MAL lines the aorta is the major source of the EI signal, were it not that the SAC mappings do not fully support this conclusion. Although the resemblance between the mappings of $\Delta A_{EI}(z_i,t)$ for the MAL lines and $\Delta A_{SIM}(z_i,t)$ is closer than for the other lines, the correspondence is too weak to draw definite conclusions.

The results so far have shown that the contributions of the different sources to the EI signal change tremendously between different subjects and depend greatly on the measurement location on the circumference of the thorax. This brings us to the last aim of the present paper, namely to investigate the sensitivity of different electrode arrays in order to determine a region where the aorta may be picked-up as a major source of the EI signal. Although no definite conclusion can be drawn from the results presented above, it might be suggested that an electrode array located on the MAL line has the best chance to pick-up the aorta as the major source of the EI signal. This might be explained by the anatomy of the thorax. The descending aorta is located somewhat left of the spine at the back of the thorax. As a result the MAL line is closest to the aorta and relatively far from other possible sources. Possibly an electrode array applied at the back of the thorax would even be more sensitive to aortic volume changes, especially of the descending aorta.

It should be noted that the difference in sensitivity between the different electrode arrays complicates matters considerably, as it means that the thorax can not be represented by the parallel cylinder model (or series model in terms of admittances). From this model it follows that the potential distribution on the circumference of the thorax should be independent of the measurement location on that circumference. Even if the electrical model of the thorax is extended to a model containing multiple sources - with the sources considered as lumped circuit elements connected in parallel - the potential distribution should not depend on the measurement location on the circumference of thorax. Consequently, such an extended electrical model could only be regarded as a first order approximation, as was already discussed in chapter 2. However, the results presented in our previous study, as well as the present study, show surprising consistency and sometimes estimated volume changes show close correspondence to volume changes measured with MRI. Furthermore, the results can be helpful to interpret results from both experimental and modeling studies found in the literature. Further research may help to better understand the relative contribution of different organs the thoracic EI signal.

Conclusion

If EI cardiography is to be an accurate non-invasive method to measure CO, it has to be established that volume changes of the aorta are the major source of the thoracic EI signal. One of the possible other sources is the conductivity change of blood due to blood flow. From the results presented here, it may be concluded that neglecting this conductivity change, introduces a relatively small error of less than 10% in volume change estimation. Additionally, this study seems to show that, although the EI signal measured across the front of thorax may contain important cardio-vascular information, the aorta is not the major source. However, from the investigated electrode arrays, the array applied on the left mid-axillary line of the thorax seems to have the best chance of picking up the aorta as the major source of the EI signal.

Appendix A

The specifications of the MRI method used for cine imaging and flow mapping are listed below. The MRI scanner was a 1.5 Tesla Siemens 'Sonata' whole body system (Siemens Medical Systems, Erlangen, Germany). A phased-array body coil with 4 elements was used as receiver. Image acquisition was prospectively triggered by the R wave of the ECG.

MRI cine imaging was performed with a 2-dimensional Steady State Free Precession pulse sequence. This sequence is also denoted as 'Fast Imaging with Steady State Precession with balancing gradients in all spatial orientations' or 'True-FISP':

Flip angle	60 deg
Echo time	1.72 ms
Number of k_y lines per heartbeat	8
Temporal resolution	13.8 ms (echo-shared)
Phase-encoding direction	anterior-posterior
Field of view	220 x 350 mm
Acquisition matrix	120 x 256 pixels
Acquisition pixel size	1.8 x 1.4 mm
Slice thickness	8 mm
Receiver bandwidth	1085 Hz/pixel

MRI phase-contrast velocity quantification was performed with a 2-dimensional gradient-echo sequence, sensitive for through-plane flow:

Flip angle	15 deg
Echo time	4.8 ms
Number of k_y lines per heartbeat	1
Temporal resolution	22 ms
Phase-encoding direction	anterior-posterior
Field of view	250 x 400 mm
Acquisition matrix	160 x 256 pixels
Acquisition pixel size	1.6 x 1.6 mm
Slice thickness	5 mm
Receiver bandwidth	190 Hz/pixel
Velocity sensitivity	150 cm/s

Appendix B

Based on the Maxwell-Fricke theory that gives the conductivity of a suspension of ellipsoids in an electrolyte the conductivity of flowing blood, say σ_{bl}, under conditions of Poiseuille flow can be written as (see chapter 4)

$$\sigma_{bl} = \frac{2}{R^2}\left\{\int_0^{r_1} \sigma_{<} r dr + \int_{r_1}^{r_2} \sigma_{<>}(r) r dr + \int_{r_2}^{R} \sigma_{>}(r) r dr\right\} \tag{B.1}$$

where R is the radius of the blood-filled tube and

$$\sigma_{<} = \sigma_p \frac{1-H}{1+\{C_{<}-1\}H} \tag{B.2}$$

where σ_p = 1.57 (Sm^{-1}) is the conductivity of plasma and H is the hematocrit expressed as a fraction and with

$$C_{<} = \frac{1}{2}\{C_b + C_r\} \tag{B.3}$$

where

$$C_r = \frac{1}{3}(C_a + 2C_b) \tag{B.4}$$

and

$$C_a = \frac{1}{M} \text{ and } C_b = \frac{2}{2-M} \tag{B.5}$$

Furthermore, if a_0 and b_0 (4 μm) are, respectively, the short and long axes of an undeformed red blood cell then

$$M(a<b)=\frac{\varphi-\frac{1}{2}\sin(2\varphi)}{\sin^3(\varphi)}\cos(\varphi) \tag{B.6}$$

with

$$\cos(\varphi)=\frac{a_0}{b_0} \tag{B.7}$$

This initial axis ratio was assumed to be $a_0/b_0 = 0.38$.

Additionally,

$$\sigma_{>}(r)=\sigma_p\frac{1-H}{1+\{C_{>}(r)-1\}H} \tag{B.8}$$

with

$$C_{>}=C_b \tag{B.9}$$

and

$$\cos\{\varphi(r)\}=\frac{a_d(r)}{b_d(r)}=\left\{1+\frac{b_0}{4\mu}\tau(r)\right\}^{-3}\frac{a_0}{b_0} \tag{B.10}$$

where $a_d(r)$ and $b_d(r)$ are, respectively, the short and long axes of the deformed red blood cells, and μ = 1,5 x 10^{-5} Nm^{-1} is the surface shear modulus of the red blood cell membrane. Furthermore, $\tau(r)$ is the shear stress and is determined from the measured reduced average velocity, say $\langle v\rangle/R$, by the following equation,

$$\tau(r)=4\eta_{bl}\frac{\langle v\rangle}{R}\frac{r}{R} \tag{B.11}$$

Where η_{bl} is the viscosity of blood and is given by

$$\eta_{bl} = \eta_{pl}\left\{1 + 2.5H + 7.37\times10^{-2}H\right\} \tag{B.12}$$

Finally,

$$\sigma_{\langle\rangle}(r) = \frac{1-H}{1+\left\{C_{\langle\rangle}(r)-1\right\}H} \tag{B.13}$$

for $r_1 \le r < r_2$ and with

$$C_{\langle\rangle}(r) = \frac{\left\{C_b(r) + f(r)C_r(r)\right\}}{1+f(r)} \tag{B.14}$$

where $f(r)$ is a linear weighting function given by

$$f(r) = \frac{\tau(r)-\tau(r_2)}{\tau(r_1)-\tau(r_2)} \qquad \text{for } r_1 \le r \le r_2 \tag{B.15}$$

that expresses that the fraction of randomly oriented RBCs linearly decreases as a function of $\tau(r)$. With (B.4)-(B.5) and (B.10)-(B.12) $C_r(r)$ and $C_b(r)$ in (B.14) are determined.

Chapter 6 Towards a Solution of the Outflow-problem in Electrical Impedance Cardiography

An Alternative to Kubicek's Approach

T.J.C. Faes; A.E. Hoetink; H.J.J. Kerkkamp; R.M. Heethaar

Medical & Biological Engineering & Computing (Submitted)

Summary

Electrical Impedance Cardiography (EIC) is a plethysmographic technique to measure cardiac stroke volume from recordings of trans-thoracic electrical impedance; special formulae (Bonjer-Nyboer, Kubicek, Sramek, Bernstein) provide means to calculate stroke volume from impedance tracings. The formulae of Kubicek, Sramek, Bernstein use the time-derivative of impedance in order to compensate for the outflow-problem (an arterial runoff of blood from the aorta during systole); an approach of which the validity was questioned previously. This study aims: i) to develop a new formula that accounts for the outflow-problem, and ii) to evaluate, in mathematical simulations, the accuracy of this formula in comparison to Bonjer-Nyboer-Kubicek-Sramek-Bernstein formulae. A three-element Windkessel model and a two-element cylinder model were used to analyse and simulate thoracic-impedance changes in relation to cardiac activity. A formula taking into account the outflow was developed. Simulation results showed that this outflow-corrected formula was: i) accurate under a wide range of physiological circumstances and; ii) superior in comparison to the Bonjer-Nyboer-Kubicek-Sramek-Bernstein approach. *Conclusion:* 1) The accuracy of a newly developed outflow-corrected formula to calculate stroke volume from thoracic impedance recordings was demonstrated in simulations. 2) The first-derivative-approach of Kubicek-Sramek-Bernstein was found to be highly inaccurate.

Introduction

Electrical Impedance Cardiography (EIC) is a plethysmographic technique developed to measure cardiac stroke volume and cardiac output from recordings of trans-thoracic electrical impedance. Trans-thoracic electrical impedance, commonly recorded from electrodes positioned at the neck and the lower side of the thorax, shows small fluctuations synchronously with the cardiac cycle. Stroke volume and cardiac output are calculated from these impedance recordings by using specially developed formulae [reviews in *e.g.* Geddes & Baker (1989), Sherwood et al. (1990), Patterson (1995), Moruccie et al. (1996), Hayes (1997)].

After the first observations of variations in trans-thoracic electrical impedance synchronously with the cardiac cycle, in the first half of the twentieth century, many attempts were made to utilise these impedance changes for non-invasive measurement of cardiac function. For many years, the following line of reasoning dominated the field. Due to the contraction of the cardiac ventricles, blood flows from the heart into the systemic and pulmonary arteries and, as a consequence of this, the volumes of the ventricles and major arteries change. These volume changes produce small changes of the trans-thoracic electrical impedance, because the conductivity of blood is slightly higher than the conductivity of the thoracic organs [Faes et al. (1999b)]. Thus thoracic impedance recordings reflect volume changes in the circulatory system, making impedance cardiography indeed a plethysmographic method. For that reason, the crucial problem in electrical impedance cardiography is having to relate the actually measured impedance changes (Ohm) to the originating volume changes (litre), and in particular stroke volume.

In the late forties of the last century, Bonjer and Nyboer provided a simple formula to relate a measured impedance change ΔZ (Ohm) to a volume change ΔV (ml),

$$\Delta V = \rho_{bl} \frac{L^2}{Z_0^2} \Delta Z_0 \qquad (6.1)$$

which holds for a cylindrical conductor with length L (cm), basal impedance Z_0 (Ω), and electric resistivity of the cylinder material ρ_{bl} (Ω cm) [Nyboer (1950); Nyboer (1970) and Bonjer (1950) (1950)]. Experiments were conducted to establish the usefulness of this formula in calculating cardiac stroke volume from impedance recordings. Results were, however, disappointing, and, as a consequence, both Bonjer and Nyboer turned their attention away from the topic [Lamberts, Visser, & Zijlstra (1984), p. 17].

In the mid-sixties of the last century, progress in space travel created an urgent need for a practical non-invasive method for measuring cardiac output. Patterson, as PhD-student, and Kubicek reinvestigated the idea of electrical impedance plethysmography and established a break-through with what is nowadays known as the Kubicek-formula [Patterson et al. (1964); Patterson (1965) and Kubicek et al. (1966)]. The modification was the replacement of the term ΔZ in the Nyboer-Bonjer formula with a term consisting of the maximum value of the first derivative to time of the impedance $Z_0(t)$, *i.e.* $(dZ_0/dt)_{MAX}$, times the left ventricular ejection time T_{LVE} (s). The Kubicek-formula reads:

$$\hat{V}_K = \rho_B \frac{L^2}{Z_0^2} \left(\frac{dZ_0(t)}{dt} \right)_{MAX} T_{LVE} \tag{6.2}$$

where $\hat{V}_K$ (ml) is the 'Kubicek-estimate' of stroke volume V_S, while ρ_{bl} (Ωcm) is the electric resistivity of blood, L (cm) is the distance between the impedance measuring electrodes, and Z_0 (Ω) is the basal thoracic electric impedance. Later on Bernstein, using ideas of Sramek [Sramek (1981) and Sramek, Rose, & Miyamoto (1983)], elaborated Kubicek's equation into the form

$$V_S = \frac{\delta}{4.25} \frac{(0.17H)^3}{Z_0} \left(\frac{dZ_0(t)}{dt} \right)_{MAX} T_{LVE} \tag{6.3}$$

where H is the physical height of the subject being investigated and δ is factor obtained from a nomogram [Bernstein (1986)].

The essential difference between the equations of Nyboer-Bonjer and Kubicek-Patterson is the replacement of the term ΔZ_0 in the former by the term

$(dZ_0/dt)_{MAX}T_{LVE}$ in the latter. A replacement copied, later on, by Sramek and Bernstein into their equations. This replacement was interpreted as a solution for the so-called 'outflow-problem' [*e.g.*: Geddes & Baker (1989) and Sherwood et al. (1990)]. This problem refers to the difficulty in finding a relationship between the aortic volume changes and the stroke volume actually pumped from the left ventricle into the aorta. That is, the thoracic impedance changes are considered to be mainly the result of volume changes of the aorta, and these aortic volume changes are, in turn, the combined result of blood entering the aorta from the left ventricle, as well as blood leaving the aorta due to further arterial runoff Geddes & Baker (1989). Thus, it was recognized that the systolic increase of the aortic volume is less than the stroke volume actually ejected by the ventrical. In order to calculate stroke volume from aortic-volume-mediated thoracic impedance changes, the equations should adequately deal with this systolic outflow of blood due to arterial runoff. The $(dZ_0/dt)_{MAX}T_{LVE}$ -approach was, quite generally, thought to adequately deal with the outflow problem [Geddes & Baker (1989) and Sherwood et al. (1990)] and has been applied, to our knowledge, ever since, in almost all applications of impedance cardiography.

Nevertheless, the $(dZ_0/dt)_{MAX}T_{LVE}$ –approach to the outflow-problem was questioned in a series of three papers by Yamakoshi and Ito. In an experimental study using expansible tubes, Yamakoshi reached the conclusion that Nyboer's equation accurately estimated stroke volume in case of a zero outflow (occluded tube), while stroke volume was underestimated in case of a non-zero outflow (non-occluded tube). For the $(dZ_0/dt)_{MAX}T_{LVE}$ –approach the conclusion is less univocal: Yamakoshi studied both sinusoidal and pulsatile waveforms of aortic inflow and found that the $(dZ_0/dt)_{MAX}T_{LVE}$ –approach was only accurate in case of the pulsatile waveform. Therefore, he concludes with: "(...) it seems to be probable that the waveform of the (...) inflow might be one of the important factors affecting the value of stroke volume calculation." [Yamakoshi et al. (1976), pp. 371]. In an accompanying paper on artificially perfused dogs which involved the same sinusoidal and pulsatile waveforms, Ito and Yamakoshi come to the same conclusion regarding the performance of Nyboer's and Kubicek's equations. Again, they stress the point that stroke volume obtained with Kubicek's formula is "(...) greatly affected by the frequency component of the

transthoracic impedance wave (...). Therefore, the main determinants of the working range of Kubicek's method should be the frequency characteristics of the blood vessels (...), the rate of blood flow into the aorta and the Fourier spectrum of the rising phase of the transthoracic impedance wave" [Ito, Yamakoshi, & Yamada (1976), pp 376-377]. Shortly later, Yamakoshi indeed demonstrated the importance of the waveform by both mathematical simulations as well as experiments on animals. He found that the $(dZ_0/dt)_{MAX}T_{LVE}$ –approach was sensitive to the rise- and fall-time of aortic flow, leading to both serious over- and underestimation of stroke volume by Kubicek's equation [Yamakoshi, Togawa, & Ito (1977)]. Many years later, we draw attention to the same problem by showing, both theoretically and experimentally, that the outflow problem was not solved with the $(dZ_0/dt)_{MAX}T_{LVE}$ term in the Kubicek-equation and Sramek-Bernstein equation [Faes et al. (1999a) and Faes et al. (2001)]. In our opinion, these results may indicate that the outflow problem in impedance cardiography is not solved with the $(dZ_0/dt)_{MAX}T_{LVE}$ –approach.

Therefore, the *aim of this study* is to reinvestigate the outflow problem and to show that the outflow problem may be solved with

$$\hat{V}_S \approx \frac{1}{1-\frac{T_{LVE}}{T_I}} \frac{\rho_{bl} L^2}{Z_o^2} \Delta Z \qquad (6.4)$$

where the right hand term closely resembles the original Nyboer-Bonjer equation (6.1) with an additional term, involving the left-ventricular ejection time T_{LVE} relative to the interbeat period T_I. Note that the additional term is: i) independent of the waveform and ii) substantial of size (typically 1.6 because T_{LVE} and T_I are 0.3s and 0.8s respectively, for a healthy resting subject. In this paper, we will derive this equation from a simple Windkessel model for the haemodynamics of the systemic circulation and a simple parallel cylinder model for the thoracic volume conductor. Moreover, we will establish the validity of our stroke-volume-formula in a simulation study.

Theory of Outflow Compensation

Approach

The rational of impedance cardiography is thought to lie in the following sequence of causes and effects; the sequence is outlined in (6.5). In systole, the left ventricle contracts, and, as a result, the left ventricular volume $V_V(t)$ decreases and blood starts to flow into the aorta $F_I(t)$. The stroke volume $V_S[k]$ is the amount of blood ejected from the ventricle during kth systole. Moreover, the aortic volume $V_A(t)$ increases; the change of the aortic volume depends on both the inflow into the aorta $F_I(t)$ and the outflow $F_O(t)$ form the aorta further into the arterial system. With this changing aortic volume $V_A(t)$, the longitudinal electrical impedance of the aorta $Z_A(t)$ changes, leading to a change of the measurable trans-thoracic impedance $Z_0(t)$. The final step in impedance cardiography, then, is to derive a formula that provides an estimate $\hat{V}_S[k]$ of left ventricular stroke volume from the measured thoracic impedance recordings $Z_0(t)$. Summarized, in a pseudo-formula:

$$\begin{array}{ccccccc} V_S[k] & & & & V_S[k] & & \\ \uparrow_{eq.\,6} & & & & \uparrow_{eq.\,8} & & \\ V_V(t) & \overset{eq.\,7}{\rightarrow} & \left.\begin{array}{l} F_I(t) \\ F_O(t) \end{array}\right\} & \overset{eq.\,10}{\rightarrow} & V_A(t) & \ldots & \\ \ldots & \overset{eq.\,16}{\rightarrow} & Z_A(t) & \overset{eq.\,17}{\rightarrow} & Z_0(t) & \overset{eq.\,25\text{-}27}{\rightarrow} & \hat{V}_S[k] \end{array} \qquad (6.5)$$

We will use simple models to describe the haemodynamics (“Windkessel”) and thoracic impedance (parallel cylinders), and to formulate explicitly the relations between the variables mentioned in (6.5) (the numbers refer to equations below). In order to derive a stroke-volume-estimator, we will first derive the dependence of $Z_0(t)$ on $V_S[k]$, and then take an inverse to obtain an estimator which provides $\hat{V}_S[k]$ as a function of $Z_0(t)$. This model-based approach finds

its roots in theories of parameter-estimation [Ljung (1987) and Söderström & Stoica (1989)]. Moreover, using the terminology developed there, we will call a formula to calculate stroke volume from impedance recordings, an estimator.

Note on the Notational Convention

We will use round and square brackets to distinguish between real and integer arguments of functions (i.e. variables). This notation emphasizes that a function with a 'square bracket argument' is of a constant value during each heart beat; e.g. the end-diastolic ventricular volume, $V_V(T_{ED}[k])$, is constant during the kth beat ($T_{ED}[k] < t < T_{ED}[k+1]$). Consequently, an integral of a square-bracketed function over a single beat is treated as a integral of constant.

In volume conductors, an inverse proportional relation exists between volume and impedance [e.g. see (6.16)], and, consequently, a volume increase results in an impedance decrease and vice versa. To facilitate an easier interpretation of impedance recordings as volume changes, most papers and textbooks show records of ΔZ and dZ/dt impedance waveforms upside down; then an impedance increase is related visually to a volume increase. Mathematically, the impedance tracings ΔZ and dZ/dt are multiplied with minus one, and, to maintain consistency, the minimum value of the dZ/dt signal is to be replaced by the maximum value of the $-dZ/dt$ signal. To avoid unnecessary bookkeeping of minus-signs, we will not follow this convention in the present chapter.

Model of Haemodynamics

Stroke Volume

Stroke volume is the amount of blood pumped out of the left ventricle per beat. In the normal heart, without regurgitation of blood due to mitral or aorta valve insufficiencies, stroke volume equals the ventricular volume change between end-diastole to end-systole. Let $V_V(t)$ be the left ventricular volume as a function of time, and let $T_{ED}[k]$ and $T_{ES}[k]$ be the time moments of end-diastole and end-systole of the kth heartbeat, respectively. Then stroke volume $V_S[k]$ is defined as,

$$V_S[k] = V_V\left(T_{ED}[k]\right) - V_V\left(T_{ES}[k]\right) \tag{6.6}$$

for the *k*th beat.

For further use it proves to be convenient to interrelate stroke volume to blood flow into the aorta. First we define aortic inflow. Let $F_I(t)$ be the time-dependent inflow of blood into the aorta from the left ventricle at the level of the aortic valve. Then, as a consequence of the physical principle of conservation of mass applied to an incompressible fluid in absence of a triscupidal valve insufficieny, the inflow $F_I(t)$ equals the left ventricular volume change $dV_V(t)/dt$ during the ejection phase, while $F_I(t)$ vanishes elsewhere in the cardiac cycle. That is,

$$F_I(t) = \begin{cases} -\dfrac{dV_V(t)}{dt} & \text{systole: } T_{ED}[k] \le t \le T_{ES}[k] \\ 0 & \text{diasystole: } T_{ES}[k] \le t \le T_{ED}[k+1] \end{cases} \tag{6.7}$$

where a minus-sign was included because a decrease of ventricular volume $V_V(t)$ results in a positive valued aortic inflow $F_I(t)$. Using this definition, it appears that stroke volume $V_S[k]$ is interrelate to aortic inflow as,

$$V_S[k] = \int_{T_{ED}[k]}^{T_{ES}[k]} F_I(t)\, dt \tag{6.8}$$

because,

$$\int_{T_{ED}[k]}^{T_{ES}[k]} F_I(t)\, dt \overset{\text{eq. 7}}{=} -\int_{T_{ED}[k]}^{T_{ES}[k]} \frac{dV_V(t)}{dt} dt = V_V\left(T_{ED}[k]\right) - V_V\left(T_{ES}[k]\right) \overset{\text{eq. 6}}{=} V_S[k] \tag{6.9}$$

where (6.6) and (6.7) where used as indicated. Note that, as a consequence of (6.7), the integration interval in (6.8) might be extended to the complete cardiac cycle, i.e. from $T_{ED}[k]$ to $T_{ED}[k+1]$.

Volume of the Aorta

Let $V_A(t)$ be the time-dependent volume of the aorta. Let $F_I(t)$ be the inflow of blood into the aorta from the left ventricle at the level of the aortic valve, and let $F_0(t)$ be the flow from the aorta further into the arterial system. Then, the aortic volume change is,

$$\frac{dV_A(t)}{dt} = F_I(t) - F_O(t) \tag{6.10}$$

by application of the physical principle of conservation of mass to an incompressible fluid. Note that $F_I(t)$ is defined at the anatomical site of the aortic valve, while $F_0(t)$ will be defined by the level of the lower sensing electrodes used in impedance cardiography.

Stroke Volume Estimators Using Aortic Volume

An estimator of stroke volume from aortic volume is easily found from (6.8) and (6.10) it follows that,

$$V_S[k] \overset{eq.\,8}{=} \int_{T_{ED}[k]}^{T_{ES}[k]} F_I(t)\,dt \overset{eq.\,10}{=} \int_{T_{ED}[k]}^{T_{ES}[k]} \frac{dV_A(t)}{dt}dt + \int_{T_{ED}[k]}^{T_{ES}[k]} F_O(t)\,dt \tag{6.11}$$

which gives stroke volume $V_S[k]$ in terms of hemodynamical variables $V_A(t)$ and $F_O(t)$.

In case we neglect the second term of the right side, we obtain a stroke volume estimator uncorrected for outflow, i.e.

$$\hat{V}_S[k] \overset{eq.\,8}{=} \int_{T_{ED}[\mathrm{k}]}^{T_{ES}[k]} \frac{dV_A(t)}{dt}dt = V_A\left(T_{ES}[k]\right) - V_A\left(T_{ED}[k]\right) \tag{6.12}$$

which is a mathematical formulation of the obvious results that the systolic volume change of an aorta occluded distally equals the stroke volume.

In order to develop an estimator which provides a correction for the outflow, we need to quantify in some way, in (6.11) the integral of the outflow $F_O(t)$ over the systole. Starting with the observation that the pulsatility of $F_O(t)$ is strongly reduced compared to $F_I(t)$, due to the windkessel-characteristics of the aorta (see simulation below), the mean value of $F_O(t)$ might be used as an estimate. Let $\bar{F}_O$ be defined as the mean of $F_O(t)$ over a complete cardiac cycle, then

$$\bar{F}_O \overset{\text{def.}}{=} \frac{1}{T_I[k]} \int_{T_{ED}[k]}^{T_{ED}[k+1]} F_O(t)\,dt \overset{\text{eq. 10}}{=} \ldots$$

$$\ldots = \frac{1}{T_I[k]} \int_{T_{ED}[k]}^{T_{ED}[k+1]} F_I(t)\,dt \;-\; \frac{1}{T_I[k]} \int_{T_{ED}[k]}^{T_{ED}[k+1]} \frac{dV_A(t)}{dt}\,dt = \ldots \tag{6.13}$$

$$\overset{\text{eqs. 7 \& 8}}{=} \frac{V_S[k]}{T_I[k]} \;-\; \frac{V_A\left(T_{ED}[k+1]\right) - V_A\left(T_{ED}[k]\right)}{T_I[k]} \;\approx\; \frac{V_S[k]}{T_I[k]}$$

where the first integral equals $V_S[k]$ as a consequence of (6.7) and (6.8), and where the term $V_A(T_{ED}[k+1]) - V_A(T_{ED}[k+1])$ vanishes because the end-diastolic volumes are assumed to be equal in consecutive beats (no interbeat accumulation of blood occurs in aorta). Thus, the mean outflow equals the stroke volume divided by the interbeat interval time $T_I[k]$.

Using this mean value estimate of $F_0(t)$ in the formula for the stroke volume estimator (6.11), yields

$$V_S[k] \overset{eq.\ 10\ \&\ 13}{=} \int_{T_{ED}[k]}^{T_{ES}[k]} \frac{dV_A(t)}{dt}\,dt \;+ \int_{T_{ED}[k]}^{T_{ES}[k]} \frac{V_S[k]}{T_I[k]}\,dt \;\approx \ldots$$

$$\ldots \approx \int_{T_{ED}[k]}^{T_{ES}[k]} \frac{dV_A(t)}{dt}\,dt \;+ \frac{T_{LVE}[k]}{T_I[k]}\; V_S[k] \tag{6.14}$$

where $T_{LVE}[k]$ is the left ventricular ejection time defined as the difference $T_{ES}[k] - T_{ED}[k]$. Collecting the terms with stroke volume $V_S[k]$ on the right side, provides an outflow corrected stroke volume estimator,

$$\hat{V}_S[k] = \frac{1}{1-\frac{T_{LVE}[k]}{T_I[k]}} \int_{T_{ED}[k]}^{T_{ES}[k]} \frac{dV_A(t)}{dt} dt = \ldots$$
$$\ldots = \frac{1}{1-\frac{T_{LVE}[k]}{T_I[k]}} \left(V_A\left(T_{ES}[k]\right) - V_A\left(T_{ED}[k]\right)\right) \quad (6.15)$$

Comparison of this outflow-corrected stroke volume estimator (6.15) with the uncorrected one (6.12) shows that the correction is obtained with the term in front, which depends on the left ventricular ejection time $T_{LVE}[k]$ relatively to the interbeat interval time $T_I[k]$. Thus, the longer the ejection time $T_{LVE}[k]$ is relatively the interbeat interval time $T_I[k]$, the larger the correction term. This is in agreement with intuition, because the volume leaving the aorta due to arterial runoff is larger with a longer duration of the systole.
Next, we have to apply this estimator to the model of thoracic impedance.

Model of Thoracic Impedance

We followed Geddes and Baker [Geddes & Baker (1989)] who amongst many others, use two cylinders to model the volume conductor properties of the thorax. One cylinder represents the time-dependent volume of the aorta, whereas the other represents the remaining thorax tissue which is assumed to be constant on the time-scale of several heart beats.

For the blood-filled aortic-cylinder: Let ρ_{bl} (Ωcm) be specific resistivity of blood, let L (cm) be the length and let $A_A(t)$ (cm^2) be the time-dependent aortic cross-sectional surface. Note that, the time-dependent aortic volume $V_A(t)$ (cm^3) of a cylinder equals L times $A(t)$. Then, the time-dependent impedance $Z_A(t)$ (Ω) is,

$$Z_A(t) = \frac{\rho_{bl} L}{A_A(t)} = \frac{\rho_{bl} L^2}{V_A(t)} \quad (6.16)$$

In a two-cylinder model, the aortic impedance and thoracic impedance are electrically connected in parallel. Hence, the time-dependent thoracic impedance $Z_0(t)$ (Ω) is

$$Z_0(t) = Z_T \,//\, Z_A(t) = \frac{1}{\frac{1}{Z_T} + \frac{1}{Z_A(t)}} \tag{6.17}$$

where we introduced // as a short hand notation for two resistors connected electrically in parallel. Additionally, note that in impedance cardiographic literature it is common to use the notion of impedance and notation of Z, while actually resistance (R) is meant. A consequence of this odd notation is that an impedance Z can be treated mathematically as a real number.

Impedance-Based Outflow-Corrected Stroke Volume Estimators

Estimators of stroke volume from impedance recording might be obtained directly by first rewriting (6.16) and (6.17) into an explicit form giving $V_A(t)$ in terms of $Z_0(t)$ and secondly substituting this explicit form into (6.15). We prefer an alternative and more tractable approach, in which $Z_0(t)$ is differentiated with respect to time.

From (6.16) and (6.17) it follows that $Z_0(t)$ is a composite function of $V_A(t)$, i.e.

$$Z_0(t) \;=\; Z_0(V_A(t)) \tag{6.18}$$

By applying the chain rule of differentiation to this composite function yields,

$$\frac{d\; Z_0\left(V_A(t)\right)}{dt} \;=\; \frac{d\; Z_0\left(V_A(t)\right)}{dV_A(t)} \;\; \frac{d\; V_A(t)}{dt} \tag{6.19}$$

and hence,

$$\frac{d\ V_A(t)}{dt} = \frac{1}{\frac{d\ Z_0\left(V_A(t)\right)}{dV_A(t)}}\ \frac{d\ Z_0\left(V_A(t)\right)}{dt} \tag{6.20}$$

which can be substituted into the estimators in (6.15). These equations show that the change of thoracic impedance and aortic volume are proportionally related by a calibration factor $dZ_0(V_A)/dV_A$ [cf. Faes et al. (1995)].

For the particular case of a two-cylinder model [(6.16) and (6.17)] the calibration factor is readily found. That is, using the chain-rule for differentiation again,

$$\frac{dZ_0\left(Z_A\left(V_A(t)\right)\right)}{dV_A(t)} = \frac{dZ_0\left(Z_A\left(V_A(t)\right)\right)}{dZ_A(t)}\ \frac{dZ_A\left(V_A(t)\right)}{dV_A(t)} = -\frac{Z_0^2(t)}{\rho_{bl}L_E^2} \tag{6.21}$$

because

$$\begin{aligned}\frac{dZ_0\left(Z_A\left(V_A(t)\right)\right)}{dZ_A(t)} &\overset{\text{eq. 17}}{=} \frac{d}{dZ_A(t)}\left(\frac{1}{Z_T}+\frac{1}{Z_A\left(V_A(t)\right)}\right)^{-1} = \ldots \\ \ldots &= \left(\frac{1}{Z_T}+\frac{1}{Z_A\left(V_A(t)\right)}\right)^{-2}\left(\frac{1}{Z_A\left(V_A(t)\right)}\right)^{2} \overset{\text{eq. 17}}{=} \frac{Z_0^2(t)}{Z_A^2(t)}\end{aligned} \tag{6.22}$$

and

$$\frac{dZ_A\left(V_A(t)\right)}{dV_A(t)} \overset{\text{eq. 16}}{=} \frac{d}{dV_A(t)}\left(\frac{\rho_{bl}L_A^2}{V_A(t)}\right) = -\frac{\rho_{bl}L_E^2}{V_A^2(t)} \overset{\text{eq. 16}}{=} -\frac{Z_A^2(t)}{\rho_{bl}L_E^2} \tag{6.23}$$

Now an impedance based stroke volume estimator corrected for outflow is found by substitution of (6.20) in (6.15)

$$V_S[k] \overset{eq.\ 15}{\approx} \frac{1}{1-\frac{T_{LVE}[k]}{T_I[k]}} \int_{T_{ED}[k]}^{T_{ES}[k]} \frac{1}{\frac{d\ Z_0\left(V_A(t)\right)}{dV_A(t)}}\ \frac{dZ_0(t)}{dt}\ dt \tag{6.24}$$

which for the particular case of a two-cylinder model [substitution of (6.21) into (6.24)] yields

$$\hat{V}_S[k] \approx -\frac{\rho_{bl} L_E^2}{1-\frac{T_{LVE}[k]}{T_I[k]}} \int_{T_{ED}[k]}^{T_{ES}[k]} \frac{1}{Z_0^2(t)} \frac{dZ_0(t)}{dt}\, dt \tag{6.25}$$

or by integration by substitution,

$$\hat{V}_S[k] \approx -\frac{\rho_{bl} L_E^2}{1-\frac{T_{LVE}[k]}{T_I[k]}} \left\{ \frac{1}{Z_0\left(T_{ED}[k]\right)} - \frac{1}{Z_0\left(T_{ES}[k]\right)} \right\} \tag{6.26}$$

Finally, this equation can be elaborated into a Nyboer-Bonjer-like-form (6.1),

$$\hat{V}_S[k] \approx -\frac{\rho_{bl} L_E^2}{1-\frac{T_{LVE}[k]}{T_I[k]}} \frac{\Delta Z_0[k]}{Z_B^2[k]} \tag{6.27}$$

where $Z_B[k]$ is a base impedance (e.g. $Z_0(t)$ averaged over a complete cardiac cycle) and $\Delta Z[k]$ is the impedance variation within the cardiac cycle. This elaboration starts from the observation that the variation $\Delta Z[k]$ is small compared to the base impedance Z_B of $Z_0(t)$ (typically, ΔZ is smaller than 5% of Z_B). Then, we define end-diastolic $Z_0(T_{ED}[k])$ and end-systolic $Z_0(T_{ES}[k])$ impedance in relation to the base impedance Z_B as (neglecting temporarily the running index k for notational brevity),

$$\begin{aligned} Z_0\left(T_{ED}\right) &\overset{\text{def}}{=} Z_B + \Delta Z_D = Z_B\left(1+\frac{\Delta Z_D}{Z_B}\right), \text{ with } 0 \le \frac{\Delta Z_D}{Z_B} \ll 1 \\ Z_0\left(T_{ES}\right) &\overset{\text{def}}{=} Z_B - \Delta Z_S = Z_B\left(1-\frac{\Delta Z_S}{Z_B}\right), \text{ with } 0 \le \frac{\Delta Z_S}{Z_B} \ll 1 \end{aligned} \tag{6.28}$$

Moreover, we define the impedance change $\Delta Z = Z_0(T_{ED}) - Z_0(T_{ES})$ and, consequently, $\Delta Z = \Delta Z_D + \Delta Z_S$. Applying a first order binominal approximation $(1 \pm \Delta x)^{-1} \approx 1 \mp \Delta x$ [Abramowitz & Stegun (1970), p. 15] to (6.28), yields

$$\frac{1}{Z_0(T_{ED}[k])} - \frac{1}{Z_0(T_{ES}[k])} \approx \frac{1}{Z_B}\left\{\left(1 - \frac{\Delta Z_D}{Z_B}\right) - \left(1 + \frac{\Delta Z_S}{Z_B}\right)\right\} = \ldots$$
$$\ldots = -\frac{\Delta Z_D + \Delta Z_S}{Z_B^2} = \frac{\Delta Z}{Z_B^2} \qquad (6.29)$$

Substitution of (6.29) into (6.26) results is (6.27). Note that it can be shown by direct substitution of (6.28) into (6.26) and a straightforward calculation, that the approximation in (6.27) and (6.29) is exact by choosing Z_B the geometrical mean, i.e. $Z_B = \sqrt{Z_0(T_{ED})\ Z_0(T_{ES})}$.

■

In conclusion (6.25)-(6.27) provide three mathematically equivalent forms of impedance based outflow-corrected stroke volume estimator.

Stroke Volume Estimators Uncorrected for Outflow

The formulae of Bonjer-Nyboer and Kubicek-Patterson are readily obtained in case the outflow-term is neglected.

In order to arrive at the uncorrected Bonjer-Nyboer formula (6.1) substitute successively (6.20) and (6.21) into (6.12). Now performing integration and then using (6.29) yields,

$$\hat{V}_S[k] \approx -\rho_{bl} L_E^2 \left\{\frac{1}{Z_0(T_{ED}[k])} - \frac{1}{Z_0(T_{ES}[k])}\right\} \approx -\frac{\rho_{bl} L_E^2}{Z_B^2[k]}\,\Delta Z_0[k] \qquad (6.30)$$

In contrast, Kubicek's equation is slightly more complicated to arrive at. A Taylor series approximation of $Z_0(t)$ is used around a yet arbitrary time moment T_M with $T_{ED} < T_M < T_{ES}$ (neglecting temporarily the running index k for notational brevity). That is,

$$\begin{aligned} T_{ED} &= T_M - \Delta T_D \\ T_{ES} &= T_M + \Delta T_S \end{aligned} \tag{6.31}$$

Hence, the left ventricular ejection time T_{LVE} defined as T_{ES} - T_{ED} equals ΔT_D $+\Delta T_S$. Then, Taylor's approximations are

$$\begin{aligned} &\frac{1}{Z_0(T_{ED})} = \frac{1}{Z_0(T_M - \Delta T_D)} \approx \ldots \\ &\ldots \approx \frac{1}{Z_0(T_M)} - \frac{1}{Z_0(T_M)^2}\frac{dZ_0(T_M)}{dt}\Delta T_D + \text{higher order terms} \\ &\frac{1}{Z_0(T_{ES})} = \frac{1}{Z_0(T_M + \Delta T_S)} \approx \ldots \\ &\ldots \approx \frac{1}{Z_0(T_M)} + \frac{1}{Z_0(T_M)^2}\frac{dZ_0(T_M)}{dt}\Delta T_S + \text{higher order terms} \end{aligned} \quad \sim \tag{6.32}$$

Hence, by substraction,

$$\begin{aligned} &\frac{1}{Z_0(T_{ED})} - \frac{1}{Z_0(T_{ES})} \approx \ldots \\ &\ldots \approx -\frac{1}{Z_0(T_M)^2}\frac{dZ_0(T_M)}{dt}\Delta T_{LVE} + \text{higher order terms} \end{aligned} \quad \sim \tag{6.33}$$

Finally, the time moment T_M need to be assigned between T_{ED} and T_{ES}. In case the higher order terms are neglected, one might use T_M in a way to maximize the first term in relation to all the higher order terms in order to improve the accuracy of this Taylor approximation. In Kubicek's approach T_M was used to maximize $dZ_0(t)/dt$, and consequently one can infer that the first of the higher order terms vanishes (as the derivative is zero for a maximum of a function). The third and higher order terms, however, are not a priori known. Hence, maximizing $dZ_0(t)/dt$ not necessarily improves accuracy of the Taylor approximation.

Successive substitution of (6.20) and (6.21) into (6.12), performing integration and then following Kubicek's approach by maximizing $dZ_0(t)/dt$ and

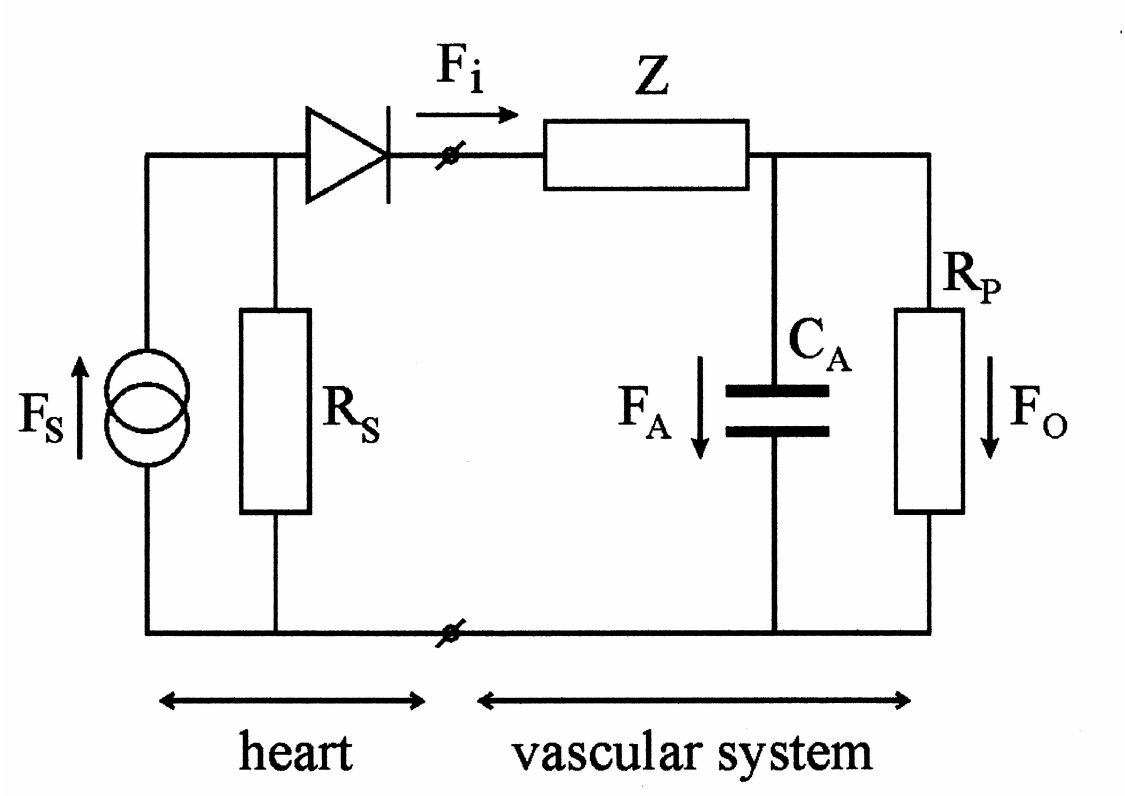

Figure 1. An electrical analogue of the cardio-vascular system.

neglecting all the higher order terms, (6.33) yields the Kubicek-Patterson equation,

$$\hat{V}_S[k] \approx -\frac{\rho_{bl} L_E^2}{Z_0(T_M)^2} \frac{dZ_0(T_{MAX})}{dt} T_{LVE} \tag{6.34}$$

where the notation $dZ_0(T_{MAX})/dt$ is used for the value of $dZ_0(t)/dt$ at time T_{max}.

Simulation Study

Methods

Cardiovascular System. An electrical analogue of the cardiovascular system is shown in figure 1. The blood flow from the left ventricle was modelled with a current source producing a current $F_S(t)$ and an internal source resistance R_S, while a diode represents the aortic valve. The blood flow from the source $F_S(t)$

was defined as an exponentially damped raised cosine in systole, while $F_S(t)$ vanished in diastole, i.e.

$$F_S(t) = \begin{cases} \frac{F_M}{2}\left\{1 - \cos\left(2\pi \frac{t-T_D}{T_S-T_D}\right)\right\} e^{a(t-T_D)} & \text{systole: } T_D \le t \le T_S \\ 0 & \text{diastole: } T_S < t < T_D + T_I \end{cases} \quad (6.35)$$

where T_D and T_S are the time moments of end-diastole and end-systole, respectively. By definition, the left ventricular ejection time T_{LVE} is T_S-T_D. The amplitude F_M is scaled such that the integral of $F_S(t)$ over the systolic period, i.e. $[T_D,T_S]$, equals a preset value of stroke volume V_S. Typical values used in simulations were: V_S = 70 ml, T_{LVE} = 0.3 s, T_I = 0.7 s (86 beats per minute) and F_M = 502 ml/s for a damping factor a = -10 and R_S = 100 mmHg s/ml.

A three-element windkessel model was used to model the haemodynamical properties of the systemic circulation [Westerhof (1993b) and Westerhof (1993a)]. The resistance of the peripheral blood vessels is pooled into a single resistor R_P (typically, 0.95 mmHg s/ml), to which Ohm's law applies. The compliance of the aorta is pooled into a single capacitor with a pressure independent compliance C_A (typically 1.5 ml/mmHg). The Z represents the haemodynamic impedance of the blood filled aorta (typically 0.033 mHg s/ml). In this study R_S = 100 mmHg s/ml was chosen large relative to the load impedance of the complete windkessel-system.

Thoracic Volume Conductor. In Kubicek's original approach, the electrical properties of the thorax were modelled using a cylinder with specific resistivity ρ_{bl} (typically 135 Ωcm), length L (typically 20 cm), time-dependent cross-sectional surface $A_A(t)$, and volume $V_A(t)$ = L $A_A(t)$. The time-dependent impedance is

$$Z_A(t) = \frac{\rho_{bl} L}{A_A(t)} = \frac{\rho_{bl} L^2}{V_A(t)} \quad (6.36)$$

where $A(t)$ follows from the haemodynamic model (mean typically 2.5 cm^2; range 2.2-2.8 cm^2). We follow Geddes and Baker in using a two-compartment

model [Geddes & Baker (1989)]. The second cylinder, enclosing Kubicek's cylinder, with specific resistivity ρ_T (typically 700 Ω cm), length L (typically 20 cm) and time-independent cross-sectional surface A_T (typically 700 cm^2). In this model the inner cylinder represents the aorta and the outer cylinder represents the remaining thoracic tissue. As both cylinders are electrically connected in parallel, the (longitudinal) impedance $Z_0(t)$ is

$$Z_0(t) = Z_T \,//\, Z_A(t) = \frac{Z_T Z_A(t)}{Z_T + Z_A(t)} \tag{6.37}$$

The appropriateness of a cylinder-model to model the thoracic volume-conducting properties has been questioned by Wang and Patterson [Wang & Patterson (1995)], but we used a two-cylinder model in this study to stick close to the original approach of Kubicek and Patterson.

Results

Figure 2 shows a typical result obtained in a simulation from the model with the parameters set at the typical values mentioned above. As a result of the pulsatile blood flow from the ventricle $F_S(t)$, the pressure $P_A(t)$ in and volume $V_A(t)$ of the aorta increase and, in turn, an outflow $F_O(t)$ flows to the peripheral resistance. Due to the change of the aortic volume $V_A(t)$, the thoracic impedance $Z_0(t)$ and its first derivative dZ_0/dt changes. Note that the model only contains the aorta and, as a result, the thoracic impedance $Z_0(t)$ and its derivative dZ_0/dt contain only aorta-related waves. Moreover, the true first derivative dZ_0/dt is shown, and not the reverse as is common in impedance cardiography (see above the note on notational convention).

For the cardiac beat shown, the interbeat interval ranged from 14 to 14.7 s; systolic interval was from 14 to 14.3 s; diastolic interval was from 14.3 to 14.7 s. At the top-left side, the inflow $F_I(t)$ (ml/s) from the ventricle into the aorta (black line) and the outflow $F_O(t)$ (ml/s) from the aorta (dashed line) clearly showed the Windkessel-effect; that is, the strong pulsatile behaviour of the inflow (ranging from 0-502 ml/s) is reduced to a rather constant outflow (over the interbeat interval the mean flow of 99.5 ml/s, range 83-116 ml/s). Note in

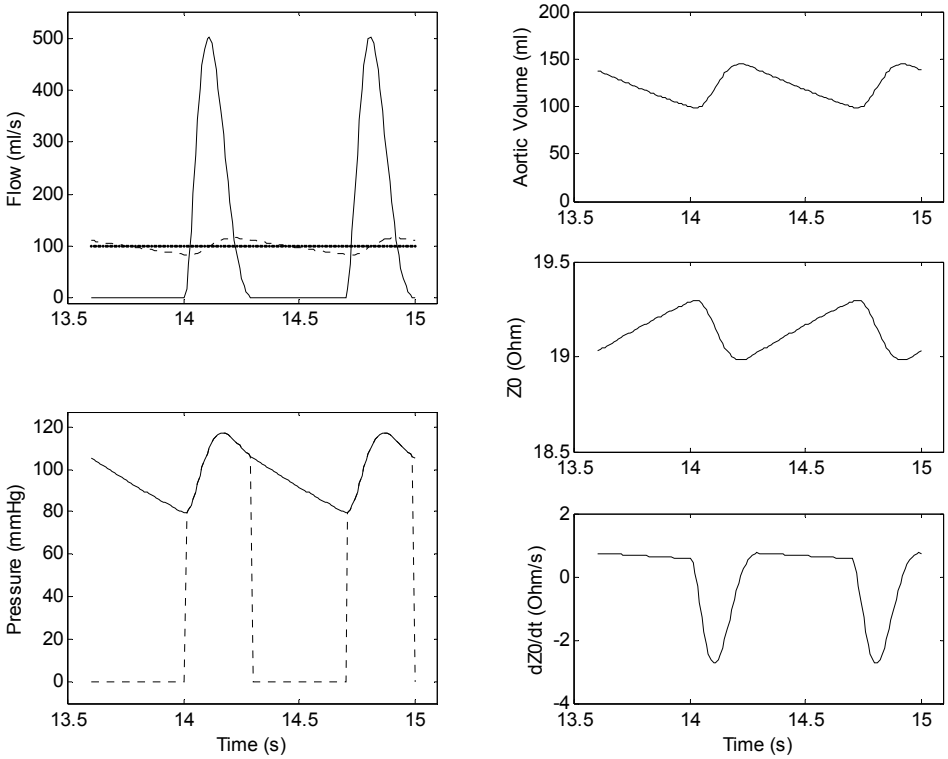

Figure 2. Typical result obtained from model in a simulation over a cardiac beat: interbeat interval from from t = 14 to 14.7 s; systole from 14 to 14.3 s; diastole from 14.3 to 14.7 s.
Leftside: (Top) the inflow (ml/s) from the ventricle into the aorta (black line) and the outflow (ml/s) from the aorta; note the horizontal line at the level of the ratio of stroke volume (70 ml) to interbeat interval (0.7s). (Bottom) the blood pressures (mmHg) in left ventricle (dashed line) and in the aorta (solid line).
Right side from top to bottom: Aortic volume (ml), thoracic impedance (Ω) and first derivative of the thoracic impedance (Ω/s).

particular, the accuracy of estimated outflow [(6.13)]; the estimate of 100 ml/s (70ml/0.7s) is close to the mean value of the outflow (103 ml/s) during systole. At the bottom-left side, the ventricular (dashed line) and aortic (solid line) pressure (mmHg) was shown. Systolic and diastolic pressures in the aorta were 117 and 90 mmHg, respectively. During diastole, the ventricular pressure was set at 0 in this indeed very simple model. At the right, from top to bottom, the aortic volume (range 98 - 145 ml), the thoracic impedance (range 19.0 - 19.3 Ω) and its first derivative (range –2.74 – 0.75 Ω/s) were shown. Note the inverse proportional relation between aortic volume $V_A(t)$ and impedance $Z_0(t)$ [(6.16)]. Simulations, similar to the one in figure 2, were used to investigate the various estimators while varying the parameters.

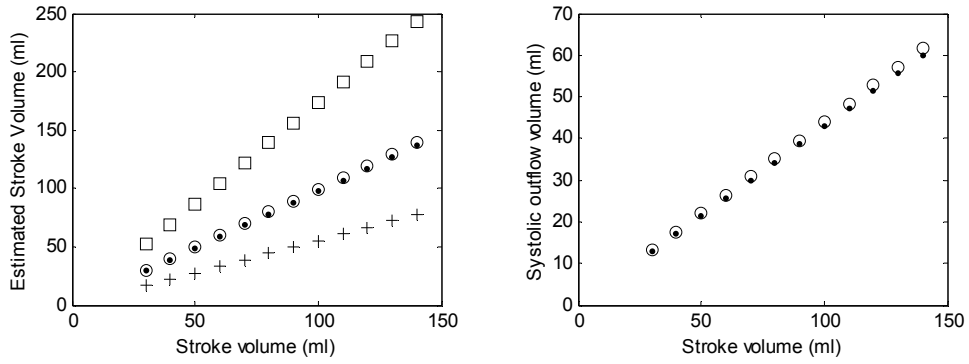

Figure 3. Performance of stroke volume estimators for different values of stroke volume (ml) (abscissa).
Left: On the ordinate the estimated stroke volumes (ml) with the outflow-corrected estimator (·) using (6.25), the Bonjer-Nyboer formula (+) using (6.30), Kubicek formula (Í) using (6.34). True stroke volume on the abscissa and true stroke volume (o) (line of identity).
Right: On the ordinate the volume of blood flowing out of the aorta during systole: estimate (·) using (6.13) and the true value (o). Stroke volume (ml) on the abscissa.
See text for further details.

Figure 3 shows the performance of different formula to estimate stroke volume from thoracic impedance (left) and systolic outflow volume (right). *Left side*: Stroke volumes in the range 40-140 ml were estimated using the outflow-corrected estimator (·) using (6.25), the Bonjer-Nyboer formula (+) using (6.30), Kubicek formula (Í) using (6.34). True stroke volumes (o) are also drawn (line of identity). This result shows that the outflow-corrected estimator is close to true value for different values of stroke volume, while the underestimation of the Bonjer-Nyboer formula (55% of true value), and the overestimation of the Kubicek-estimator (170% of true value) are considerably and, moreover, proportional to the true stroke volume. *Right side*: The volume of blood flowing out the aorta during systole (o) was calculated (integral of outflow $F_O(t)$ over systole) and, moreover, this true value was compared to the estimated value (·) using (6.13). For the latter, the mean outflow from the aorta was estimated [(6.13)] as the ratio of stroke volume (V_S) by the interbeat interval (T_I), and, hence, the amount of blood flowing from the aorta during the systole interval (i.e. left ventricular ejection time: T_{LVE}) is estimated as $V_S\, T_{LVE} / T_I$. The results in figure 3 clearly demonstrate i) the considerable size of the outflow (43% of stroke volume), and ii) the close correspondence of the mean-value estimator to the true-value for different values of stroke volume. Note that, as expected, the

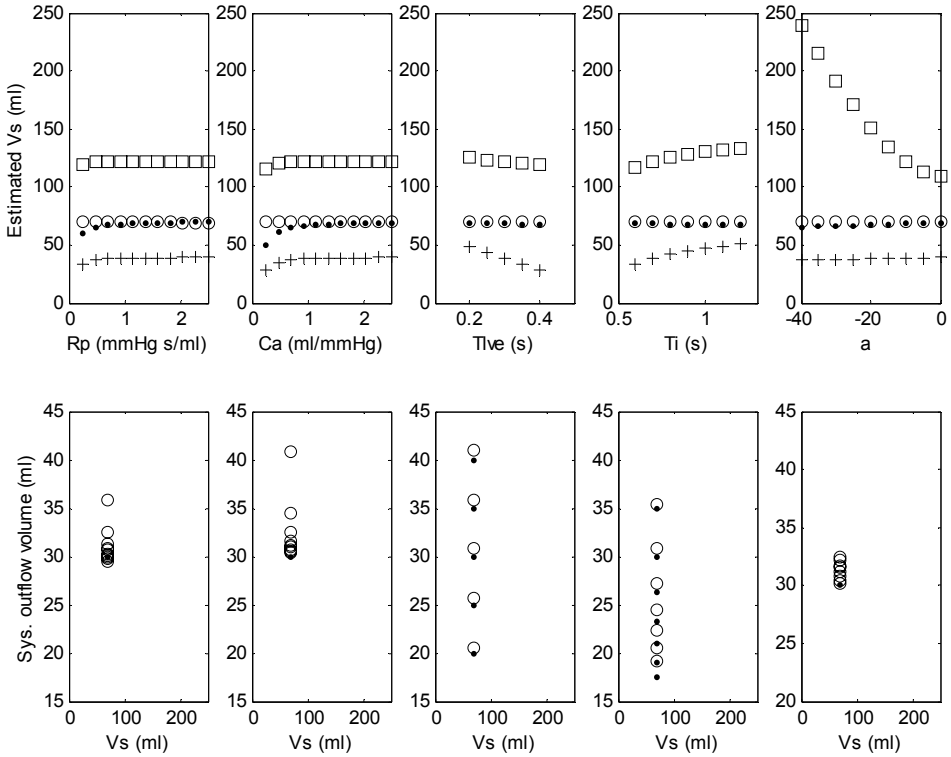

Figure 4. Performance of estimators of stroke volume (top) and systolic outflow volume (bottom) for different values of peripheral resistance (R_P), aortic compliance (C_A), left ventricular ejection time (T_{LVE}), interbeat interval (T_I), and steepness of inflow (as controlled by parameter *a*).
Top row: On the ordinate the estimated stroke volumes (ml) with the outflow-corrected estimator (·) using (6.25), the Bonjer-Nyboer formula (+) using (6.30), Kubicek formula using (6.34) and the true stroke volume (o) for one varying parameters on the abscissa
Bottom row: True systolic outflow volume (o) and its estimate (·) using (6.13) for varying parameters (see top row). Stroke volume (ml) was 70 ml in all cases.
See results for further details.

difference between the Bonjer-Nyboer estimate and the true stroke volume (left side: underestimation at 55% of the true value) is approximately equal to systolic outflow volume (right side: 43% of stroke volume).

Figure 4 shows the performance of the estimators again, but now, from left to right, for variations of the peripheral resistance R_P (range 0.25-2.25 mmHg s/ml), the aortic compliance C_A (range 0.25 – 2.5 ml/mmHg), the left ventricular ejection time T_{LVE} (range 0.2 – 0.4 s), the interbeat interval T_I (range 0.6 – 1.2 s) and the steepness of the inflow $F_I(t)$ as controlled by the parameter *a* in (6.35) (range: –40 – 0). *Top row*: stroke volumes as estimated with the outflow-corrected estimator (·) using (6.25), the Bonjer-Nyboer formula (+) using (6.30), Kubicek formula (Î) using (6.34). True stroke volumes (o) was set at 70

ml. Note that, the difference between the outflow-corrected estimator and the true stroke volume is small, except for the smallest values of R_p and C_A, while the Bonjer-Nyboer-formula underestimates and Kubicek-formula overestimates considerable in all cases. *Bottom row*: estimated systolic outflow volume (·) using (6.13) and multiplied with left ventricular ejection time (see previous paragraph) compared to the true systolic outflow volume (o). Because of the definition of the estimated outflow volume, this estimate changes only in case of variation of left ventricular ejection time (T_{LVE}) and interbeat interval (T_I), while the value is 30 ml in the three other cases. Note that the difference between the true value (o) and the estimated value (·) is smaller than 5 ml, except for the smallest values of R_p and C_A.

Note that in figure 4 only one parameter is varied a time, while all other parameters are set at the values used in figure 2. This explains, for example, the results obtained for varying T_{LVE}. Increasing T_{LVE} at a constant stroke volume V_S, leads to a decreased amplitude F_M of the inflow $F_I(t)$ (6.35), and as a result the impedance change ΔZ in the Bonjer-Nyboer formula and the derivative of the impedance dZ_0/dt in the Kubicek-formula decreases. Henceforward, the estimated stroke volumes with the formula of Nyboer-Bonjer and Kubicek decrease with increasing left ventricular ejection times.

Discussion

In this study we reinvestigated the outflow-problem in electrical impedance cardiography using a simple mathematical model of the cardiovascular system and the thoracic impedance. This simple model was employed in order to evaluate in simulations the stroke volume estimators known as the Bonjer-Nyboer and Kubicek formulae. Moreover, the model was used to develope and evaluate a new formula with an adequate correction for the outflow-problem. To be more specific: we showed that: i) the outflow-problem is inadequately treated in the formulae of Bonjer-Nyboer, Kubicek, and Sramek-Bernstein, ii) that the outflow-problem can be solved adequately with the formulae in (6.25)-(6.27) which requires only the interbeat interval length extra in comparison to the information used in the Bonjer-Nyboer and Kubicek formulae. In this present

study, the adequateness of this outflow solution was evaluated using simulations with the model.

It was generally agreed that the outflow-problem was not properly dealt with in the Nyboer-Bonjer equation [see for example Sherwood et al. (1990)] and, indeed, our simulation results indicated a significant underestimation of 55% of the true value. For many years, the replacement of the term ΔZ_0 by $(dZ_0/dt)_{MAX} T_{LVE}$ by Kubicek was thought to be a solution to the outflow problem. This study showed, however, that this solution is very disappointing. The results obtained with the Kubicek-equation showed very large overestimations up to 170% and more of the true stroke volume. Moreover, and most peculiar for an solution of the outflow-problem, these overestimations were found to be almost independent of the peripheral resistance and aortic compliance (the main determinants of the actual outflow), and strongly dependent on the steepness of the arterial inflow (figure 4). The same is expected to hold, mutatis mutandis, for the Sramek-Bernstein equation, because Kubiceks replacement of the term ΔZ_0 by $(dZ_0/dt)_{MAX} T_{LVE}$ was copied by Sramek-Bernstein. Hence, the outflow problem is unsolved in impedance cardiography; a conclusion already reached in 1976 and 1977 by Yamokoshi in simulation and experimental studies [Yamakoshi et al. (1976) and Yamakoshi, Togawa, & Ito (1977)].

The error in Kubicek's solution to the outflow problem can be found in two subtleties in the derivation of Kubicek's equation. Using a one-cylinder model (6.5) for the sake of simplicity, the relation between volume and impedance is

$$V_A(t) = \frac{\rho_{bl} L^2}{Z_A(t)} \quad \Rightarrow \quad \frac{dV_A(t)}{dt} = -\frac{\rho_{bl} L^2}{Z_A(t)^2} \frac{dZ_A(t)}{dt} \tag{6.38}$$

Applying differential calculus,

$$\Delta V = \frac{dV_A(t)}{dt} \Delta t = -\frac{\rho_{bl} L^2}{Z_A(t)^2} \frac{dZ_A(t)}{dt} \Delta t \tag{6.39}$$

which holds only for infinitesimal small values of Δt. Substitution of the *non*-infinitesimal value of T_{LVE} for Δt yields,

$$\Delta V = \frac{dV_A(t)}{dt}\Delta t \approx -\frac{\rho_{bl} L^2}{Z_A(t)^2}\frac{dZ_A(t)}{dt}T_{LVE} \qquad (6.40)$$

That is, the Kubicek equation on the right-hand side when the maximum value of the derivative is taken. There is, however, no mathematical or physiological argument to conjecture that ΔV equals stroke volume V_S, as was take for granted in many studies. In fact, 1) ΔV is the change of the *aortic* volume, under 2) the condition that T_{LVE} is very small (a condition most likely not met for physiological values of T_{LVE} in the order of 0.3 (s). These two subtleties make all the difference between the "Kubicek-Sramek-Bernstein $(dZ_0/dt)_{MAX}T_{LVE}$ estimate" of stroke volume and its true value.

To solve the outflow-problem, we estimated the amount of blood flowing out of the aorta during systole using a very simple reasoning. Starting from the observation that the outflow is relatively constant in time due to the storage capacity of the aorta ascendens (figure 2), this constant outflow was estimated (6.13) as the ratio of stroke volume (*i.e.*, the total amount of blood flowing from the aorta into the periphery each heart beat) to interbeat interval (i.e. the time available to pass this stroke volume). In simulations this estimate of the systolic outflow volume proved to be accurate up to a few milliliters under most physiological conditions (right side of figure 3 and bottom row of figure 4). Using this estimate of systolic outflow volume, it required only a few lines to arrive at an outflow corrected stroke volume estimator [(6.15) and (6.25)-(6.27)]; provided the availability of the mathematical machinery developed in (6.6)-(6.29). In simulations the robustness for parameter variations and accuracy of the outflow-corrected estimator proved to be realy satisfying (figure 3 and 4).

In the present study we assumed that the aorta as the main source of thoracic impedance changes; an assumption, however, questioned in the literature. We will discuss the tenability of this assumption in light of literature. Mohapatra summarizes a number of experimental studies in human and animal models on the origne of cardiac synchroneous thoracic impedance changes

performed over the preceding fifty years [Mohapatra (1981)]. A clear conclusion was impossible to draw: changes of thoracic impedance synchronously with cardiac activity were related to volume changes of the ventricle, the aorta, the pulmonary arteries and the lungs itself. Since then a shift from experimental studies to studies using computer models occurred. Starting with a Sakamoto's paper, a series of papers was published to study the origin of cardiac synchronous impedance changes. These studies rather diverge in the realism of the used geometry of the thorax anatomy (from Sakamoto's 'plumbers pipe' model to more or less realistic geometries obtained from anatomical textbooks or MR images), the used resistivities to model the electric properties of the various thoracic tissues (difference between resistivities of various tissues are over exaggerated [Faes et al. (1999b)], as well as the resistivity change of pulsatile flow of blood (see chapter 4) and the way in which volume changes within the cardiac cycle are modeled. As a result the studies also diverge in their result: comparing all the studies on the reported estimated contribution of different organs to the total thoracic impedance change shows that the between study variability is larger than the variability between organs. Moreover, the experimental validation of the model in these studies is poor or even absent. Hence, from all these we conclude that there is no consensus on the contribution of various thoracic organs to thoracic impedance, although multiple origins are to be expected. In contrast our own experimental study showed a clear relation to aortic volume changes during systole (chapter 2), provided that an appropriate electrode configuration is used for the voltage sensing electrodes (chapter 3), while the resistivity change of flowing blood might be neglected (chapters 4 and 5). In the light of these findings it may be worthwhile to reinvestigate a stroke volume estimator based on an assumption of the aorta as a major contributor of thoracic impedance changes.

This study illustrates the strong influence of the steepness of the aortic inflow on the stroke volume estimation in the $(dZ/dt)_{MAX}T_{LVE}$ approach of the Kubicek-Sramek-Bernstein equations (dependence on parameter *a* in figure 4). These results reconfirm the findings of Ito et al. on the influence of rise times of aortic flow [Ito, Yamakoshi, & Yamada (1976)]. This influence of steepness or rise time might explain one of our observations that impedance cardiography performs significantly poorer in cardiac patients compared to obstetrical and

critically ill patients [Raaijmakers et al. (1999)], because the steepness and rise time of aortic flow are expected to be reduced considerable and to show more interindivual variation in cardiac patients. Avoiding the $(dZ/dt)_{MAX}T_{LVE}$ approach might improve results and, moreover, change the meta-evaluation of impedance cardiography because most validation studies are made in cardiac patients [Raaijmakers et al. (1999)].

The measurement of stroke volume with impedance cardiography is a plethysmographic method. However, there is close resemblance with the so-called pressure pulse contour methods, which were originally developed by Otto Frank [Noordergraaf (1978)]. In the pulse contour method, stroke volume is determined from an aortic pressure $P_A(t)$ recording by calculating the area under the pulsatile part of the pressure wave during a complete beat, and deviding this area by the haemodynamic resistance of the systemic circulation. That is,

$$V_S = \frac{1}{R_P} \int_{T_D[k+1]}^{T_D[k+1]} \left\{ P_A(t) - P_A\left(T_D[k]\right) \right\} dt \tag{6.41}$$

Cardiographic stroke volume estimation can be elaborated into the form of

$$V_S = \frac{\rho_B L^2}{R_P C_A} \int_{T_D[k]}^{T_D[k+1]} \left(\frac{1}{Z_0(t)} - \frac{1}{Z_0\left(T_D[k]\right)} \right) dt \tag{6.42}$$

Comparing the formulae for the pressure contour method and the impedance method shows the close resemblance between both methods. That is, in both cases a measured signal (pressure and impedance) are integrated over a complete cardiac beat where the integrand was diminished with its end-diastolic value. To scale the value of these integrals to stroke volume, the haemodynamic resistance R_P was used in the pulse contour method, while time-constant ($R_P C_A$) of the diastolic decline in combination with the resistivity and electrode distance in impedance cardiography. In the pressure pulse contour method, the scaling to the peripheral resistance was always difficult, because of the following vicious argument: this resistance necessary for stroke

volume calculations follows from the measured mean pressure and cardiac output calculated from stroke volume. In case of the impedance cardiography, this vicious circle is broken, because the time-constant $R_P C_A$ might be calculated directly from e.g. the decay of impedance during late diastole.

So far, we restricted the evaluation of the outflow-corrected stroke volume estimator to a simulations study. The reason for that is that it is generally recognized that impedance cardiography suffers from a number of problems which have to be solved simultaneously to save impedance cardiographic stroke volume estimation from obscurity. The problems nowadays recognized as major are: 1) the possible multiple origins of the thoracic impedance changes, 2) the detection of the start and end of the left ventricular ejection time in impedance recordings, 3) the influence of resistivity pulsatile flowing blood, 4) de length of the aorta in combination with the distance between the voltage sensing electrodes, and 5) an optimal position of the electrodes. These problems need to be solved before it becomes worthwhile to perform evaluation studies in animal or human models.

Conclusion

An outflow-corrected stroke volume estimator was developed for use in electrical impedance cardiography. In this simulation studies, the accuracy formula was demonstrated in simulations. Moreover, the first-derivative-approach of Kubicek-Sramek-Bernstein was found to be highly inaccurate. The real challenge is, of course, to demonstrate the quality of the estimator on data recorded from patients.

Appendix: Simulation of the Model

In order to make simulations, the model of figure 1 needs to be brought into a computational form. In this appendix, we will discuss: i) the equations of the haemodynamic and volume-conductor model, ii) a computational suitable form of these models to simulate the variables $V_S[k]$, $V_A(t)$, $Z_0(t)$ and dZ_0/dt, and iii) the applied numerical methods.

Equations of the Haemodynamic Model

Figure 1 shows the haemodynamic model in an analogous form of an electrical network to which standard theory of network analysis applies. That is: Kirchhoff's current law applies to the nodes; Ohm's law applies to the resistors representing the source resistance of the ventricle (R_H), the proximal impedance of the aorta (R_Z), and the resistance of the peripheral vasculature (R_P) [Westerhof (1993b) and Westerhof (1993a)]. The aortic compliance is represented by a pressure dependent capacitor

$$C_W(P_W) = \frac{dV_W}{dP_W} = \frac{\frac{dV_W(t)}{dt}}{\frac{dP_W(t)}{dt}} \qquad \text{(A.1)}$$

The left ventricle is represented by a current source $F_S(t)$ with a source resistance (R_H) and the aortic valve is represented by a diode. To be more specific: the pressures at both sides of the diode determine the presence of a non-ejecting phase or ejecting phase, i.e.

$$\begin{aligned} &P_V(t) < P_A(t) \Rightarrow \; F_I(t) = 0 \Rightarrow \text{ non-ejecting phase} \\ &P_V(t) = P_A(t) \Rightarrow \; F_I(t) > 0 \; \Rightarrow \text{ ejecting phase} \end{aligned} \qquad \text{(A.2)}$$

Furthermore, we define $F_S(t)$ as

$$F_S(t) \overset{def.}{=} \begin{cases} F_M\left(1-\cos\left(\dfrac{2\pi\left(t-T_D[k]\right)}{T_S[k]-T_D[k]}\right)\right)e^{a\left(t-T_D[k]\right)} & \text{systole} \\ 0 & \text{diastole} \end{cases} \qquad \text{(A.3)}$$

which makes $F_S(t)$ an exponentially damped raised cosine in systole, whereas $F_S(t)$ vanishes in diastole. The amplitude F_M is scaled such that the integral of $F_S(t)$ over the systolic period $[T_D,T_S]$ equals a preset value of stroke volume V_S (details of this non-linear problem are left undiscussed). Note that, this definition of $F_S(t)$ has the advantages that: i) the wave form closely resembles normal aortic blood flow, ii) the steepness of $F_S(t)$ is controlled by the exponential parameter a (a<0), iii) both $F_S(t)$ and its derivative to time are continuous functions of time which improves the numerical accuracy of the computations.

We now derive the state equation, which gives the state variable $P_W(t)$ as a function of exogenous variable $F_S(t)$. Applying standard network analysis to the network in figure 1 and using (A.1) and (6.10) yields,

$$\left.\begin{aligned} \frac{dV_W(t)}{dt} &\overset{\text{eq. A1}}{=} C_A(P_W)\frac{dP_W(t)}{dt} \\ \frac{dV_W(t)}{dt} &\overset{\text{eq. 10}}{=} F_I(t)-F_O(t) \\ F_O(t) &= \frac{P_W(t)}{R_P} \end{aligned}\right\} \Rightarrow\ C_A(P_W)\frac{dP_W(t)}{dt}+\frac{1}{R_P}P_W(t)=F_I(t) \qquad \text{(A.4)}$$

In order to relate $F_I(t)$ to $F_S(t)$, we have to distinguish two phases in which the ventricular is ejecting ($F_I(t)$>0) and non-ejecting ($F_I(t)$=0).

In the *ejecting phase*, for a conducting diode (aortic valve open), the following relations hold: $P_V(t) = P_A(t)$ and consequently, $F_S(t) = F_I(t) + F_H(t)$. Hence,

$$\left.\begin{aligned} F_I(t) &= F_S(t)-F_H(t) \\ F_H(t) &= \frac{P_V(t)}{R_H} \\ P_V(t) &= P_A(t) \\ P_A(t) &= P_W(t)+R_Z F_I(t) \end{aligned}\right\} \Rightarrow F_I(t)=\frac{R_H}{R_H+R_Z}F_S(t)-\frac{1}{R_H+R_Z}P_W(t) \qquad \text{(A.5)}$$

Substitution of (A.5) into (A.4) yields the state equation for the ejecting phase,

$$C_A(P_W)\frac{dP_W(t)}{dt}+\left\{\frac{1}{R_P}+\frac{1}{R_H+R_Z}\right\}P_W=\frac{R_H}{R_H+R_Z}F_S(t) \tag{A.6}$$

In the *non-ejecting* phase, for a non-conducting diode (aortic valve closed), the following relations holds: $P_V(t) < P_A(t)$ and consequently, $F_I(t) = 0$ and $P_A(t) = P_W(t)$. Effectively, the network is separated into independent left and right parts. For the right part the state (A.4) with $F_I(t) = 0$ becomes,

$$C_A(P_W)\frac{dP_W(t)}{dt}+\frac{1}{R_P}P_W=0 \tag{A.7}$$

and for the left side of the circuit,

$$P_V(t)=R_H F_S(t) \tag{A.8}$$

Using (A.1) as well as both derivatives to solve the state equations numerically provides state variables $P_W(t)$ and $V_W(t)$. All other variable can be calculated form this state variable together with the known exogenous variable $F_S(t)$ (see below).

Equations for Thoracic Impedance Model

With the calculated $V_W(t)$ and its derivative the thoracic impedance $Z_0(t)$ and its derivative are calculated using the two-cylinder [(6.16) and (6.17)]. That is,

$$Z_0(t)=Z_T \,//\, Z_A(t)=\frac{1}{\frac{1}{Z_T}+\frac{1}{Z_A(t)}} \tag{A.9}$$

with

$$Z_A(t) = \frac{\rho_{bl} L_E}{A_A(t)} = \frac{\rho_{bl} L_A^2}{V_A(t)} \tag{A.10}$$

The first derivative dZ_0/dt is computed from

$$\frac{dZ_o(t)}{dt} = \frac{dZ_o(V_A(t))}{dV_A(t)} \frac{dV_A(t)}{dt} = -\frac{Z_0(t)^2}{\rho_{bl} L^2} \frac{dV_A(t)}{dt} \tag{A.11}$$

using (6.21). We choose to compute dZ_0/dt from $dV_A(t)/dt$, in order to avoid a numerical differentiation of $Z_0(t)$, an operation notoriously known for its inaccuracies.

Computational Form

The state and auxiliary equations [(A.6)-(A.8)] present an initial value problem. The non-linear diode-element complicates the numerical integration of the initial value problem, which we solved in the following way:

Firstly, we assume a non-ejecting phase at time moment T_0 and compute accordingly, the pressures at both sides of the diode. That is, from $F_S(T_0)$ and the initial value $P_W(T_0)$ the pressures $P_V(T_0) = P_W(T_0)$ and $P_A(T_0) = R_S F_S(T_0)$ follow.

Secondly, if indeed the calculated pressures $P_V(T_0)$ and $P_A(T_0)$ confirm a non-ejecting phase (i.e. $P_V(T_0) < P_A(T_0)$), then the variables P_W and V_W at the next time moment $T_0+\Delta T$ are computed from

$$\begin{aligned} \frac{dP_W(t)}{dt} &= -\frac{1}{R_P C_W(P_W)} P_W(t) \\ \frac{dV_W(t)}{dt} &= -\frac{1}{R_P} P_W(t) \end{aligned} \tag{A.12}$$

using a numerical differential equation solver. If, on the other hand, the calculated pressures $P_V(T_0)$ and $P_A(T_0)$ reject a non-ejecting phase [i.e. $P_V(T_0) = P_A(T_0)$], the variables P_W and V_W at the next time moment $T_0+\Delta T$ are computed from

$$\frac{dP_W(t)}{dt} = \frac{R_H}{R_H + R_Z}\frac{1}{C_W(P_W)}F_S(t) - \frac{1}{R_P // (R_H + R_Z) C_W(P_W)}P_W(t)$$
$$\frac{dV_W(t)}{dt} = \frac{R_H}{R_H + R_Z}F_S(t) - \frac{1}{R_P // (R_H + R_Z)}P_W(t) \qquad \text{(A.13)}$$

where we used the notation

$$\frac{1}{R_P // (R_H + R_Z)} = \frac{1}{\frac{1}{R_P} + \frac{1}{R_H + R_Z}} \qquad \text{(A.14)}$$

(a parallel connection of R_P with the resistors R_H and R_Z in series).

Thirdly, this computational process is repeated, using the computed $P_W(T_0+\Delta T)$ each time as the new initial value until the end of the simulation period is reached.

Fourthly, the other variables are calculated as follows: the flows, using Kirchhoff's and Ohm's laws, follow from the auxiliary equations

$$F_0(t) = \frac{P_W(t)}{R_P}, \quad F_I(t) = F_0(t) + \frac{dV_W(t)}{dt}, \quad F_H(t) = F_S(t) - F_I(t) \qquad \text{(A.15)}$$

whereas the pressures at both sides of the valve (diode) follow from

$$P_V(t) = R_H F_H(t), \quad P_A(t) = P_W(t) + \mathrm{R_Z}\ F_I(t) \qquad \text{(A.16)}$$

Finally, $Z_0(t)$ and dZ_0/dt were computed from $V_A(t)$ and $dV_A(t)/dt$ using (A.9)-(A.11).

Chapter 7 General Discussion and Conclusion

The validity of Electrical Impedance (EI) cardiography as a non-invasive method to estimate Stroke Volume (SV) or Cardiac Output (CO) depends first of all on the possibility to measure aortic volume changes. Only if this condition is met, an estimator can be developed that accurately estimates SV or CO from the EI signal. In the introduction of this thesis (see chapter 1) this is translated into three fundamental questions:

1. Can the contribution of the aorta to the thoracic EI signal be separated from the contribution of other possible sources?
2. Can the contribution to the thoracic EI change of the blood resistivity change due to blood flow be quantified?
3. Can the outflow-problem be solved?

The answer to the first question will indicate if the aorta can be considered as the major source of the thoracic EI signal. The answer to question two will show whether this aortic contribution reflects mainly volume changes of the aorta or whether it is due to a combination of volume changes and resistivity changes of blood due to blood flow. Only if aortic volume changes are the major source of the EI signal, and blood resistivity changes can be ignored, question three becomes relevant.

A more practical question was also raised in the introduction:

4. Can the number of voltage pickup electrodes needed for EI cardiography be reduced to a minimum?

This question only is relevant of course if the first three questions indicate that EI cardiography is at all a valid method for SV or CO estimation. However, comparing the EI signals measured on both sides of the thorax with such signals measured on the left-hand and right-hand side of the thorax can indicate whether the simple parallel cylinder model is a valid representation of the

thorax. Remember that as a consequence of this model (axis-symmetry) the equipotential lines should be perpendicular to the axis of the cylinders and therefore, voltage pickup electrodes on the left-hand side, right-hand side, and both sides of the thorax should give equal results. This explains why this question was investigated in chapter three and not, as would be more natural, at the end of this thesis.

Is the Aorta the Major Source of the EI signal?

Chapter 2 introduced a method to estimate thoracic blood volume changes during the heart cycle from regional thoracic EI measurements. An estimator was developed that calculates segmental surface area changes of the organs in the thorax. The EI data was collected with a linear electrode array that resembles the 'Woltjer-arrangement'. The difference being that where the latter arrangement uses voltage pickup electrodes that are separated by a relatively large distance, the voltage pickup electrodes in the array used in chapter 2 were separated by a relatively short distance. Results from EI measurements on three healthy male subjects where compared to the surface area changes of the thoracic organs obtained from MRI measurements. These latter images included contributions of the aorta, the vena cava, the carotid arteries and the heart. Furthermore, volume changes across the whole thorax and in the region of the aortic arch were calculated from the EI signals and the MRI images.

The results show that the total volume changes measured with EI across the whole thorax (i.e. from the xiphoid process up to the neck) show remarkable similarity with the volume change measured with MRI. The EI volume change measured at the mid-clavicular lines corresponded closely to MRI volume changes including contributions of the aorta, vena-cava, carotid arteries, and the heart. The EI volume change measured at mid-axillary lines, on the other hand, showed close correspondence to MRI volume changes including contributions of the aorta, vena-cava, carotid arteries, but without the heart. This indicates that the aorta is not the only source of the EI signal measured across the whole thorax and consequently the parallel cylinder model is not a valid representation of the whole thorax. The contribution of the heart is considerable as the total volume change decreases by approximately one third in systole.

The results also show, however, that reducing the region across which the EI signal is measured, changes matters considerably. If the EI signal is measured across the region of the ascending aorta, aortic arch, and upper part of the descending aorta, the estimated volume changes show close correspondence to the volume change of only the aorta measured with MRI. Moreover, the EI volume changes measured at the mid-clavicular lines and mid-axillary lines are almost identical (correlation coefficients of these volume changes ranging from 0.932-0.987). This suggests that in the region of the aortic arch the aorta is the major source of the EI signal and as a result the parallel cylinder model is valid. Three objections can be made at this point, two being of a fundamental nature and the other of a more practical nature.

The first fundamental objection concerns the electrode array: all EI signals were simultaneously measured at the left-hand and right-hand side of the thorax. As a result these signals are a weighed sum of underlying EI signals. Although close correspondence exists in the composite signals measured at the mid-clavicular lines and mid-axillary lines, there is no guarantee that the underlying signals correspond equally well. Signals measured, for example, at the mid-axillary line on the left-hand side and right-hand side of the thorax may not show this close correspondence. Therefore, no definite conclusion concerning the validity of the parallel cylinder model can be drawn at this point.

The second fundamental objection that can be raised, concerns the contribution of the resistivity change of blood due to blood flow. The estimator developed in chapter 2 was based on the assumption that the magnitude of the resistivity of flowing blood is about 10% smaller than the magnitude of blood resistivity in the absence of flow. First of all the magnitude of the resistivity change in-vivo should be estimated. Secondly, the pulsatile nature of the resistivity change of blood in-vivo has to be accounted for.

The third objection that is of a more practical nature involves the use of the EI method in the clinic. It is not desirable that the accuracy of the method depends greatly on the exact placement of the voltage pickup electrodes. Ideally, application of the electrodes on the thorax should be easy and quick, and the location where the electrodes are placed should not interfere with medical treatment. It is highly questionable that having to place the electrodes

in the region of the aortic arch meets these demands. For example, the exact region of the aortic arch will vary between individual subjects, as it depends on the anatomy of the subject. If the voltage pickup electrodes are misplaced and pickup EI signals from below the region of the aortic arch, part of the contribution of the heart will be picked up. This may result in measured volume changes that are smaller than the volume changes of the aorta, and thus SV will be underestimated. This example demonstrates that having to place the voltage pickup electrodes in the region of the aortic arch is, for practical purposes, far from desirable.

Chapter 3 dealt with the fundamental objection about the electrode array in an indirect way. The aim was to investigate whether the number of electrodes for EI cardiography can be reduced, removing part of the practical objection concerning electrode placement. In the process, however, an indication of the validity of the parallel cylinder model can be obtained. Six different electrode arrangements were used to obtain the thoracic EI impedance signal. One arrangement was the ‘Woltjer-arrangement’, another arrangement was similar to the ‘Woljer-arrangement’, but placed the upper voltage pickup electrodes as closely as possible to the clavicles at the lateral aspect of the base of the neck. In this way the contribution of the neck is removed. Two other arrangements reduced the number of current injection electrodes from four to two. They differed by placing them at the left-hand side and right-hand side of the thorax, respectively. The last two arrangements reduced the number of voltage pickup electrodes from four to two, also placing them on opposite lateral sides of the thorax.

The results show that the EI signal measured on the right-hand side of the thorax differs considerably from that measured on the left-hand side of the thorax. Consequently, the fundamental objection concerning the electrode array that was used in chapter 2 seems to be substantiated. Therefore, the suggestion that the parallel cylinder model is a valid representation of the thorax in the region of the aortic arch has to be re-examined. However, before returning to this matter, let us discuss the second fundamental objection concerning the contribution of the conductivity change of blood.

Can the Magnitude of Blood Resistivity Change be Quantified?

Although there is general consensus that blood conductivity changes due to blood flow (caused by deaggregation, orientation and deformation of erythrocytes), the magnitude of this effect in-vivo is still a matter of debate. Where some concluded on the basis of in-vitro experiments that the magnitude of the decrease of blood resistivity due to blood flow may be as large as 20% relative to blood with undeformed and randomly orientated erythrocytes, others argued that this is an overestimation of the so-called resistivity effect, as in-vivo it is questionable whether a state of complete deorientation exists before the onset of blood flow. The magnitude of the resistivity change due to pulsatile blood flow, they estimated, was about 5%. Before the contribution of blood resistivity change in-vivo can be discussed at all, better theoretical understanding of this phenomenon is needed.

In chapter 4 a theory on blood conductivity (i.e. the reciprocal of the resistivity) was proposed that showed good agreement with the conductivity change of blood measured in-vitro. This theory was developed assuming a stationary and laminar flow profile in a rigid tube, so-called Poiseuille flow. In-vivo, however, the flow profile is much more erratic and surely not stationary. The theoretical model, however, may be considered to give an upper bound of the conductivity change in-vivo. In chapter 5 the theory presented in chapter 4 is combined with the method introduced in chapter 2. Cross-sectional surface area changes and average flow velocities were measured with MRI in four subjects. The relative error introduced in neglecting the pulsatile nature of blood conductivity change was estimated.

The results show that neglecting this pulsatile nature introduces an error in volume estimation that ranges from roughly 2-10% during the systolic part of the heart cycle, depending largely on the flow pattern in the aorta. Consequently, it may be inferred that the conductivity change of blood is only a minor cause for any disagreement of EI volume changes and volume changes measured with MRI.

Where on the Thorax is the Aorta the Major Source of the EI Signal?

Before returning to the discussion of the aorta as a source of the thoracic EI signal, let us summarize the findings on this matter so far. First of all it was established in chapter 2 that the aorta is not the only source of the EI signal measured across the whole thorax. When measured in the region of the aortic arch, on the other hand, it did seem to be the major source. Additionally, in that region the parallel cylinder model seemed a valid representation of the thorax. However, the EI signals were measured on the left-hand side and right-hand side simultaneously and thus no discrimination was possible between the EI signals measured on different lateral sides of the thorax. The results of chapter 3 indicated that differences in EI signal between both lateral sides of the thorax do indeed exist, when the signal is measured across the whole thorax.

In chapter 5 the method of chapter 2 was used again, but now on four subjects the EI signals were measured with electrode arrays applied on mid-axillary and mid-clavicular lines on the left-hand and right-hand side of the thorax separately. In addition, the EI signal was also measured on the sternal line of the thorax. The results confirm what was already found in chapter 3: large differences exist between the EI signals measured at different locations on the thorax. Moreover, where it could be argued in chapter 2 that in the region of the aortic arch the aorta is the major source of the EI signal, irrespective of the location of the electrode array, the results presented in chapter 5 refute this. Considerable differences exist in the cross-sectional surface area change mappings obtained with the different arrays and it is impossible to identify any of these changes as being the result of the cross-sectional surface area changes of the aorta. The volume changes calculated from these cross-sectional surface area changes confirm this, with the possible exception of the volume changes measured at the mid-axillary line on the left-hand side of the thorax. This is the only location on the thorax where the volume change measured with EI resembles the volume change of the aorta, although the resemblance is not strong.

One conclusion can be drawn with certainty from these findings: the parallel cylinder model is not a valid representation of the thorax, not even in the

region of the aortic arch. Extending the parallel cylinder model to a parallel conductor model, as was done in chapter 2, does not overcome this problem. The only solution is replacing the parallel cylinder model with a model that takes into account the multiple sources of the EI signal. Such a model should be able to predict the different contributions of the thoracic organs in different regions of the thorax.

It seems that the linear electrode array that was used in chapter 5 of this thesis is highly sensitive to changes that occur in the proximity of the electrode pairs. Close to the heart, for example, the contribution of the heart is clearly dominant, whereas at locations farther away from the heart, it does not contribute to the EI signal. This property of the array could be of some advantage. Placing the electrode array directly on the descending aorta, e.g. at the back of the thorax slightly left of the spine, might result in relatively accurate estimation of the volume change of the descending aorta. However, such an electrode arrangement is less practical in a clinical setting, as it involves more movement of the patient when applying the electrodes or when checking whether the electrodes are still attached. Therefore, this arrangement was not investigated in this thesis.

Can the Outflow-Problem be Solved?

As was demonstrated in chapter 6 the outflow-problem was not adequately dealt with in the Nyboer-Bonjer equation or in the Kubicek-Patterson equation. To tackle the outflow-problem, a model of heamodynamics has been introduced that leads to an estimator of stroke volume that corrects for the outflow of blood from the aorta due to arterial runoff. This estimator contains three independent variables: the time interval between two consecutive heartbeats (T_I), the time interval in which the heart ejects blood into the aorta (T_{LVE}), and the aortic volume change between end-diastole and end-systole (ΔV_A). Additionally, using the parallel cylinder model as an electrical model of the thorax, the aortic volume change ΔV_A was related to thoracic impedance change (ΔZ). Simulation results established the superiority of this new estimator over the Nyboer-Bonjer equation and the Kubicek-Patterson equation. The obvious question now is how this new estimator will perform on patients or healthy subjects. Before the new

estimator can be used on patients or healthy subjects, however, two major obstacles must be taken.

First of all, it has been demonstrated in this thesis that the parallel cylinder model is not a valid representation of the electrical properties of the thorax. This does not imply that the outflow correction is invalid, as the correction follows from the heamodynamics and therefore is independent of the thoracic model. The thoracic model is only necessary to relate aortic volume changes to thoracic impedance changes, but as was argued above it can not be concluded beyond reasonable doubt yet what model or which electrode configuration are best suited to tackle this first obstacle. It can only be suggested that a linear electrode array applied at a mid-axillary line on the left-hand side of the thorax seems the best candidate.

Secondly, to correct for the outflow the interbeat time interval (T_I) and the left ventricular ejection time (T_{LVE}) must be measured. The first time interval can easily be obtained from an ECG that is recorded simultaneously with the EI-signal. Estimating the second time interval has not been dealt with in this thesis. Traditionally it is estimated from the B-point and X-point in the EI cardiogram (see figure 2 in chapter 1). However, these points are not always easily identifiable, especially when data from critically ill patients are used. Using wrong estimations of T_{LVE} will introduce possibly large errors in SV estimations.

Can the Number of Voltage Pickup Electrodes be Reduced to a Minimum?

As was discussed above, chapter 3 investigated the reduction of the number of electrodes to measure the EI cardiogram. Different arrangements were considered to be equivalent if the results obtained with these arrangements did not differ in their group means, and yielded small differences in the results obtained for individual subjects.

It was found that reducing the number of current injecting electrodes has little effect on the measured values of Z_0, $(dZ/dt)_{min}$ and T_{LVE}. Reducing the number of voltage pickup electrodes, on the other hand, substantially changes the measured values of these variables, especially when the voltage pickup electrodes are located on the right-hand side of the thorax. A reduced number

of electrodes applied on the right-hand side of the thorax resulted in a considerable reduction in the group mean of the estimated stroke volume, due to a higher value of the measured base impedance Z_0. A reduced number of voltage pickup electrodes applied on the left-hand side of the thorax did not change the group means of the measured variables or calculated stroke volume. However, differences in these variables for individual subjects can be considerable. For some subjects the value of the estimated SV (using the Kubicek-estimator) was up to 45 ml lower than that of the estimated SV with the 'Woltjer-arrangement'.

Thus, a reduction of the number of electrodes is payed for by a possible decrease in estimated SV. This does not mean that an electrode array with two voltage pickup electrodes on the left-hand side of the thorax is less optimal than the 'Woltjer-arrangement'. The only conclusion that can be drawn from chapter 3 is that the arrangements are not equivalent. In order to establish the superiority of either arrangement, their validity should be investigated by comparison to a reference method like MRI or dilution methods. Before this can be done however, the SV-estimator presented in chapter 6 should be validated and robust estimation of T_{LVE} has to be investigated.

Conclusion

1) The aorta is only the major source of the thoracic EI signal when it is measured in the region of the aortic arch with voltage pickup electrodes located on both sides of the thorax.
2) Voltage pickup electrodes applied on different sides of the thorax, however, show large differences in measured volume changes.
3) As a consequence the parallel cylinder model is not a valid representation of the thorax.
4) When voltage pickup electrodes are applied on only one side of the thorax, the left-hand side seems to be the best side to pick up the aorta as the major source.
5) The resistivity change of blood due to pulsatile blood flow is not a major contributor to the EI signal. At most 10% of the EI signal stems from blood resistivity change.
6) The outflow problem can be solved by a heamodynamic model of the systemic circulation, independent of the validity of the parallel cylinder model.

Amsterdam, July 2004

Bibliography

Abramowitz, M. & Stegun, I. A. 1970, *Handbook of mathematical functions* Dover Publ., New York.

Bernstein, D. P. 1986, "A new stroke volume equation for thoracic electrical bioimpedance: theory and rationale", Critical Care Medicine, vol. 14, no. 10, pp. 904-909.

Bird, R. B., Steward, W. E., & Lightfoot, E. N. 1966, *Transport Phenomena* Wiley International, New York.

Bland, J. M. & Altman, D. G. 1986, "Statistical methods for assessing agreement between two methods of clinical measurement", *Lancet*, vol. 1, no. 8476, pp. 307-310.

Bonjer, F. H. 1950, *Circulatie onderzoek door impedantiemeting (Investigation of circulation by impedance measurements)*, PhD. thesis of the University of Groningen The Netherlands (in Dutch).

Bonjer, F. H., van den Berg, Jw., & Dirken, M. N. J. 1952, "The origin of the variations of body impedance of body impedance occurring during the cardiac cycle", *Circulation*, vol. 6, pp. 415-420.

Coulter, N. & Pappenheimer, J. R. 1949, "Development of turbulence in flowing blood", *American Journal of Physiology*, vol. 159, pp. 401-408.

Dellimore, J. W. & Gosling, R. G. 1975, "Change in blood conductivity with flow rate", *Medical & Biological Engineering*, vol. 13, no. 6, pp. 904-913.

Duck, F. A. 1990, *Physical properties of Tissue* Academic Press Limited, London.

Edgerton, R. H. 1974, "Conductivity of sheared suspensions of ellipsoidal particles with application to blood flow", *IEEE Transactions on Biomedical Engineering*, vol. 21, no. 1, pp. 33-43.

Evans, E. A. 1973, "New membrane concept applied to the analysis of fluid shear- and micropipette-deformed red blood cells", *Biophysical Journal*, vol. 13, no. 9, pp. 941-954.

Evans, E. A. & Skalak, R. 1979a, "Mechanics and thermodynamics of biomembranes: Part 1", *CRC Critical Reviews in Bioengineering*, vol. 3, no. 3, pp. 181-330.

Evans, E. A. & Skalak, R. 1979b, "Mechanics and thermodynamics of biomembranes: Part 2", *CRC Critical Reviews in Bioengineering*, vol. 3, no. 4, pp. 331-418.

Faes, T. J., Kerkkamp, H. J. J., Hoetink, A. E., & Heethaar, R. M. 2001, "The unsolved outflow problem in impedance cardiography", *Proceedings of XI ICEBI*, 17-21 juni Oslo, pp. 527-530.

Faes, T. J., Raaijmakers, E., Meijer, J. H., Goovaerts, H. G., & Heethaar, R. M. 1999a, "Towards a theoretical understanding of stroke volume estimation with impedance cardiography", *Annals New York Acadamy of Sciences*, vol. 873, pp. 128-134.

Faes, T. J., van der Meij, H. A., de Munck, J. C., & Heethaar, R. M. 1999b, "The electric resistivity of human tissues (100 Hz-10 MHz): a meta- analysis of review studies", *Physiological Measurement*, vol. 20, no. 4, pp. R1-10.

Faes, T. J., Vonk-Noordegraaf, A., Raaijmakers, E., de Vries P.M.J.M., & Heethaar, R. M. 1995, "Mathematical analysis of electrical impedance tomografic data in venous occlusion plethysmography and impedance cardiography", Proceedings of the IX ICEBI, Heidelberg Sept. 26-30, pp. 480-483.

Frewer, R. A. 1974, "The electrical conductivity of flowing blood", *Bio-Medical Engineering*, vol. 9, no. 12, pp. 552-555.

Fricke, H. 1924, "A mathematical treatment of the electric conductivity and capacity of disperse systems I", *Phys.Rev.*, vol. 24, pp. 575-587.

Fujii, M., Nakajima, K., Sakamoto, K., & Kanai, H. 1999, "Orientation and deformation of erythrocytes in flowing blood", *Annals New York Acadamy of Sciences*, vol. 873, pp. 245-261.

Geddes, L. A. & Baker, L. E. 1989, *Principle of applied biomedical instrumentation* John Wiley & Sons, New York.

Geddes, L. E. & Baker, L. E. 1972, "Thoracic impedance changes following saline injection into right and left ventricles", *Journal of Applied Physiology*, vol. 33, no. 2, pp. 278-281.

Geselowitz, D. B. 1971, "An application of electrocardiographic lead theory to impedance plethysmography", *IEEE Transactions on Biomedical Engineering*, vol. 18, no. 1, pp. 38-41.

Goldsmith, H. L. 1999, "Flow-induced interactions in the circulation," in *Advances in the flow and rheology of non-Newtonian Fluids*, vol. 8 D. A. Siginer, ed., Elsevier, Amsterdam, pp. 1-62.

Gollan, F. & Namon, R. 1970, "Electrical impedance of pulsatile blood flow in rigid tubes and in isolated organs", *Annals New York Acadamy of Sciences* pp. 568-576.

Goovaerts, H. G., Raaijmakers, E., & Heethaar, R. M. 1995, "High frequency impedance cardiography", Proceedings of the IX ICEBI, Heidelberg Sept. 26-30, pp. 125-128.

Hayes, B. 1997, *Non-invasive cardiovascular monitoring* BMJ Publishing Group, London.

Hoetink, A. E., Faes, Th. J. C., Marcus, J. T., Kerkkamp, H. J. J., & Heethaar, R. M. 2002, "Imaging of thoracic blood volume changes during the heart cycle with electrical impedance using a linear spot-electrode array", *IEEE Transactions on Medical Imaging*, vol. 21, no. 6, pp. 653-661.

Ito, H., Yamakoshi, K., & Yamada, A. 1976, "Physiological and fluid-dynamic investigations of the transthoracic impedance plethysmography method for measuring cardiac output: Part II Analysis of the transthoracic impedance wave by perfusing dogs", *Medical & Biological Engineering* pp. 373-378.

Kauppinen, P. K., Hyttinen, J. A., & Malmivuo, J. A. 1998, "Sensitivity distributions of impedance cardiography using band and spot electrodes analyzed by a three-dimensional computer model", *Annals of Biomedical Engineering*, vol. 26, no. 4, pp. 694-702.

Kim, D. W., Baker, L. E., Pearce, J. A., & Kim, W. K. 1988, "Origins of the impedance change in impedance cardiography by a three- dimensional finite element model", *IEEE Transactions on Biomedical Engineering*, vol. 35, no. 12, pp. 993-1000.

Kim, D. W., Song, C. G., & Lee, M. H. 1992, "A new ensemble averaging technique in impedance cardiography for estimation of stroke volume during treadmill exercise", *Frontiers Medical Biological Engineering*, vol. 4, pp. 179-188.

Kornet, L., Jansen, J. R., Gussenhoven, E. J., Hardeman, M. R., Hoeks, A. P., & Versprille, A. 1999, "Conductance method for the measurement of cross-sectional areas of the aorta", *Annals of Biomedical Engineering*, vol. 27, no. 2, pp. 141-150.

Kosicki, J., Chen, L. H., Hobbie, R., Patterson, R., & Ackerman, E. 1986, "Contributions to the impedance cardiogram waveform", *Annals of Biomedical Engineering*, vol. 14, no. 1, pp. 67-80.

Kubicek, W. G., Karnegis, J. N., Patterson, R. P., Witsoe, D. A., & Mattson, R. H. 1966, "Development and evaluation of an impedance cardiac output system", *Aerospace Medicine*, vol. 37, no. 12, pp. 1208-1212.

Lababidi, Z., Ehmke, D. A., Durnin, R. E., Leaverton, P. E., & Lauer, R. M. 1970, "The first derivative thoracic impedance cardiogram", *Circulation*, vol. 41, no. 4, pp. 651-658.

Lamberts, R., Visser, K. R., & Zijlstra, W. G. 1984, *Impedance Cardiography* Van Gorcum, Assen, The Netherlands.

Liebman, F. M. 1970, "Electrical impedance pulse tracings from pulsatile blood flow in rigid tubes and volume-restricted vascular beds: theoretical explanations", *Annals New York Acadamy of Sciences*, vol. 170, pp. 437-451.

Lih, M. M. 1975, *Tranport phenomena in medicine and biology* John Wiley and Sons, New York.

Ljung, L. 1987, *System identification Theory for the user* Prentice Hall, New York.

Maxwell, J. C. 1954, *A treatise on electricity and magnetism*, 3rd ed. edn, Dover, New York.

Merrill, E. 1969, "Rheology of blood", *Physiological Reviews*, vol. 49, no. 4, pp. 863-888.

Mohapatra, S. N. 1981, *Non-invasive Cardiovascular monitoring by electrical impedance technique* Pittman Medical Ltd, London.

Mohapatra, S. N. & Hill, D. W. 1975, "The changes in blood resistivity with haematocrit and temperature", *European Journal of Intensive Care Medicine*, vol. 1, pp. 153-162.

Montgomery, D. C. 1997, "Design and Analysis of Experiments," 5th edn, John Wiley & Sons, New York.

Moruccie, J. P., Valentinuzzi, M. E., Rigaud, B., Felice, C. J., Chauveau, N., & Marsili, P. M. 1996, "Bioelectrical impedance techniques in medicine", *Critical Reviews in Biomedical Engineering*, vol. 24, pp. 361-385.

Mueller, J. L., Isaacson, D., & Newell, J. C. 2001, "Reconstruction of conductivity changes due to ventilation and perfusion from EIT data collected on a rectangular electrode array", *Physiological Measurement*, vol. 22, no. 1, pp. 97-106.

Ninomiya, M., Fujii, M., Niwa, M., Sakamoto, K., & Kanai, H. 1988, "Physical properties of flowing blood", *Biorheology*, vol. 25, no. 1-2, pp. 319-328.

Noordergraaf, A. 1978, *Circulatory system dynamics* Academic Press, New York.

Nyboer, J. 1950, "Electrical impedance plethysmography", *Circulation*, vol. 11, pp. 811-821.

Nyboer, J. 1970, *Electrical impedance plethysmography*, 2nd edn, Thomas Publishers, Springfield, IL.

Patterson, R., Wang, L., McVeigh, G., Burns, R., & Cohn, J. 1993, "Impedance cardiography: the failure of sternal electrodes to predict changes in stroke volume", *Biol.Psychol.*, vol. 36, no. 1-2, pp. 33-41.

Patterson, R. P. 1965, *Cardiac output determinations using impedance plethysmography*, PhD. thesis of the University of Minnesota, Minneapolis, Minnesota.

Patterson, R. P. 1989, "Fundamentals of impedance cardiography", *IEEE Engineering in Medicine and Biology Magazine* pp. 35-38.

Patterson, R. P. 1995, "Bioelectric Impedance Measurements," in *The Biomedical Engineering Handbook*, J. D. Bronzino, ed., CRC press & IEEE press, pp. 1223-1230.

Patterson, R. P., Kubicek, W., Kinnen, E., Witsoe, D., & Noren, G. 1964, "Developement of an electrical impedance plethysmograph system to monitor cardiac output", Proceedings of the First Annual Rocky Mountain bioengineeing symposium, May 4-5 at US Air Force Academy Colorado, pp. 56-71.

Patterson, R. P., Wang, L., Raza, B., & Wood, K. 1990, "Mapping the cardiogenic impedance signal on the thoracic surface", *Medical & Biological Engineering & Computing*, vol. 28, no. 3, pp. 212-216.

Patterson, R. P., Wang, L., & Raza, S. B. 1991, "Impedance cardiography using band and regional electrodes in supine, sitting, and during exercise", *IEEE Transactions on Biomedical Engineering*, vol. 38, no. 5, pp. 393-400.

Raaijmakers, E. 1998, *Towards an Understanding of Impedance Cardiography*, PhD. thesis of the Vrije Universiteit, Amsterdam.

Raaijmakers, E., Faes, T. J., Goovaerts, H. G., de Vries, P. M., & Heethaar, R. M. 1997a, "The inaccuracy of Kubicek's one-cylinder model in thoracic impedance cardiography", *IEEE Transactions on Biomedical Engineering*, vol. 44, no. 1, pp. 70-76.

Raaijmakers, E., Faes, T. J., Goovaerts, H. G., Meijer, J. H., de Vries P.M.J.M., & Heethaar, R. M. 1998, "Thoracic geometry and its relation to electrical current distribution: Consequences for electrode placement in electrical impedance cardiography", *Medical & Biological Engineering & Computing*, vol. 36, pp. 592-597.

Raaijmakers, E., Faes, T. J., Scholten, R. J., Goovaerts, H. G., & Heethaar, R. M. 1999, "A meta-analysis of three decades of validating thoracic impedance cardiography", *Critical Care Medicine*, vol. 27, no. 6, pp. 1203-1213.

Raaijmakers, E., Marcus, J. T., Faes, T. J., Meijer, J. H., Goovaerts, H. G., de Vries, P. M. J. M., & Heethaar, R. M. 1996b, "The influence of pulsatile flow on blood resistivity in impedance cardiography", Proc. of the 8th Annu. Int. Conf. IEEE, pp. 1957-1958.

Raza, S. B., Patterson, R. P., & Wang, L. 1992, "Filtering respiration and low-frequency movement artefacts from the cardiogenic electrical impedance signal", *Medical & Biological Engineering & Computing*, vol. 30, no. 5, pp. 556-561.

Sakamoto, K. & Kanai, H. 1979, "Electrical characteristics of flowing blood", *IEEE Transactions on Biomedical Engineering*, vol. 26, no. 12, pp. 686-695.

Sakamoto, K., Muto, K., Kanai, H., & Iizuka, M. 1979, "Problems of impedance cardiography", *Medical & Biological Engineering & Computing*, vol. 17, no. 6, pp. 697-709.

Shankar, T. M. R., Webster, J. G., & Shao, S. Y. 1985, "The contribution of vessel volume change and blood resistivity change to the electrical impedance pulse", *IEEE Transactions on Biomedical Engineering*, vol. 32, no. 3, pp. 192-198.

Sherwood, A., Allen, M. T., Fahrenberg, J., Kelsey, R. M., Lovallo, W. R., & van Doornen, L. J. 1990, "Methodological guidelines for impedance cardiography", *Psychophysiology*, vol. 27, no. 1, pp. 1-23.

Sigman, E., Kolin, A., Katz, L. N., & Jochim, K. 1937, "Effect of motion on the electrical conductivity of the blood", *American Journal of Physiology*, vol. 118, pp. 708-719.

Skalak, R., Keller, S. R., & Secomb, T. W. 1981, "Mechanics of blood flow", *Journal of Biomechanical Engineering*, vol. 103, no. 2, pp. 102-115.

Söderström, T. & Stoica, P. 1989, *System identification* Prentice Hall, New York.

Sramek, B. B. 1981, "Noninvasive technique for measurement of cardiac output by means of electrical impedance", Proceedings of the Vth ICEBI August, Tokyo, pp. 39-42.

Sramek, B. B., Rose, D. M., & Miyamoto, A. "Stroke volume equation with a linear base impedance model and its accuracy, as compared to thermodilution and magnetic flowmeter techniques in humans and animals", pp. 38-41.

Troutman, E. D. & Newbower, R. S. 1983, "A practical analysis of the electrical conductivity of blood", *IEEE Transactions on Biomedical Engineering*, vol. 30, pp. 141-153.

van de Water, J. M., Miller, T. W., Vogel, R. L., Mount, B. E., & Dalton, M. L. 2003, "Impedance cardiography the next vital sign technology?", *Chest*, vol. 123, pp. 2028-2033.

Visser, K. R. 1989, "Electric properties of flowing blood and impedance cardiography", *Annals of Biomedical Engineering*, vol. 17, no. 5, pp. 463-473.

Visser, K. R. 1992, "Electric conductivity of stationary and flowing human blood at low frequencies", *Medical & Biological Engineering & Computing*, vol. 30, no. 6, pp. 636-640.

Visser, K. R., Lamberts, R., Korsten, H. H., & Zijlstra, W. G. 1976, "Observations on blood flow related electrical impedance changes in rigid tubes", *Pflugers Archiv - European Journal of Physiology*, vol. 366, no. 2-3, pp. 289-291.

Wang, L. & Patterson, R. 1995, "Multiple sources of the impedance cardiogram based on 3-D finite difference human thorax models", *IEEE Transactions on Biomedical Engineering*, vol. 42, no. 2, pp. 141-148.

Wang, Y., Haynor, D. R., & Kim, Y. 2001, "A finite-element study of the effects of electrode position on the measured impedance change in impedance cardiography", *IEEE Transactions on Biomedical Engineering*, vol. 48, no. 12, pp. 1390-1401.

Westerhof, N. 1993a, "Arterial haemodynamics," in *The physics of heart and circulation*, J. Strackee & N. Westerhof, eds., Institute of Physics Publishing, Bristol & Philadelphia, pp. 355-382.

Westerhof, N. 1993b, "Cardiac pump function," in *The physics of heart and circulation*, J. Strackee & N. Westerhof, eds., Institute of Physics Publishing, Bristol & Philadelphia, pp. 207-221.

Woltjer, H. H., Arntzen, B. W., Bogaard, H. J., & de Vries, P. M. 1996a, "Optimalisation of the spot electrode array in impedance cardiography", *Medical & Biological Engineering & Computing*, vol. 34, no. 1, pp. 84-87.

Woltjer, H. H., Bogaard, H. J., Sheffer, G. J., van der Spoel, H. I., Huybregts, A. J. M., & de Vries P.M.J.M. 1996b, "Standardization of non-invasive impedance cardiography for assessment of stroke volume: comparison with thermodilution", *British Journal of Anaesthesiology*, vol. 77, pp. 748-752.

Woltjer, H. H., van der Meer, B. J., Bogaard, H. J., & de Vries, P. M. 1995, "Comparison between spot and band electrodes and between two equations for calculations of stroke volume by means of impedance cardiography", *Medical & Biological Engineering & Computing*, vol. 33, no. 3, pp. 330-334.

Wtorek, J. 2000, "Relations between components of impedance cardiogram analyzed by means of finite element model and sensitivity theorem", *Annals of Biomedical Engineering*, vol. 28, no. 11, pp. 1352-1361.

Wtorek, J. & Polinski, A. 1995, "Examination of impedance cardiography properties--FEM model studies", *Biomedical Sciences Instrumentation*, vol. 31:77-82., pp. 77-82.

Yamakoshi, K., Ito, H., Yamakoshi, K., Miura, S., & Tomino, T. 1976, "Physiological and fluid-dynamic investigations of the transthoracic impedance plethysmography method for measuring cardiac output.: Part 1-A fluid-dynamic approach to the theory using an expansible tube model", *Medical & Biological Engineering*, vol. 14, pp. 365-372.

Yamakoshi, K., Togawa, T., & Ito, H. 1977, "Evaluation of the theory of cardiac-output computation from transthoracic impedance plethysmography", *Biological Engineering & Computing*, vol. 15, pp. 479-488.

Zhang, Y. J., Qu, M. H., Webster, J. G., Tompkins, W. J., Ward, B. A., & Bassett, D. J. 1986, "Cardiac output monitoring by impedance cardiography during treadmill exercise", *IEEE Transactions on Biomedical Engineering*, vol. 33, no. 11, pp. 1037-1042.

Summary

Electrical impedance cardiography, sometimes called bio-impedance cardiography or thoracic impedance cardiography, was introduced as a low-cost non-invasive method to monitor function parameters of heart and circulation. The method aims to calculate heart function related parameters from a change in the electrical impedance measured across the thorax. To do so, an electrical current is injected into the body by means of one set of electrodes and with a different set of electrodes voltage changes across the thorax are measured as a function of time. From the measured voltage and current the magnitude and of the thoracic impedance can be calculated, which is generally revered to as the electrical impedance (EI) of the thorax.

One of the heart function related parameters that might be determined from the thoracic EI signal is the amount of blood pumped by the heart into the aorta, i.e. Stroke Volume (SV) or Cardiac Output (CO). The rational behind the method is that when blood is injected into the aorta, its cross-sectional surface area increases and consequently its EI decreases. Therefore, a heart contraction synchronous decrease of the measured thoracic EI is assumed to be related to SV and CO. Although this line of reasoning seams simple, the extensive literature on the subject shows that it contains several pitfalls.

The most fundamental point of critique is that the electrical representation of the thorax, the parallel cylinder model, is not adequate. This model assumes that the only source of the EI signal is the aorta (represented by a cylinder) and that the aorta is enclosed by another cylinder that represents the thorax (of which the electrical properties are assumed time-invariant, at least in a period of several heart beats). However, other possible origins of the thoracic EI change are the other major blood vessels in the thorax (e.g. pulmonary artery, vena cava etc.), the heart, muscle tissue, the lungs, and possibly even the electrical resistivity change of blood due to blood flow. In order to calculate SV or CO from the measured thoracic EI change, the contribution of the aorta to the

thoracic EI change should first of all be separable in time and location on the thorax from the contribution of the other sources.

Even if it is possible to isolate the contribution of the aorta, the problem of the electrical resistivity change of blood due to blood flow complicates matters considerably. If the heart pumps blood into the aorta, two different processes may cause a measurable EI change. On the one hand, the increase of cross-sectional surface area of the aorta will result in a decrease of the measured EI. On the other hand, in flowing blood shear stresses result in orientation and deformation of red blood cells. The orientation and deformation of red blood cells alters the pathway of the electrical current. As a consequence the electrical resistivity of blood decreases and this in turn will also produce a decrease of the measured EI. Consequently, if SV is to be obtained from a measured EI change, theoretical knowledge about the relation between inflow of blood into the aorta, cross-sectional surface area change of the aorta and blood resistivity change is of eminent importance.

Suppose that the measured thoracic EI change can be related only to the cross-sectional surface area change (or equivalently to the volume change) of the aorta, still another problem remains. How can SV or CO be calculated from the volume change of the aorta? During the cardiac cycle, blood is not only entering the aorta, but simultanously blood is also leaving the aorta due to arterial runoff. This is the so-called outflow problem and it still remains unsolved. As a consequence, a theoretically founded estimator of SV from thoracic EI changes is still not available.

This thesis focuses on these problems by answering the following fundamental questions:

1. Can the contribution of the aorta to the thoracic EI signal be separated from the contribution of other possible sources?
2. Can the contribution to the thoracic EI change of the blood resistivity change due to blood flow be quantified?
3. Can the outflow-problem be solved?

A more practical question is also discussed:

4. Can the number of voltage pickup electrodes needed for EI cardiography be reduced to a minimum?

Reducing the number of electrodes needed for EI cardiography is more comfortable for the patient and more practical for medical personnel, especially in the Intensive Care Unit and after extensive surgery.

Is the Aorta the Major Source of the EI signal?

Chapter 2 introduced a method to estimate thoracic blood volume changes during the heart cycle from regional thoracic EI measurements. An estimator was developed that calculates segmental surface area changes of the organs in the thorax. The EI data was collected with a linear electrode array that resembles traditional electrode arrangements. The difference being that where the traditional arrangements use voltage pickup electrodes that are separated by a relatively large distance, the voltage pickup electrodes in the array used in *chapter 2* were separated by a relatively short distance. Results from EI measurements on three healthy male subjects where compared to the surface area changes of the thoracic organs obtained from MRI measurements. These latter images included contributions of the aorta, the vena cava, the carotid arteries and the heart. Furthermore, volume changes across the whole thorax and in the region of the aortic arch were calculated from the EI signals and the MRI images.

The results showed that the total volume changes measured with EI across the whole thorax show remarkable similarity with the volume change measured with MRI. The EI volume change measured close to the heart corresponded closely to MRI volume changes including contributions of the aorta, vena-cava, carotid arteries, and the heart. The EI volume change measured further away from the heart at the lateral sides of the thorax, on the other hand, showed close correspondence to MRI volume changes including contributions of the aorta, vena-cava, carotid arteries, but without the heart. This indicates that the aorta is not the only source of the EI signal measured across the whole thorax and consequently the parallel cylinder model is not a valid

representation of the whole thorax. The contribution of the heart is considerable as the total volume change decreases by approximately one third in systole.

The results also showed, however, that reducing the region across which the EI signal is measured, changes matters considerably. If the EI signal is measured across the region of the ascending aorta, aortic arch, and upper part of the descending aorta, the estimated volume changes show close correspondence to the volume change of only the aorta measured with MRI. Moreover, the EI volume changes measured at the anterior side of the thorax and lateral side of the thorax are almost identical (correlation coefficients of these volume changes ranging from 0.932-0.987). This suggests that in the region of the aortic arch the aorta is the major source of the EI signal and the parallel cylinder model is valid.

Three objections can be made at this point, two being of a fundamental nature and the other of a more practical nature. The first fundamental objection concerns the electrode array: all EI signals were simultaneously measured at the left-hand and right-hand side of the thorax. Signals measured, for example, at the left-hand side or right-hand side of the thorax only may not show this close correspondence. The second fundamental objection that can be raised, concerns the contribution of the resistivity change of blood due to blood flow. The estimator developed in *chapter 2* was based on the assumption that the magnitude of the resistivity of flowing blood is about 10% smaller than the magnitude of blood resistivity in the absence of flow. The third objection that is of a more practical nature involves the use of the EI method in the clinic. It is not desirable that the accuracy of the method depends greatly on the exact placement of the voltage pickup electrodes.

Chapter 3 dealt with both the fundamental and practical objection about the electrode array in an indirect way. The aim was to investigate whether the number of electrodes for EI cardiography can be reduced, removing part of the practical objection concerning electrode placement. In the process, however, an indication of the validity of the parallel cylinder model was obtained. Six different electrode arrangements were used to obtain the thoracic EI impedance signal. The results showed that the EI signal measured on the right-hand side of the thorax differs considerably from that measured on the left-hand side of the

thorax. Consequently, the fundamental objection concerning the electrode array that was used in *chapter 2* seems to be substantiated.

Can the Magnitude of Blood Resistivity Change be Quantified?

Although there is general consensus that blood conductivity changes due to blood flow (caused by deaggregation, orientation and deformation of erythrocytes), the magnitude of this effect in-vivo is still a matter of debate. Where some concluded on the basis of in-vitro experiments that the magnitude of the decrease of blood resistivity due to blood flow may be as large as 20% relative to blood with undeformed and randomly orientated erythrocytes, others argued that this is an overestimation of the so-called resistivity effect, as in-vivo it is questionable whether a state of complete deorientation exists before the onset of blood flow. The magnitude of the resistivity change due to pulsatile blood flow, they estimated, was about 5%. Before the contribution of blood resistivity change in-vivo can be discussed at all, better theoretical understanding of this phenomenon is needed.

In *chapter 4* a theory on blood conductivity (i.e. the reciprocal of the resistivity) was proposed that showed good agreement with the conductivity change of blood measured in-vitro. This theory was developed assuming a stationary and laminar flow profile in a rigid tube, so-called Poiseuille flow. In-vivo, however, the flow profile is much more erratic and surely not stationary. The theoretical model, however, may be considered to give an upper bound of the conductivity change in-vivo. In *chapter 5* the theory presented in *chapter 4* is combined with the method introduced in *chapter 2*. Cross-sectional surface area changes and average flow velocities were measured with MRI in four subjects. The relative error introduced in neglecting the pulsatile nature of blood conductivity change was estimated.

The results show that neglecting this pulsatile nature introduces an error in volume estimation that ranges from roughly 2-10% during the systolic part of the heart cycle, depending largely on the flow pattern in the aorta. Consequently, it may be inferred that the conductivity change of blood is only a minor cause for any disagreement of EI volume changes and volume changes measured with MRI.

Where on the Thorax is the Aorta the Major Source of the EI Signal?

Where on the thorax can the In *chapter 5* the method of *chapter 2* was used again, but now on four subjects the EI signals were measured with electrode arrays applied on mid-axillary and mid-clavicular lines on the left-hand and right-hand side of the thorax separately. In addition, the EI signal was also measured on the sternal line of the thorax. The results confirmed what was already found in *chapter 3*: large differences exist between the EI signals measured at different locations on the thorax. Moreover, where it could be argued in *chapter 2* that in the region of the aortic arch the aorta is the major source of the EI signal, irrespective of the location of the electrode array, the results presented in *chapter 5* refute this. Considerable differences exist in the cross-sectional surface area change mappings obtained with the different arrays and it is impossible to identify any of these changes as being the result of the cross-sectional surface area changes of the aorta. The volume changes calculated from these cross-sectional surface area changes confirm this, with the possible exception of the volume changes measured at the mid-axillary line on the left-hand side of the thorax. This is the only location on the thorax where the volume change measured with EI resembles the volume change of the aorta, although the resemblance is not strong.One conclusion can be drawn with certainty from these findings: the parallel cylinder model is not a valid representation of the thorax, not even in the region of the aortic arch. Extending the parallel cylinder model to a parallel conductor model, as was done in *chapter 2*, does not overcome this problem. The only solution is replacing the parallel cylinder model with a model that takes into account the multiple sources of the EI signal. Such a model should be able to predict the different contributions of the thoracic organs in different regions of the thorax.

Can the Outflow-Problem be Solved?

To tackle the outflow-problem, in *chapter 6* a model of heamodynamics was introduced that leads to an estimator of stroke volume that corrects for the outflow of blood from the aorta due to arterial runoff. This estimator contains three independent variables: the time interval between two consecutive heartbeats (T_I), the time interval in which the heart ejects blood into the aorta (T_{LVE}), and the aortic volume change between end-diastole and end-systole (ΔV_A). Additionally, using the parallel cylinder model as an electrical model of the thorax, the aortic volume change ΔV_A was related to thoracic impedance change (ΔZ). Simulation results established the superiority of this new estimator over traditional estimators. The obvious question now is how this new estimator will perform on patients or healthy subjects. Before the new estimator can be used on patients or healthy subjects, however, two major obstacles must be taken.

First of all, it has been demonstrated in this thesis that the parallel cylinder model is not a valid representation of the electrical properties of the thorax. This does not imply that the outflow correction is invalid, as the correction follows from the heamodynamics and therefore is independent of the thoracic model. The thoracic model is only necessary to relate aortic volume changes to thoracic impedance changes, but as was argued above it can not be concluded beyond reasonable doubt yet what model or which electrode configuration are best suited to tackle this first obstacle.

Secondly, to correct for the outflow the interbeat time interval (T_I) and the left ventricular ejection time (T_{LVE}) must be measured. The first time interval can easily be obtained from an ECG that is recorded simultaneously with the EI-signal. Estimating the second time interval has not been dealt with in this thesis. Using wrong estimations of T_{LVE} will introduce possibly large errors in SV estimations.

Can the Number of Voltage Pickup Electrodes be Reduced to a Minimum?

As was discussed above, *chapter 3* investigated the reduction of the number of electrodes to measure the EI cardiogram. It was found that reducing the number of current injecting electrodes has little effect. Reducing the number of voltage pickup electrodes, on the other hand, substantially changes stroke volume estimation, especially when the voltage pickup electrodes are located on the right-hand side of the thorax. A reduced number of electrodes applied on the right-hand side of the thorax resulted in a considerable reduction in the group mean of the estimated stroke volume, due to a higher value of the measured base impedance Z_0. A reduced number of voltage pickup electrodes applied on the left-hand side of the thorax did not change the group means of the measured variables or calculated stroke volume. However, differences in these variables for individual subjects can be considerable. For some subjects the value of the estimated SV (using the Kubicek-estimator) was up to 45 ml lower than that of the estimated SV with a traditional arrangement. Thus, a reduction of the number of electrodes is payed for by a possible decrease in estimated SV. This does not mean that an electrode array with two voltage pickup electrodes on the left-hand side of the thorax is less optimal than the traditional arrangement. The only conclusion that can be drawn from *chapter 3* is that the arrangements are not equivalent. In order to establish the superiority of either arrangement, their validity should be investigated by comparison to a reference method like MRI or dilution methods. Before this can be done however, the SV-estimator presented in chapter 6 should be validated and robust estimation of T_{LVE} has to be investigated.

Conclusion

1) The aorta is only the major source of the thoracic EI signal when it is measured in the region of the aortic arch with voltage pickup electrodes located on both sides of the thorax.
2) Voltage pickup electrodes applied on different sides of the thorax, however, show large differences in measured volume changes.
3) As a consequence the parallel cylinder model is not a valid representation of the thorax.
4) When voltage pickup electrodes are applied on only one side of the thorax, the left-hand side seems to be the best side to pick up the aorta as the major source.
5) The resistivity change of blood due to pulsatile blood flow is not a major contributor to the EI signal. At most 10% of the EI signal stems from blood resistivity change.
6) The outflow problem can be solved by a heamodynamic model of the systemic circulation, independent of the validity of the parallel cylinder model.

Samenvatting

Electrische Impedantie cardiograpy, ook wel bio-impedantie cardiografie genoemd, is ooit geïntroduceerd als een goedkope en niet-invasieve manier om parameters van de hartfunctie en bloedscirculatie te meten. Met deze methode wordt geprobeerd om de hartfunctie parameters te bepalen uit electrische impedantie veranderingen die gemeten worden over de borstkas. Hiervoor wordt door middel van een aantal electrodes een stroom door het lichaam gestuurd en met andere electrodes wordt de spanning over de borstkas gemeten als functie van de tijd. Met de gemeten spanning en bekende geïnjecteerde stroom kan de magnitude van de electrische impedantie (EI) van de borstkas berekend worden.

Een van de hartfunctie gerelateerde parameters die mogelijk met de EI van de borstkas bepaald kan worden is de hoeveelheid bloed die per hartslag in de aorta wordt gepompt. Dit heet het Slag Volume (SV). Het idee is dat door het pompen van bloed in de aorta, de diameter van de aorta toeneemt en als gevolg daarvan de EI van de borstkas afneemt. Daarom wordt aangenomen dat een hartsynchrone afname van het EI-signaal, gerelateerd is aan SV. Alhoewel deze denkwijze simpel lijkt, laat de uitgebreide literatuur over dit onderwerp zien dat er een aantal valkuilen zijn.

De meest fundamentele tegenwerping is dat het meest gebruikte electrische model van de thorax, het zogenoemde parallele cilinder model, niet adequaat is. Dit model gaat er vanuit dat de enige bron van het EI-signaal de aorta is (die gerepresenteerd wordt door een cilinder) en dat de aorta omsloten wordt door een andere cilinder die de thorax voorstelt. De electrische eigenschappen van de thorax worden als tijdsonafhankelijk gezien, in ieder geval als de tijdspanne van een aantal hartslagen wordt beschoud. Er zijn echter andere mogelijke bronnen van het EI-signaal, zoals andere grote bloedvaten (longslagader, vena cava), het hart, spierweefsel, de longen. Om het slagvolume te kunnen berekenen moet de bijdrage van de aorta aan het EI-signaal dus gescheiden kunnen worden van de bijdragen van de andere bronnen.

Zelfs als het mogelijk is de bijdrage van de aorta te isoleren, dan blijft er een ander probleem bestaan. De electrische eigenschappen van bloed veranderen als dit gaat stromen. Als het hart bloed pompt in de aorta, zorgen mogelijk twee verschillende processen voor een meetbare verandering van het EI-signaal. Ten eerste zal een toename van de diameter van de aorta zorgen voor een afname van de EI. Ten tweede zullen door het gaan stromen van het bloed de rode bloedcellen zich gaan oriënteren in de stroomrichting en bij hogere stroomsnelheden zelfs van vorm gaan veranderen. Als gevolg hiervan zal de soortelijke weerstand van bloed afnemen en dit veroorzaakt ook een afname van de EI. Als SV uit het EI-signaal bepaald moet worden is het dus van belang om te weten wat de relatie is tussen het pompen van bloed in de aorta, de diameter verandering van de aorta en de verandering van soortelijke weerstand van het bloed.

Stel dat een gemeten EI verandering van de borstkas veroorzaakt zou worden door alleen diameter veranderingen (of equivalent daar aan volume veranderingen) van de aorta. Dan moet de vraag gesteld worden hoe SV uit de volume verandering van de aorta bepaald kan worden? Tijdens de hartcyclus stroomt bloed niet alleen de aorta in, maar gelukkig stroomt er ook bloed uit de aorta naar de rest van het lichaam. Hiervoor moet gecorrigeerd worden als SV bepaald wordt uit volume veranderingen van de aorta. Dit wordt het ‘uitstroom-probleem’ (Engels: Outflow-problem) genoemd en het is tot nu toe nog niet adequaat opgelost. Er is dus nog geen goede schatter van SV op basis van het EI-signaal.

In dit proefschrift worden de bovenstaande problemen behandeld door het stellen van de volgende fundamentele vragen:

1. Kan de bijdrage van de aorta aan het EI-signaal gescheiden worden van de bijdragen van andere mogelijke bronnen?
2. Kan de bijdrage aan het EI-sigaal van de verandering van de soortelijke weerstand van bloed door stroming gequantificeerd worden?
3. Kan het ‘uitstroom-prombleem’ worden opgelost.

Een meer practische vraag die ook aan de orde komt is:

4. Kan het aantal electrodes dat nodig is voor EI cardiografie worden gereduceerd?

Het reduceren van het aantal electrodes dat nodig is om het EI-signaal te meten is comfortabeler voor de patiënt en practischer voor medisch personeel, met name als gemeten moet worden op de Intensive Care.

Is de aorta de belangrijkste bron van het EI-signaal?

In *hoofdstuk 2* wordt een methode geïntroduceerd waarmee bloed volume veranderingen van organen in de borstkas gemeten kunnen worden. Het EI-signaal wordt gemeten met een rij electrodes die dicht bij elkaar zijn geplaatst over de hele borstkas. Met een special ontworpen schatter wordt zo de totale oppervlakte verandering van alle organen in plakken van de borstkas gemeten. Deze metingen zijn uitgevoerd op drie mannelijke proefpersonen en de resultaten zijn vergeleken met oppervlakte veranderingen van de organen die met Magnetic Resonance Imaging (MRI) zijn gemeten. Uit deze laatste metingen zijn oppervlakte veranderingen van de aorta, vena cava, de carotiden en het hart gemeten. Met de EI-metingen en MRI-metingen zijn de volume veranderingen van deze organen in de hele borstkas bepaald en in het gedeelte van de borstkas waar de aorta boog zich bevindt.

De resultaten tonen een opmerkelijke overeenkomst tussen de volume veranderingen gemeten met EI en met MRI. De volume veranderingen gemeten met EI dicht bij het hart corresponderen goed met volume veranderingen gemeten met MRI waarbij bijdragen van de aorta, vena cava, carotiden en het hart zijn meegenomen. Als de volume veranderingen op een grotere afstand van het hart worden gemeten met EI (met de electrodes aan de zijkant van de borstkas geplaatst), dan is de overeenkomts goed met gemeten MRI volume veranderingen waarbij de bijdrage van het hart is weggelaten. Dit resultaat toont aan dat de aorta niet de enige bron van het EI signaal is, als het signaal over de hele borstkas gemeten wordt. Het gevolg hiervan is dat het parallele cilinder model geen goede representatie is van (de electrische eigenschappen van) de borstkas. De bijdrage van het hart is aanzienlijk en verkleint de totale gemeten volume verandering met eenderde tijdens systole (dit is de fase van

de hartcyclus waarin bloed in de aorta gepompt wordt en het hart in volume afneemt).

De resultaten in dit hoofstuk laten echter ook zien dat de zaken anders liggen als het gebied waarin volume veranderingen worden gemeten, wordt gereduceerd tot het gebied in de borstkas waarin de aorta boog zich bevindt. In dit geval komen de volume veranderingen die met EI zijn gemeten goed overeen met volume veranderingen van de aorta die met MRI gemeten zijn. Daarbij komt nog dat EI-metingen dicht bij het hart bijna gelijk zijn aan EI-metingen verder weg van het hart (correlatie coëfficiënten tussen deze metingen lagen tussen de 0.932 en 0.987). Dit suggereert dat in het gebied van de aorta boog de aorta de belangrijkste bron is en dat het parallele cilinder model valide is.

Drie bezwaren kunnen op dit moment aangetekend worden, waarvan twee van fundamentele aard en een van een meer practische aard. Het eerste fundamentele bezwaar betreft de electrode configuratie waarmee gemeten is. De EI-signalen zijn gelijktijdig aan de linker kant en rechter kant van de borstkas gemeten. Als het EI-signalen alleen links of rechts gemeten worden, dan wordt de goede overeenkomst met MRI mogelijk niet gevonden. Het tweede fundamentele bezwaar betreft de bijdrage van de afname van de soortelijke weerstand van bloed door het gaan stromen van bloed. Bij het ontwikkelen van de EI schatter in *hoofdstuk 2* is ervan uitgegaan dat de soortelijke weerstand van stromend bloed 10% kleiner is dan dat van stilstaand bloed. Deze aanname zal hard gemaakt moeten worden. Het derde bezwaar van meer practische aard betreft de plaatsing van de electrodes. Voor klinisch gebruik is het niet wenselijk dat de electrodes precies in het gebied van de aorta boog moeten worden geplaatst om een goede schatting te van de volume verandering van de aorta te kunnen krijgen.

In *hoofdstuk 3* worden zowel het fundamentele als het practische bezwaar van de electrode configuratie onderzocht. Het doel was om te onderzoeken of het aantal electrodes voor EI cardiografie gereduceerd kan worden. Daarmee wordt een gedeelte van het practische bezwaar wegenomen. Tijdens het onderzoek werd echter ook een indicatie verkregen of EI-signalen die afzonderlijk links en rechts gemeten worden, overeenkomen met signalen die gelijktijdig links en

rechts gemeten worden. Uit vergelijking van zes verschillende electrode configuraties blijkt dat er een groot verschil is tussen de verschillende signalen. Dit wijst er op dat het fundamentele bezwaar betreffende de electrode configuratie terrecht lijkt.

Kan de bijdrage aan het EI-sigaal van de verandering van de soortelijke weerstand van bloed door stroming gequantificeerd worden?

Alhoewel er in de literatuur consensus is over het feit dat de soortelijke weerstand van bloed verandert als bloed gaat stromen, is de grootte van het effect in-vivo nog onderwerp van debat. Waar sommigen op basis van in-vitro experimenten concluderen dat de afname wel 20% kan zijn ten opzicht van stilstaand bloed, beargumenteren anderen dat dit een overschatting van het zogenoemde resistiviteit-effect is. Sommige schattingen komen niet verder dan een afname van 5% van de soortelijke weerstand van stomend bloed in-vivo.

In *hoofdstuk 4* wordt een theorie ontwikkeld, die de conductiviteit (dit is het reciproke van de soortelijke weerstand) van stromend bloed berekent, op basis van oriëntatie en vervorming van rode bloedcellen door schuifspanning. De resultaten verkregen met deze theorie laten een goede overeenkomst zien met resultaten verkregen uit in-vitro experimenten. De theorie is ontwikkeld op basis van de aanname dat bloed laminair en stationair stroomt in een starre buis, de zogenaamde Poisseuille-stroom. In-vivo, echter, is het stroom-profiel van bloed niet laminair en zeker niet stationair. Het theoretische resultaat kan echter beschouwd worden als een ‘worst-case’ scenario van het te verwachten effect, omdat het niet laminair en stationair zijn van de bloedstroom in-vivo, de mate van oriëntatie en vervorming vermindert. Het gevolg is dat de te verwachten afname van de soortelijke weerstand in-vivo dus altijd minder zal zijn dan de berekende afname op basis van Poisseuille-stroom.

In *hoofstuk 5* wordt de theorie uit *hoofdstuk 4* gecombineerd met de methode die geïntroduceerd is in *hoofdstuk 2*. Weer zijn EI-signalen gemeten op de borstkas met electrodes die dicht bij elkaar zijn geplaatst. Ook zijn met MRI weer de oppervlakte veranderingen van de organen in de borstkas gemeten, maar daar bovenop is ook de stroomsnelheid van bloed in de aorta bepaald. De metingen zijn verricht op vier proefpersonen (twee mannen en

twee vrouwen). Uit de metingen is een schatting van de fout verkregen die optreedt als de pulstiele verandering van de soortelijke weerstand van bloed tijdens de hartcyclus wordt verwaarloosd in de berekening van het aorta volume. De resultaten laten zien dat de fout die geïntroduceerd wordt ligt tussen de 2% en 10%, afhankelijk van het stroomprofiel van bloed. Er mag dus geconcludeerd worden dat de verandering van de soortelijke weerstand van bloed maar een kleine bijdrage levert aan een eventueel gemeten verschil tussen volume veranderingen van de aorta die gemeten zijn met EI en MRI.

Waar op de borstkas is de aorta de belangrijkste bron van het EI-signaal?

In *hoofstuk 5* is de methode die in *hoofdstuk 2* is ontwikkeld weer toegepast op vier proefpersonen, maar nu zijn de EI-sigalen links en rechts op de borstkas afzonderlijk gemeten. Ook zijn de EI-signalen op de centrale lijn over het borstbeen gemeten. De resultaten bevestigen wat al was gevonden in *hoofdstuk 3*, namelijk dat er grote verschillen bestaan tussen de EI-signalen die links en rechts worden gemeten. Daar komt nog bij dat waar in *hoofdstuk 2* in het gebied van de aorta boog goede overeenstemming was tussen de EI-signalen die dichtbij en verder weg van het hart gemeten waren, de resultaten uit *hoofdstuk 5* dit tegenspreken. Er zijn grote verschillen gevonden tussen de volume veranderingen die gemeten zijn met verschillende electrode configuraties en geen van deze configuraties lijkt de volume verandering van de aorta goed te kunnen meten, met als mogelijke uitzondering een configuratie waarbij de electroden aan de linker zijkant van de borstkas geplaatst worden. Dit is de enige configuratie die enige overeenkomst laat zien tussen de volume veranderingen die met EI zijn gemeten en de volume verandering van de aorta die met MRI gemeten is.

Een conclusie kan met zekerheid getrokken worden: het parallele cilinder model is geen goede representatie van de electrische eigenschappen van de borstkas, zelfs niet in het gebied van de aorta boog. Het uitbreiden van het parallele cilinder model naar een parallele geleidersmodel (dus onafhankelijk van de geometrie van de geleider), zoals gedaan is in *hoofdstuk 2*, lost het probleem niet op. De enige oplossing is het parallele cilinder model te vervangen door een model dat de meervoudige bronnen van het EI-signaal in

rekening brengt. Zo een model moet tenminste aan de eis voldoen dat het de verschillende bijdragen van de organen in de borstkas op verschillende plaatsen op de borstkas op een correcte manier voorspelt.

Kan het 'uitstroom-probleem' worden opgelost?

Om het 'uitstroom-probleem' aan te pakken, is in *hoofdstuk 6* een heamodynamisch model gebruikt, op basis waarvan een SV-schatter is ontworpen die corrigeert voor het wegstromen van bloed uit de aorta tijdens de hartcyclus. Deze schatter bevat drie onafhankelijke variabelen: het tijdinterval tussen twee opeenvolgende hartslagen; het tijdinterval waarin het hart bloed pompt in de aorta; en de volume verandering van de aorta tussen eind-diastole en eind-systole. Verder is het parallele cilinder model gebruikt om de volume verandering van de aorta te relateren aan de EI verandering van de aorta. Simulatie resultaten laten zien dat deze schatter beter presteert dan traditionele schatters die ofwel niet, danwel niet adequaat corrigeren voor de uitstroom van bloed uit de aorta. De voor de hand liggende vraag is nu hoe deze schatter presteert op signalen gemeten aan patiënten of gezonde proefpersonen. Voor dat dit kan gebeuren, moeten echter twee belangrijke obstakels overwonnen worden.

Ten eerste is in dit proefschrift aangetoond dat het parallele cilinder model geen goede representatie van de thorax is. Dit betekent niet dat de, in dit proefschrift geïntroduceerde, uitstroom correctie niet valide is. De uitstroom correctie is gebaseerd op het heamodynamische model en is dus onafhankelijk van het electrische model van de thorax. Het electrische model is alleen nodig om volume veranderingen van de aorta te relateren aan gemeten EI veranderingen, maar zoals hierboven uiteen is gezet is nog niet vast te stellen welk electrisch model of welke electrode configuratie het meest geschikt is om de klus te klaren.

Ten tweede moeten voor een goede correctie het tijdinterval tussen twee opeenvolgende hartslagen en het tijdinterval waarin het hart bloed pompt in de aorta bepaald worden. Het eerste interval kan makkelijk uit het ECG bepaald worden, dat gelijktijdig met het EI-signaal geregistreerd wordt. Het schatten van het tweede interval echter is niet in dit proefschrift behandeld en

kan in sommige (pathalogische) gevallen tot problemen leiden. Verkeerde schattingen van het tijdinterval waarin het hart bloed pompt in de aorta kan leiden tot grote fouten in SV schattingen.

Kan het aantal electrodes dat nodig is voor EI cardiografie worden gereduceerd?

Zoals eerder al was gezegd, is in *hoofdstuk 3* onderzocht of het aantal electodes dat nodig is om het EI-cardiogram te meten, gereduceerd kan worden. De resultaten laten zien dat het reduceren van electrodes die de stroom in het lichaam injecteren, weinig effect hebben op de schatting van het SV.

Het reduceren van het aantal electroden die de spanning over de borstkas meten, geeft echter aanzienlijke verschillen in SV schatting, met name als de electrodes alleen aan de rechter kant van de borstkas worden geplaatst. Deze configuratie resulteerde in een aanzienlijke verlaging van het gemiddelde SV gemeten over de hele groep proefpersonen. Als de electrodes alleen aan de linkerkant van de borstkas worden geplaatst, dan veranderd het gemiddelde slagvolume gemeten over de hele groep niet significant, maar kunnen aanzienlijke verschillen (meestal reductie) optreden in SV schattingen van individuele proefpersonen. De prijs die betaald wordt voor het verminderen van het aantal spanningsmetende electroden is een mogelijke reductie in het geschatte slagvolume.

Dit betekent echter niet dat een configuratie met twee spanning metende electrodes links minder goed presteert dan de traditionele configuratie (met spanning metende electroden aan beide zijden van de borstkas). De enige conclusie die getrokken kan worden is dat de twee configuraties niet equivalent zijn. Om de superioriteit van een van beide electrode configuraties aan te tonen, moeten de SV schattingen van deze configuraties worden vergeleken met een referentie methode (MRI of dilutie methoden). Voordat dit gedaan kan worden moet echter de SV schatter die in *hoofdstuk 6* is ontwikkeld gevalideerd worden. Zoals gezegd moet dan eerst onderzocht worden hoe het tijdinterval waarin het hart bloed pompt in de aorta robuust en accuraat gemeten kan worden.

Conclusie

1) De aorta is de belangrijkste bron van het EI-signaal van de borstkas als het signaal gemeten wordt in het gebied van de aorta boog met spanning metende electrodes die aan beide zijden van de borstkas geplaatst zijn.
2) Als spanning metende electrodes echter aan verschillende kanten van de borstkas afzonderlijk worden geplaatst, dan worden er grote verschillen gevonden tussen gemeten volumes.
3) Een gevolg hiervan is dat het parallele cilinder model geen goede representatie is van de electrische eigenschappen van de borstkas.
4) Als spannings metende electroden aan maar een kant van de borstkas geplaatst worden, dan lijkt de linkerkant de beste kant om de aorta als belangrijkste bron te kunnen meten.
5) De verandering van de soortelijke weerstand van bloed door pulsatiele bloed stroming is geen grote bijdrager aan het EI-signaal. In het ergste geval zal niet meer dan 10% van het EI-signaal het gevolg zijn van de verandering van de soortelijke weerstand.
6) Het ‘uitsroom-probleem’ kan opgelost worden door gebruik te maken van een heamodynamisch model van de systemische bloedcirculatie, onafhankelijk van de validiteit van het parallele cilinder model.

Nawoord

Het gevoel bij het beginnen van dit nawoord is onbeschrijvelijk. Dat dit proefschrift dan toch echt bijna klaar is geeft een gevoel van uitzinnige euforie. Aan de andere kant wordt dit gevoel getemperd door het besef dat ik in die staat van euforie waarschijnlijk iemand onrecht ga aan doen door diegene niet de o zo verdiende dankbaarheid te betuigen. Verder moet mij nog van het hart dat de volgorde waarin personen genoemd worden geenzins een weerspiegeling is van mate van mijn dankbaarheid. Hoe het ook zij, nog een paar passen naar de top en laat de afgrond dan maar komen.

Allereerst wil ik mijn waardering uitspreken voor mijn promotor Rob Heethaar. Afgezien van het feit dat een promotieonderzoek niet tot stand kan komen zonder de bereidwilligheid van een promotor, moet mij van het hart dat de manier waarop ik aan mijn promotieonderzoek heb kunnen werken en de vrijheid die ik daarbij heb gehad me altijd bij zullen blijven.

Waar een promotor is, is een co-promotor. In mijn geval is dat Theo Faes. Toen ik voorstelde om als motto van het proefschrift ‘The assumption is the mother of all fuck-ups’ te nemen, zei Theo meteen: ‘niet de aanname, maar het dogmatisch vasthouden aan een aanname is de moeder aller vergissingen’. Zoiets zou mijn vader waarschijnlijk ook gezegd hebben en dat bedoel ik als een compliment. Het is tekenend voor de grondige manier waarop je placht te redeneren en de kritische kijk waarmee je in elke redeneer wijze de zwakke punten weet aan te wijzen. Ik denk met genoegen terug aan alle discussies voor het bord met markers die altijd maar op lijken te zijn en het waren de momenten die mij als onderzoeker het meest gevormd hebben.

Naast alle andere collega’s die ik uiteraard dankbaar ben voor de geweldige tijd die mijn verblijf op de afdeling Klinische Fysica is geweest, wil ik er twee bijzonder bedanken, omdat het mijn kamergenoten zijn geweest: Joost Kuijer en Frank de Vries. Met jullie heb ik mijn liefde voor het muziek maken kunnen delen, alleen jammer dat jullie gitaristen zijn en geen drummer. Behalve dat heb ik mede door jullie humor en relaxedheid altijd een werkplek gehad waar je je kunt thuisvoelen. Van mijn niet kamergenoten verdient Jan Meijer

nog een eervolle vermelding, omdat we op zijn kamer altijd gezellig een sigaretje konden roken. Het feit dat Jan nu gestopt is met roken, doet daar niets aan af.

Mijn speciale dank gaat uit naar Erwin Borrias die op een blauwe maandag nog metingen voor mij heeft zitten uitwerken. Dit deed hij niet voor de lol en ook niet omdat hij toch niets te doen had en daarom verdient hij een dikke pluim. Ook Isabela Kadzinska heeft erg veel werk verricht om de bergen data die de MRI metingen opleverden uit te werken, hulde hiervoor.

Uiteraard verdienen mijn paranimfen Sergei Herczog en Arjan Borrias speciale aandacht, want zonder paranimfen kan de promovendus niet. De grote dag die nu nog voor me ligt en ooit ver achter me, zal niet tot stand kunnen komen zonder hulp van deze twee reuzen.

Natuurlijk ben ik mijn promotie commissie zeer dankbaar voor het lezen van mijn proefschrift. I would like to express my special gratitude to Dr. Kanai who took the trouble to read my thesis and to travel half the from Japan to The Netherlands to be a member of the commitee

Lieve Vianda, in jouw proefschrift staat het al, namelijk van dat naast elkaar gaan zitten tijdens de verplichte cursus Medische Ethiek van het Mensgebonden onderzoek en zo. Daar heb ik verder weinig aan toe te voegen.. Wat me nog wel van het hart moet is dat zonder jouw liefde en steun (wel practisch dat je eerder bent gepromoveerd) de laatste loodjes een stuk zwaarder zouden zijn geweest.

Curriculum Vitae

Alexander Emanuel Hoetink was born in Apeldoorn, The Netherlands, on Februari 25, 1971. In 1989 he passed the secondary school (Atheneum B), at the 'Amsterdams Lyceum' in Amsterdam. He started to study at the department of Applied Physics of the Delft University of Technology in Delft, The Netherlands, in 1989. During his study he participated in the USA Technology Project, visiting several companies in the USA that are active in the fields of Telecomunication, Solid State Physics and Process Technology. Additionally, several universities and institutions in the USA were visited, amongst others Harvard, MIT, Stanford University, CalTech, Jet Propulsion Labaratories. In 1998 he graduated the study at the laboratory of Seismics and Acoustics. In August 1998 he started as Assistant Researcher at the department of Medical Physics of the VU University Medical Center in Amsterdam, where he performed the research described in this thesis. In August 1992 he started as a researcher at the Stichting Wetenschappelijk Onderzoek Verkeersveiligheid (SWOV), where he wrote a report on the safety aspects of Advanced Cruise Control. Since October 1993 he is employed at the department of Clinical and Experimental Audiology, where he is in trainging as a Clinical Physicist in the field of Audiology.

Color Figures

Chapter 3

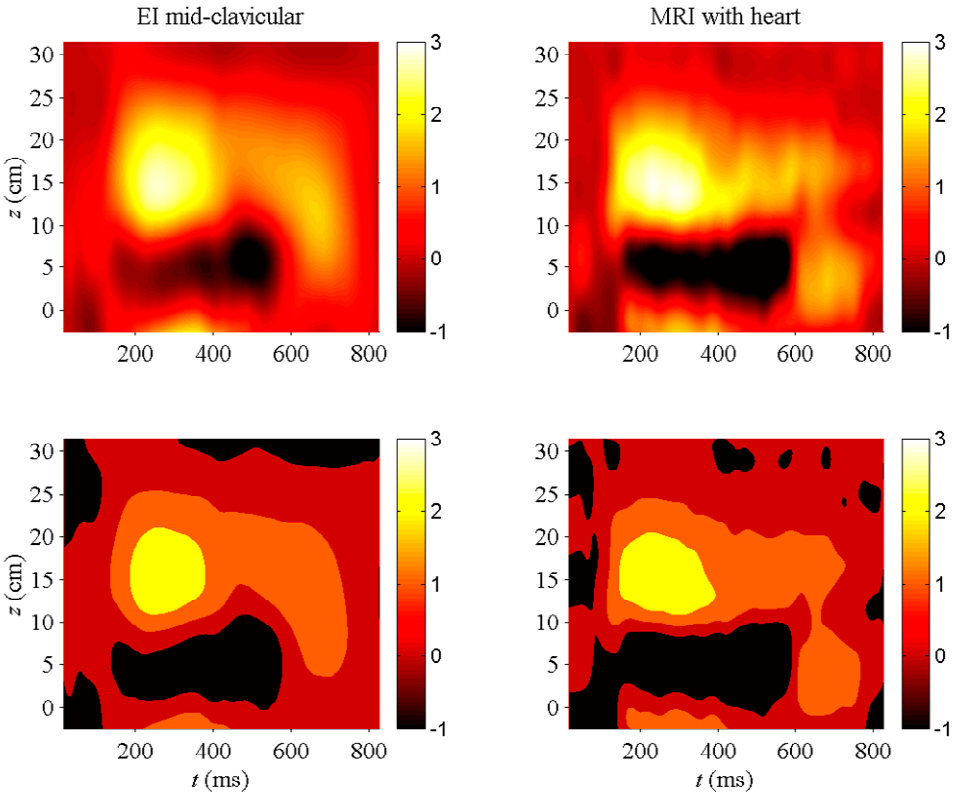

Figure 3. (top left) SAC image (cm^2) estimated from mid-clavicular EI measurements; (bottom left) Contour map obtained from the mid-clavicular EI SAC image; (top right) SAC image (cm^2) calculated from MRI measurements including the contribution of the aorta, the vena cava, the carotid arteries and the heart; (bottom right) Contour map obtained from the MRI SAC image.

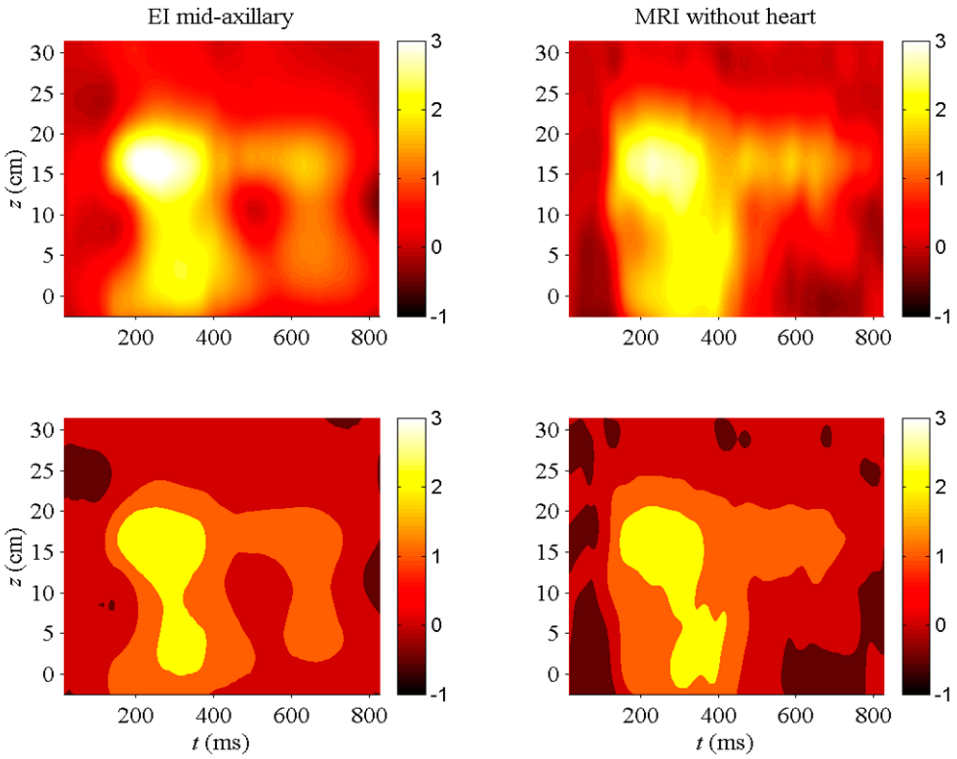

Figure 4. (top left) SAC image (cm^2) estimated from mid-axillary EI measurements; (bottom left) Contour map obtained from the mid-axillary EI SAC image; (top right) SAC image (cm^2) calculated from MRI measurements including the contributions from aorta, the vena cava and the carotid arteries, but without the contribution of the heart; (bottom right) Contour map obtained from the MRI SAC image.

Chapter 5

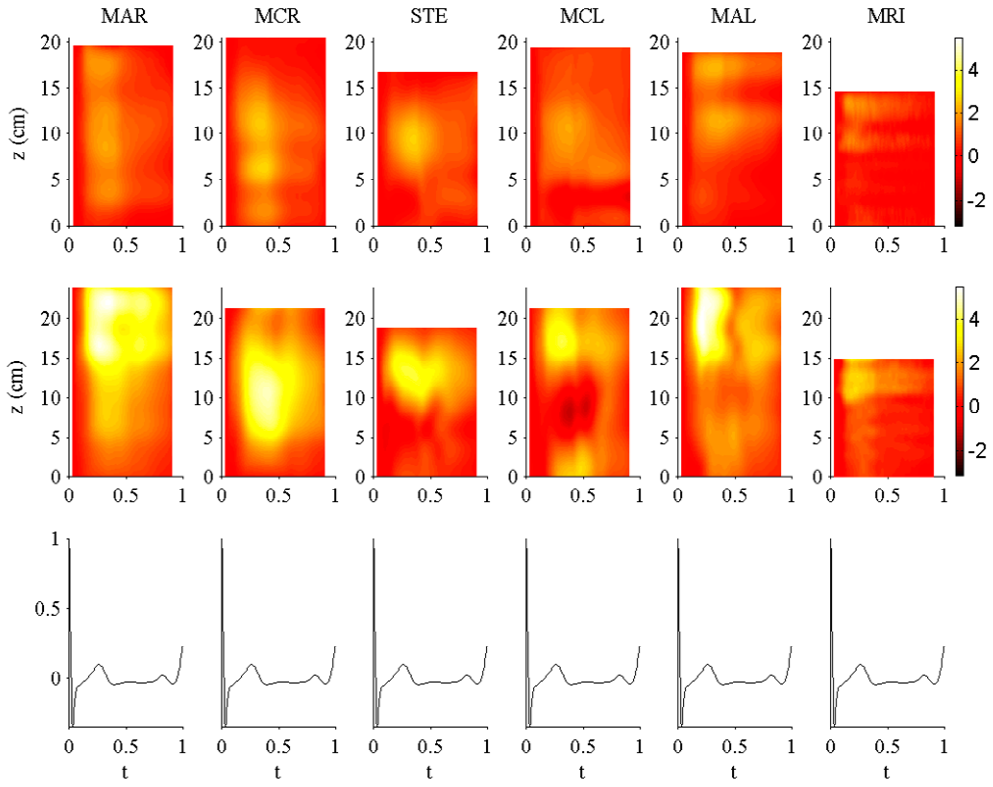

Figure 5. Mappings of the SAC for the male subjects as a function of time (horizontal axis) and location on the thorax (vertical axis). The top row gives the results for subject 1 and the second row for subject 2. The bottom row gives an example of an ECG.

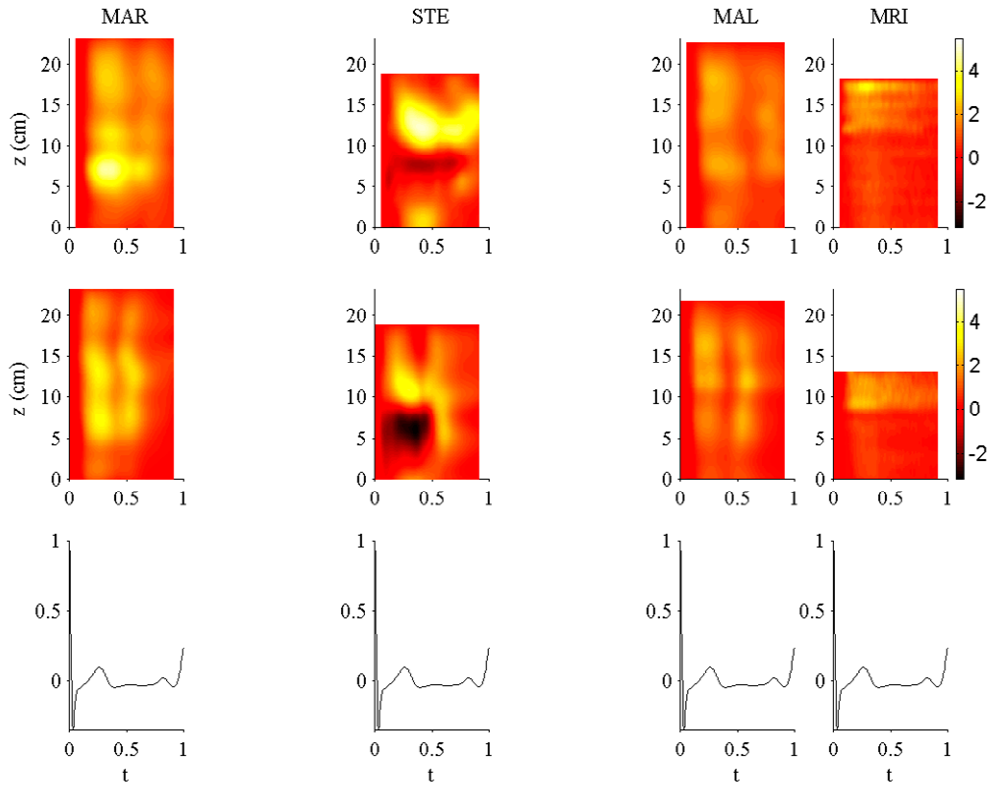

Figure 6. Mappings of the SAC for the female subjects as a function of time (horizontal axis) and location on the thorax (vertical axis). The top row gives the results for subject 3 and the second row for subject 4. The bottom row gives an example of an ECG.